공학박사 학위논문

Diffusion mechanism of excited charge-transfer states

여기 상태 전하 이동 상의 확산 기작

2020년 2월

서울대학교 대학원

재료공학 전공

김 황 범

Abstract

Diffusion mechanism of excited charge-transfer states

Hwang-Beom Kim
Department of Materials Science and Engineering
The Graduate School
Seoul National University

Excited-state CT complexes (exciplexes) have become an important research issue since the triplet harvesting ability of them was reported. Organic light-emitting diodes (OLEDs) could transform only singlet excited states into photons in the past when non-phosphorescent dyes were employed. The singlet generation probability from recombination of electrons and holes in OLEDs is just 25%, and triplet excited states which are generated three times more than singlet excited states are wasted into phonons. However, exciplexes were discovered to enable to transform triplet excited states into singlet excited states, and successfully have been employed in OLEDs as triplet harvesters, recently. It has become a new way for achieving the efficiency of phosphorescent OLEDs without using phosphorescent dyes containing

heavy atoms such as iridium and platinum.

Exciplexes are also important research topics in organic photovoltaics (OPVs). The objective of OPVs is the conversion of excitons generated by light to free charges. For the dissociation of excitons into charges, heterojunctions have been employed in OPVs. Heterojunctions induce the exciton dissociation, and free charges could be collected in electrodes. When exciton dissociation happens, exciplexes could be precursors for free charges because exciplexes are weakly bound electron-hole pair. The understanding of exciton dissociation into free charges including exciplex states should be preceded for scientific approach to improve efficiencies of OPVs.

Despite the application and importance of exciplexes in organic optoelectronic devices, the exciplex diffusion in optoelectronic devices was not considered in the device. It is because optical absorption was considered to be not present for exciplexes. The diffusion of excited states in optoelectronic devices takes place by excitation energy transfer (ET), and the ET takes place when spectral overlap between emission spectra of energy donors and absorption spectra of energy acceptors is present. The absence of absorption to exciplex states has excluded the discussion on the exciplex diffusion.

First of all, we report the optical absorption to exciplex states in this thesis. The absorption to exciplex states was detected by ultraviolet-visible-near infrared (UV-Vis-NIR) spectrophotometer employing exciplex-forming films with thickness

of 1~2 micrometers. The extraction of extinction coefficients for intermolecular CT absorption band was carried out by two methods. One is to employ an ellipsometry measurement, and the other is not.

Second, discussion on the exciplex diffusion is provided. The measured intermolecular CT absorption band indicates that exciplex-exciplex ETs could take place because of the presence of the spectral overlap between emission spectrum and absorption spectrum of exciplexes. In order to figure out exciplex-exciplex ETs take place, we fabricated organic films where high-energy exciplexes and low-energy exciplexes are doped. The transient analysis for photoluminescence (PL) for the exciplexes was conducted for various doping concentrations of the films. The exponential decrease of ET rate constants with exciplex separation as well as the spectral overlap between emission and absorption spectra of the exciplexes indicate that the exciplex-exciplex ET takes place and the dominant mechanism is Dexter ET.

Finally, we report exciton generation from exciplexes by ET. The spectral overlap between the emission spectrum of the exciton and the absorption spectrum of the exciplex is present, and it is grounds for exciton-exciplex ETs. We fabricated organic films where the exciton and exciplex are doped for the purpose of observing the exciton-exciplex ET. The excited-state lifetime of the exciton decreases and that of the exciplex increases. Not only the spectral overlap but also the quantitative analysis of the excited-state lifetimes of the exciton and exciplex indicates that the exciton-exciplex ET takes place in the organic semiconductor.

Keyword: exciplex, diffusion, energy transfer, charge-transfer absorption, Dexter-type energy transfer

Student Number: 2014-21494

Table of contents

List of Tables

List of Figures

Chapter 1. Introduction

1.1. Motivation and outline of thesis

Excited charge-transfer (CT) states stand for electronic states for excited-state CT complexes (exciplexes). Exciplexes were discovered by new redshifted, broad, and featureless emission bands different from exciton emission bands in mixtures of different molecules even though excitons are generated by photoexcitation. It indicates that different molecules simultaneously participate in an emission process, and the complex of the different molecules is called 'exciplex'.[1,2]

Exciplexes usually formed in type-II heterojunctions where energy levels of the lowest unoccupied molecular orbital (LUMO) and the highest occupied molecular orbital (HOMO) of one molecule are higher than those of a different molecule. In type-II heterojunctions, the former could partially transfer an electron into the latter when one of them is in the excited state because the electronic energy for the CT configuration is lower than that for the excited configuration without CT, leading to the generation of exciplexes.[1,3–5]

The type-II heterojunctions are often found in optoelectronic devices such as organic light-emitting diodes (OLEDs) and organic photovoltaics (OPVs) because they usually exploited heterojunctions between hole-transporting materials and electron-transporting materials and the heterojunctions are easy to satisfy the conditions of type-II heterojunction. In early stage of research for OLEDs, exciplexes were considered as obstacles for highly efficient devices because the photoluminescence

quantum yield (PLQY) of exciplexes is usually low. Recently, high reverse intersystem crossing yield (RISC) of exciplexes was discovered and actively employed in OLEDs.[6,7,16,8–15] In OPVs, exciplexes usually act as precursors for the generation of free polarons.[4,17–25]

Exciplex properties such as excited-state transition rates, dissociation and recombination rates, and energetics are actively researching because they have a great influence on the device characteristics.[1,3,32,7,8,26–31] However, exciplex diffusion in organic optoelectronic devices was lacking in spite of the influence of excited-state diffusion on the device characteristics. Excitation energy transfer (ET) is the mechanism for the excited-state diffusion. There are two kinds of excitation ET. One is Förster-type resonance ET (FRET) and the other is Dexter-type exchange ET (DET).[2,33] FRET is dominant mechanism for singlet exciton diffusion. On the other hand, DET is the only mechanism for triplet exciton diffusion of non-phosphorescent molecules.[33] ETs require the spectral overlap between an emission spectrum of an energy donor and an optical absorption spectrum of an energy acceptor because of the energy conservation law during the quantum transition.[2,33]

Exciplex diffusion was not considered because the generation of an exciplex from a nearby exciplex by ET was unlikely to be realized considering that the optical absorption band corresponding to the CT transition from the ground state to the exciplex state was considered not to be present.[2] Recently, the CT absorption bands with very small intensities was observed in blends of polymer/[6,6]-phenyl C_{61} butyric acid methyl ester (PCBM) exhibiting exciplex emission bands employing elaborated absorption measurements such as a Fourier transform photocurrent spectroscopy (FTPS) and a photothermal deflection spectroscopy (PDS).[4,20,25,34,35] Also,

the exciplex diffusion was reported using an optical microscope with a scanning detector, and the geminate recombination of exciplexes was proposed to be the mechanism of the exciplex diffusion.[36] However, the mechanism for the exciplex diffusion is hard to be concluded until now, considering the lacking discussion on the ET for the mechanism of the exciplex diffusion. The discussion on the possible mechanisms of the exciplex diffusion is provided in this thesis.

In the rest part of Chapter 1, study backgrounds for this thesis are provided. Theoretical backgrounds for CT characteristics and optical properties of exciplexes are given for understanding the optical absorption and photoluminescence (PL) spectra of exciplexes. The analysis of them is crucial in this thesis. The origin and theoretical model for the thermally activated delayed fluorescence (TADF) of exciplexes are also provided for the quantitative analysis of the transient PL profiles of exciplexes in the other chapters. Finally, the diffusion of excited states in organic films is theoretically reviewed, and it helps to understand the discussion on the possible mechanisms of the exciplex diffusion.

In Chapter 2, we report very small extinction coefficients for the CT transition from the ground state to the exciplex state. The very small extinction coefficients were obtained from exciplex-forming films consisting of small molecules which are usually employed in OLEDs. Two simple methods extracting the very small extinction coefficients from absorbance of the films using an ultraviolet-visible-near infrared (UV-Vis-NIR) spectroscopy were described in the chapter. The first one is employing the ellipsometry measurements additionally in order to obtain the thicknesses and refractive indices of the organic films. Going one step further, the second one is just employing the absorbance measurements using the ultraviolet-

visible-near infrared (UV-Vis-NIR) spectroscopy in order to obtain the thicknesses and refractive indices of the organic films.

In Chapter 3, we discuss on the mechanism of the exciplex diffusion in organic semiconductors. The CT absorption bands obtained in Chapter 2 provide a basis for the ET to be the mechanism of the exciplex diffusion considering that the exciplex-exciplex ET requires spectral overlap between optical absorption spectra of exciplex states and emission spectra of exciplex states. In order to figure out whether the exciplex-exciplex ET operates, we fabricated organic films in which two kinds of exciplexes are close together. Time-resolved PL analysis for the two kinds of exciplexes was conducted, and we could conclude that the exciplex-exciplex ET works in the films. As a result of the quantitative analysis of various mechanisms for the exciplex diffusion, we could conclude that DET is the dominant mechanism for the exciplex diffusion.

In Chapter 4, the exciplex generation from excitons by ET is reported. Even though the exciton generation from exciplexes by CT or ET and the exciplex generation from excitons by CT were reported, the exciplex generation from excitons by ET was not reported. It is because of a common belief that the CT absorption band for exciplexes is absent like the reason of the lacking discussion on exciplex diffusion. Exciton-exciplex ET was investigated using the films where excitons and exciplexes are co-doped. The PL emission from the excitons and exciplexes were analyzed by the time-resolved PL spectroscopy. We could conclude that exciton-exciplex ET operates in the organic semiconductors by the quantitative analysis for the transient PL profiles.

1.2. Charge-transfer characteristics of excited-state charge-transfer complexes

Exciplexes are formed by CT at the excited state between donor and acceptor molecules, from which the name of exciplex originates. The exciplex emission is usually observed in type-II heterojunctions, which consist of a pair of two molecules with the energy levels of HOMO and LUMO of a donor molecule being higher than those of an acceptor molecule as shown in Figure 1.1.

The exciplex consists of a pair of an electron donor molecule and an electron acceptor molecule. Here, electron donor molecules generally contain electron-donating moieties such as carbazoles, triarylamines, and 9,10-dihydroacridines.[37–41] Electron acceptor molecules typically have electron-withdrawing moieties such as 1,3,5-triazines, quinoxalines, pyrazines, pyrimidines, quinolines, phenanthrolines, pyridines, 1,3,4-oxadiazoles, benzimidazoles, benzotriazoles, triarylboranes, siloles, phosphine oxides, sulfones, cyano groups, fluoro groups, and carbonyl groups.[37,39,49,40,42–48]

The CT forming exciplexes can be considered as the partial CT, and the exciplex wavefunction can be expressed as the mixed state of pure locally ground (LG), locally excited (LE) and CT states as a result of the configuration interaction which is the superposition of the configurations described by Equation (1.1).[50,51]

$$\Psi_m(x) = \sum_{i,j} C^m_{\mathrm{LG},i,j}(x)\Psi_{\mathrm{LG},i,j} + \sum_{i,j} C^m_{\mathrm{LE},i,j}(x)\Psi_{\mathrm{LE},i,j} + \sum_{i,j} C^m_{\mathrm{CT},i,j}(x)\Psi_{\mathrm{CT},i,j} \quad \cdots\cdots\cdots\cdots (1.1)$$

where $\Psi_m(x)$ is the m^{th} wavefunction of the mixed vibronic states, $\Psi_{\mathrm{LG},i,j}$ is the wavefunction of the pure LG vibronic states, $\Psi_{\mathrm{LE},i,j}$ is the wavefunction of the pure

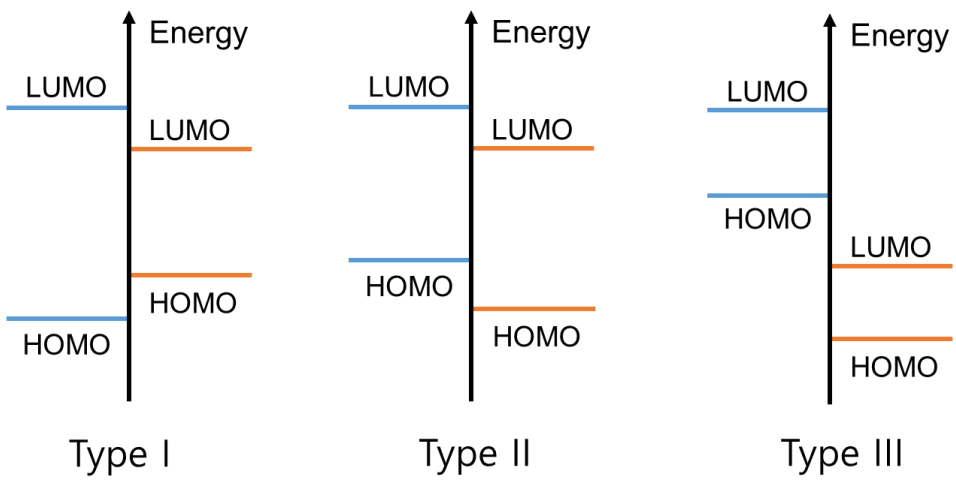

Figure 1.1. Molecular orbital energy diagram for type-I, II, III heterojunctions.

LE vibronic states, $\Psi_{\mathrm{CT},i,j}$ is the wavefunction of the pure CT virbonic states, *i* and *j* are the quantum numbers of the high-frequency skeletal vibrational normal modes, *x* is the configuration coordinate which is influenced by the low-frequency (classical) modes, and *C*'s are the corresponding expansion coefficients. The fraction of CT, $f_{\mathrm{CT}}(x)$ in the exciplex is defined at configuration, *x*.

$$f_{\mathrm{CT}}(x) = \sum_{i,j} \left| C^{m}_{\mathrm{CT},i,j}(x) \right|^2 \quad \cdots\cdots (1.2)$$

The thermal average of $f_{\mathrm{CT}}(x)$ gives the overall percentage of CT, $\%_{\mathrm{CT}}$ in the exciplex.

$$\%_{\mathrm{CT}} = 100 \int f_{\mathrm{CT}}(x) \exp\left(-\frac{E_{\mathrm{Ex}}(x)}{k_{\mathrm{B}}T} \right) dx \quad \cdots\cdots (1.3)$$

where $E_{\mathrm{Ex}}(x)$ is the energy of the mixed excited state at configuration *x*, k_{B} is the Boltzmann constant, and *T* is the absolute temperature.

The HOMO and LUMO of the exciplex are spatially separated, and the exciplex state is close to the pure CT state.[52–54] Figure 1.2 shows the geometry of an exciplex-forming pair of 9,9′,9″-triphenyl-9H,9′H,9″H-3,3′:6′,3″-tercarbazole (Tris-PCz) and 3′,3‴,3⁗-(1,3,5-triazine-2,4,6-triyl)tris(([1,1′-biphenyl]-3-carbonitrile)) (CN-T2T) in the equilibrium geometry of the ground state.[53] The geometry optimization was calculated with the DFT at the B3LYP/6-31g(d) levels using the dichloromethane as the medium, which would be the geometry in the local minimum. In this geometry, there is a complexation energy of 0.0451 eV between cyano-biphenyl and carbazole moieties, the distance between two molecules is calculated to be 4.50 Å, and the calculated LUMO and HOMO of this complexation are located at CN-T2T and Tris-PCz, respectively. The transition from the ground state to the

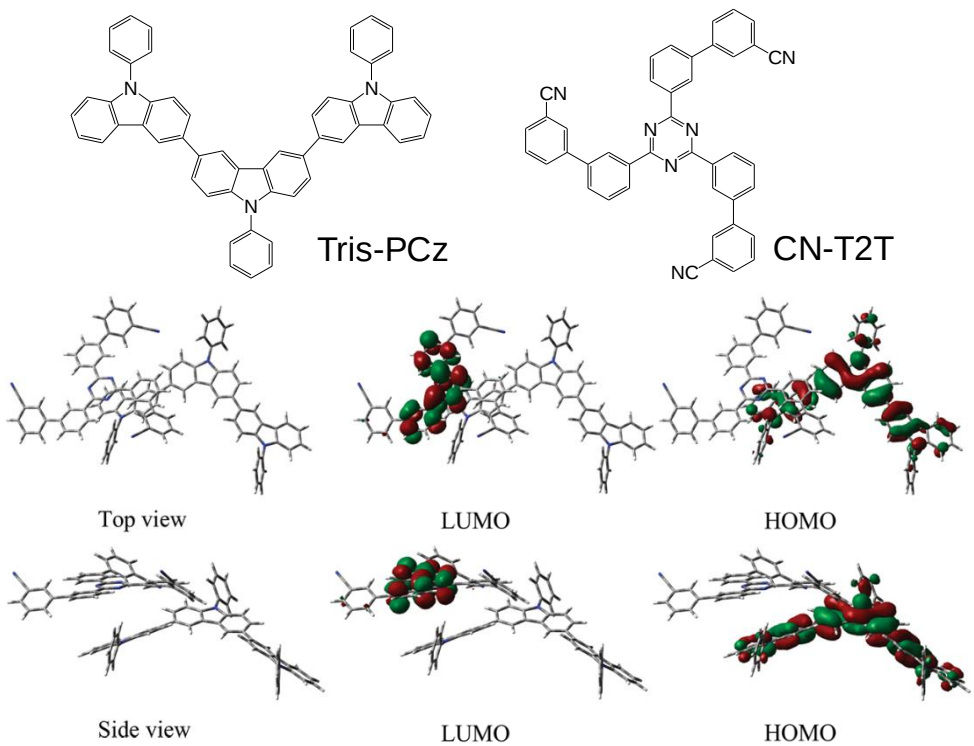

Figure 1.2. Molecular structures of Tris-PCz and CN-T2T and the geometry of a pair of them in the ground state and HOMO and LUMO of the exciplex.[53]

lowest excited singlet state is assigned to $\phi_{\mathrm{HOMO}} \rightarrow \phi_{\mathrm{LOMO}}$ (96 %), which indicates the high fraction of CT in the exciplex. Tris-PCz and CN-T2T form exciplexes close to contact radical ion pairs.

1.3. Optical properties of exciplexes

A significant feature of exciplexes is their PL spectra. As $\%_{CT}$ in the exciplex increase, the PL spectra of exciplexes are redshifted from the PL spectra of the constituent molecules, and broad and featureless without the vibrational progression. Figure 1.3(a) shows the PL spectra of the exciplexes consisting of 9,10-dicyanoanthracene (DCA) and various alkylbenzene donors in cyclohexane.[50] The decrease of the oxidation potentials of the donors corresponding to the increase of the energy levels of the HOMO of the donors lead to the decrease of the energy of the pure CT state. It gives rise to the increase of $\%_{CT}$ of exciplexes, resulting in the decrease of the vibrational progression caused by the pure LE state, and the influence increment of the broad and redshifted PL spectra on exciplex emission. Even though $\%_{CT}$ of the exciplex ensemble is given in one value, exciplexes participating in emission have various f_{CT} which is dependent on the microscopic environment and librational displacement as shown in Figure 1.3(b). The simulated PL spectra (red curves) of exciplexes are well matched with the experimental ones (black curves) in Figure 1.3(a).

There are two main reasons that PL spectra of exciplexes are redshifted than those of the constituent molecules. One reason comes from the energy difference between the pure LE and CT states. The increase of the energy difference between them leads to the increase of $\%_{CT}$ indicating that the increase of the influence of the pure CT state on the exciplex state. In other words, the PL spectra of the exciplexes are gradually redshifted compared to the PL spectra of the constituent molecules as $\%_{CT}$ increases if other parameters remain constant. Therefore, the

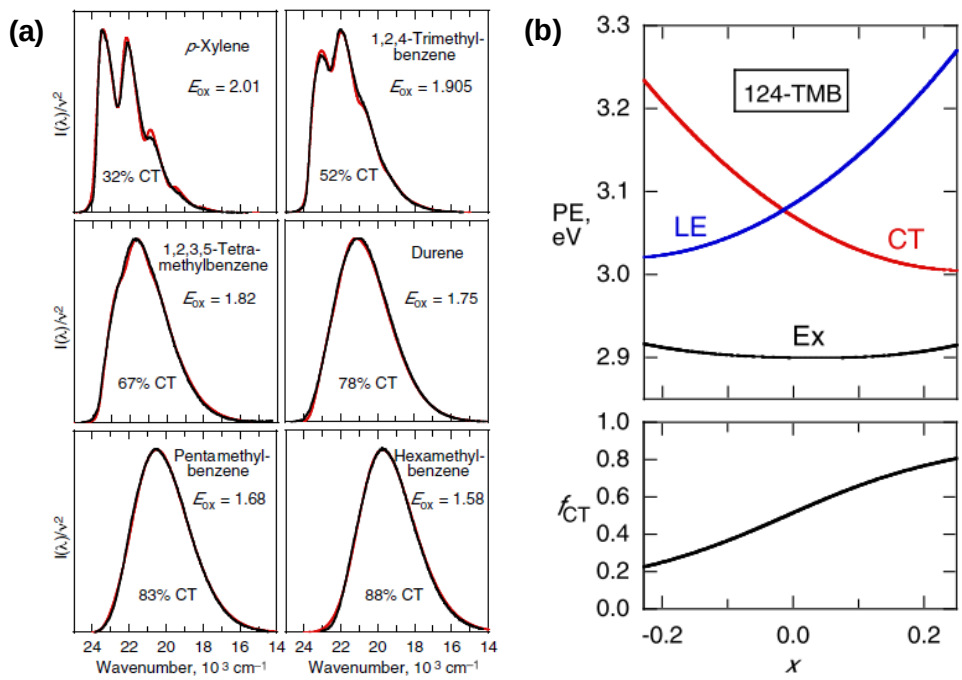

Figure 1.3. (a) PL spectra (black) and simulated curves (red) of exciplexes with different $\%_{CT}$ consisting of DCA and various alkylbenzene donors in cyclohexane. (b) Potential energy curve for the pure singlet LE state, the pure CT state, and the singlet exciplex state as well as f_{CT} as a function configuration coordinate (x) for the 1,2,4-trimethyl-benzene exciplex $(\%_{CT} = 52)$.[50]

higher HOMO energy levels of donors than acceptors and the lower LUMO energy levels of acceptors than donors are the one main reason that the observed emission of exciplexes is redshifted from that of the constituent molecules, and the increase of the energy difference of the HOMOs or LUMOs between donors and acceptors usually lead to the increase of the degree of the redshift of the exciplex PL spectra. Another main reason that PL spectra of exciplexes are redshifted than those of the constituent molecules is the reorganization energy caused by different equilibrium geometries between the pure LE state and the pure CT state.[50,55]

In contrast to the PL spectra of exciplexes, the optical absorption spectra of exciplexes are usually not observed. Figure 1.4 shows that the PL and absorption spectra of the 1,1-bis[4-[*N*,*N*-di(p-tolyl)amino]phenyl] cyclohexane (TAPC) and 6,6′-bis(2-4diphenylquinoline) (B1PPQ) neat films, and the TAPC:B1PPQ blended films.[56] TAPC and B1PPQ form the highly ionic exciplex, which could be inferred by the redshifted, broad, and featureless PL spectra of the blended films as shown in Figure 1.4(a), where TAPC serves as electron donors and B1PPQ as electron acceptors. Only exciplex emissions with no emission from each molecule appear in the range of 10 to 50 mol% B1PPQ of the blended films. This indicates that almost all the excitons in the blended films participate in forming exciplexes. Despite of this fact, new absorption peaks corresponding to the exciplex PL do not appear in the absorption spectra (Figure 1.4(b)) of the blended films. In addition, the absorption spectra of the TAPC:B1PPQ blended films with various ratios can be fitted to the linear sum of the absorption spectra of the neat films of constituent molecules. The absorbance is linearly proportional to the number of molecules in the path of light under the assumption that there is little interaction between the donor and acceptor

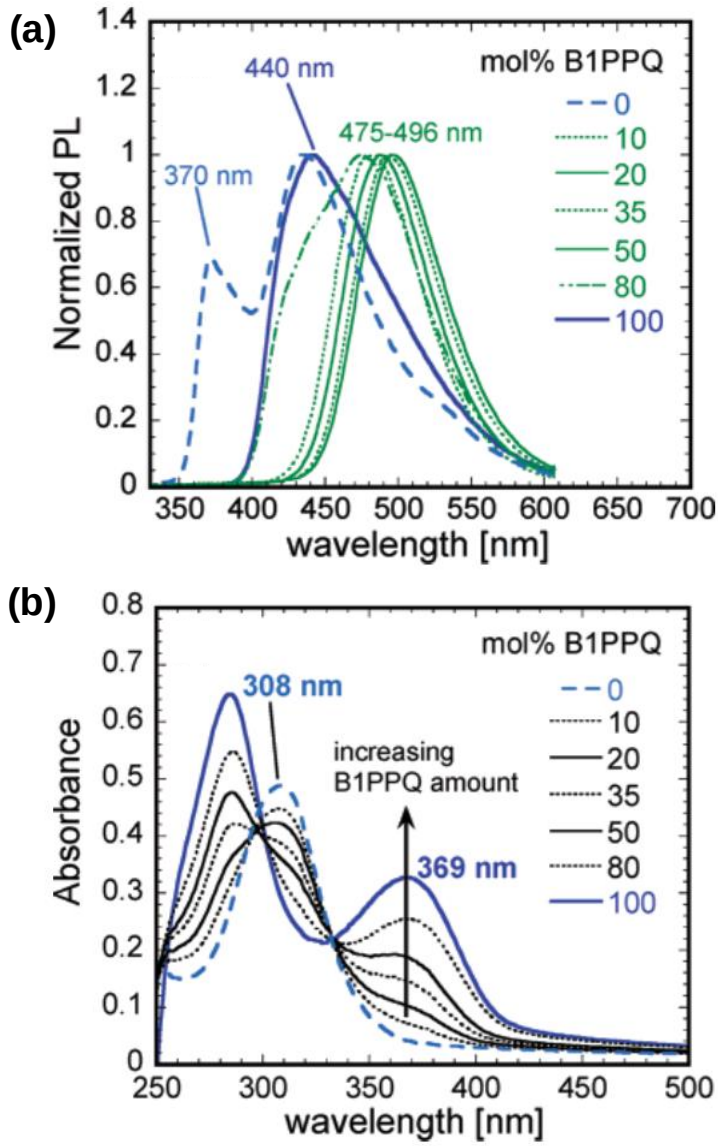

Figure 1.4. (a) PL and (b) absorption spectra of the TAPC and B1PPQ neat films and TAPC:B1PPQ blended films with various molar ratio.[56]

molecules in the ground state. This indicates that the exciplexes are not directly formed from the ground state by photo-excitation, but formed from the excitons of the constituent molecules. In other words, excitons of the constituent molecules play a role as precursors to exciplexes. It is the reason that these species are termed the excited-state CT complex.

However, there are elaborate studies that new optical absorption peaks corresponding to the exciplex PL appear in the donor-acceptor blended films.[4,20,21,25,34,35,57,58] These new optical absorption peaks originate from the direct optical excitation from the ground state to the exciplex state.[4] Poly(2-methoxy-5-(3′,7′-dimethyloctyloxy)-1,4-phenylenevinylene) (MDMO-PPV):PCBM exciplexes are one of the examples. Figure 1.5(a) shows that the PL spectrum of the MDMO-PPV:PCBM (1:4) blended film.[59] Given the PL spectra for the pristine films of the constituent molecules shown in the inset, there is a new redshifted and broad peak around 1.35 eV which originates from the transition from the exciplex state to the ground state. Figure 1.5(b) shows the linear and logarithmic external quantum efficiencies (EQEs) of the solar cell whose structure is ITO/ poly(2,3-dihydrothieno-1,4-dioxin)-poly(styrene sulfonate) (PEDOT:PSS)/ MDMO-PPV:PCBM (1:4)/ Ca/ Al using FTPS.[20] FTPS is the extremely sensitive technique for measuring low absorption, which was introduced for the purpose of measuring defect-related optical absorption in microcrystalline silicon thin films.[60] A new redshifted, broad peak around 1.65 eV with low absorption coefficients below the onsets of the absorption spectra of MDMO-PPV and PCBM is observed, which is fitted to the CT complex (CTC) fit curve in Figure 1.5(b).[20] The new redshifted broad peak is unrecognizable

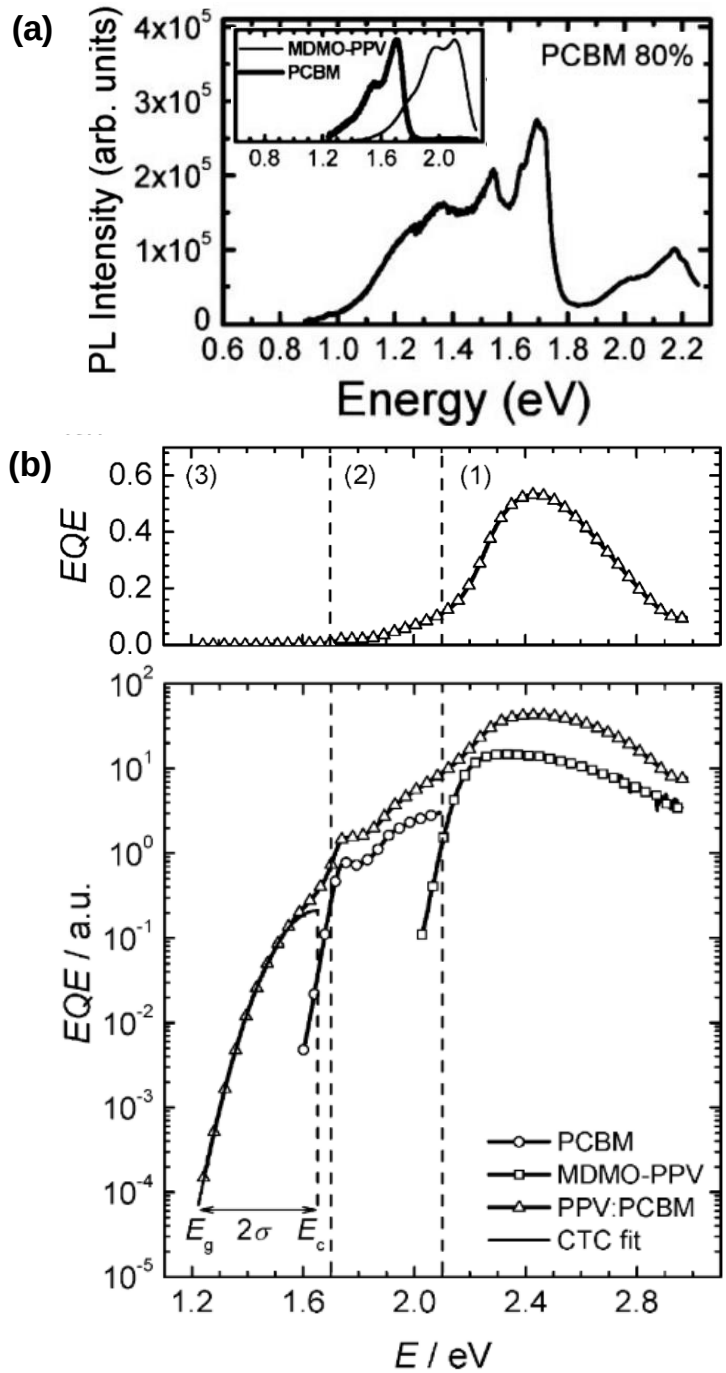

Figure. 1.5. (a) PL[59] and (b) FTPS[20] spectra of the MDMP-PPV:PCBM (1:4) blended film.

in the linear absorption data. The low absorption coefficients of the singlet exciplex state is attributed to the CT characteristics of exciplexes.

1.4. Thermally activated delayed fluorescence

TADF of exciplexes has become the center of attention since it was reported in the OLED research field. In the past, OLEDs employing pure organic molecules without heavy atoms had the limit of 25% for generating singlet excitons from polarons. Considering that only the singlet excitons is the radiative species in room temperature without heavy atoms, it had served as the obstacles for achieving highly efficient OLEDs over the internal quantum efficiency (IQE) of 25%. Beginning with the report of the OLEDs exploiting the TADF of exciplexes, however, the theoretical limit for generating singlet excited states from polarons reaches 100% without heavy atoms. The TADF of exciplexes has been the core value for the third generation OLEDs along with intramolecular CT molecules.

The CT characteristics of exciplexes induces the small singlet-triplet energy splitting because the decrease of overlap between electron and hole orbitals leads to the decrease of exchange energy in the same orbital configuration. It indicates that highly ionic singlet exciplexes could have small singlet-triplet energy splitting which is the energy difference between the lowest excited singlet state (S_1) and the lowest excited triplet state (T_1) if the CT configuration considerably contributes the orbital configurations of T_1. This small singlet-triplet energy splitting of exciplexes causes the TADF. In other words, the transition from the triplet exciplex state to the singlet exciplex state plays a major role in the TADF. The singlet exciplex state undergoes transitions to the ground state by the radiative (fluorescent) and nonradiative ways (internal conversion) as well as the transition to the triplet exciplex state by the non-radiative way (intersystem crossing (ISC)). The triplet exciplex state also undergoes

the transitions to the singlet exciplex state by the nonradiative way (RISC) and to the ground state with the radiative (phosphorescent) and the nonradiative ways. Conventional fluorescent molecules have very small RISC rate constant at room temperature due to large singlet-triplet energy splitting, so the lowest triplet excited state has little transition probability to the lowest singlet excited state. On the other hand, exciplexes could have large transition probability for the RISC from the triplet excited state to the singlet excited state at room temperature. It is attributed to small singlet-triplet energy splitting of exciplexes, resulting in strong delayed fluorescence originated from efficient RISC process, followed by the fluorescence process. This is called TADF.[7,16,61]

The state energy diagram of the exciplex-forming system which is typically employed in exciplex-emitting OLEDs is shown in Figure 1.6(a). The basis states of the exciplex-forming system are denoted as S_{LE}, S_{CT}, T_{LE}, and T_{CT} which are the lowest singlet LE state, the lowest singlet CT state, the lowest triplet LE state, and the lowest triplet CT states, respectively, based on the three-state mixing model for the singlet and triplet states.[29] S_{CT} and T_{CT} which are formed in the exciplex-forming system induce the effective state mixing between the states with the same spin multiplicity, resulting in S_1, S_2, T_1, and T_2 states, which are the lowest singlet state, the second lowest singlet state, the lowest triplet state, and the second lowest triplet state in exciplex-forming system. They have the both the CT character and the LE character by virtue of the state mixing. The mixing coefficients decide the degrees of CT of the mixed states.[29,50] The highly neutral triplet exciplex state exhibits large LE character. The effective ISC and RISC could occur by virtue of the state mixing between the singlet and triplet states when their energy levels are close.[2,7,62–64]

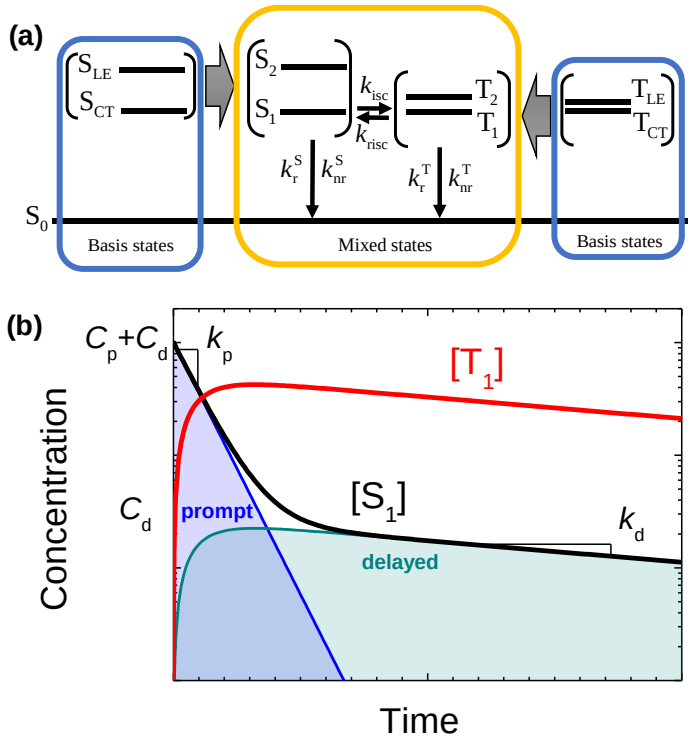

Figure 1.6. (a) State energy diagram of the exciplex-forming system. (b) Typical semilogarithmic plots for concentration profiles of singlet (black) and triplet (red) excited states exhibiting TADF characteristics along with the decay rate constants for the prompt (blue) and delayed (green) parts for the concentration profile of the singlet excited state when the excitation source is applied as the delta function.

The rate equations for the concentrations of singlet and triplet exciplex states could be given in Equation (1.4) and (1.5).

$$\frac{d[S_1]}{dt} = G_S - \left(k_r^S + k_{nr}^S + k_{isc}\right)[S_1] + k_{risc}[T_1] \quad \cdots\cdots (1.4)$$

$$\frac{d[T_1]}{dt} = G_T - \left(k_r^T + k_{nr}^T + k_{risc}\right)[T_1] + k_{isc}[S_1] \quad \cdots\cdots (1.5)$$

where $[S_1]$ and $[T_1]$ are the concentrations of singlet and triplet exciplexes, and G_S and G_T are the generation rates of singlet and triplet exciplexes, respectively, from the excitation source or any states other than the exciplex states. G_T is zero for photo-excitation and G_S:G_T = 1:3 for electrical excitation.

In the transient PL experiments generation rates of singlet exciplexes from the excitation source could be considered as the delta function at t = 0, and the concentration of the exciplex states by solving Equation (1.4) and (1.5) could be described by

$$[S_1] = \left(C_p + C_d\right)\exp\left(-k_p t\right) + C_d\left[\exp\left(-k_d t\right) - \exp\left(-k_p t\right)\right], \quad \cdots\cdots (1.6)$$

$$[T_1] = -C_T \exp\left(-k_p t\right) + C_T \exp\left(-k_d t\right) \quad \cdots\cdots (1.7)$$

where k_p and k_d are the decay rate constants of the prompt and delayed terms of the singlet exciplex state, respectively, C_p and C_d are the pre-exponential factor of the prompt and delayed terms of the singlet exciplex state, respectively, and C_T is the pre-exponential factor of the triplet exciplex state which are expressed by

$$k_p, k_d = \frac{1}{2}\left(k_S + k_T\right)\left\{1 \pm \left[1 - \frac{4k_S k_T - 4k_{isc}k_{risc}}{\left(k_S + k_T\right)^2}\right]^{0.5}\right\}, \quad \cdots\cdots (1.8)$$

$$C_p = \frac{k_S - k_d}{k_p - k_d}[S_1]_0, \quad \cdots\cdots (1.9)$$

$$C_{\mathrm{d}} = \frac{k_{\mathrm{p}} - k_{\mathrm{S}}}{k_{\mathrm{p}} - k_{\mathrm{d}}}\left[\mathrm{S}_1\right]_0, \quad \cdots\cdots (1.10)$$

$$C_{\mathrm{T}} = \frac{k_{\mathrm{isc}}\left(k_{\mathrm{S}} - k_{\mathrm{d}}\right)}{\left(k_{\mathrm{p}} - k_{\mathrm{d}}\right)\left(k_{\mathrm{p}} - k_{\mathrm{T}}\right)}\left[\mathrm{S}_1\right]_0, \quad \cdots\cdots (1.11)$$

where $\left[\mathrm{S}_1\right]_0$ is the concentration of the singlet exciplex state at t = 0, $k_{\mathrm{S}} = k_{\mathrm{r}}^{\mathrm{S}} + k_{\mathrm{nr}}^{\mathrm{S}} + k_{\mathrm{isc}}$, and $k_{\mathrm{T}} = k_{\mathrm{r}}^{\mathrm{T}} + k_{\mathrm{nr}}^{\mathrm{T}} + k_{\mathrm{risc}}$. The first term on the right-hand side of Equation (1.6) represents the concentration profile of S_1 except for that of S_1 regenerated from T_1, and the second tem represents the concentration profile of S_1 regenerated by RISC process from T_1 which is 0 at t = 0 which is plotted in Figure 1.6(b) as blue and green lines, respectively. One example following the equations is depicted in Figure 1.6(b) as black and red lines. The population of the singlet state is usually dominant in the prompt time region, and that of the triplet state is usually dominant in the delayed time region because the lifetime of the singlet states is usually shorter than that of the triplet states. The transient PL intensities of exciplexes follow the black curve in Figure 1.6(b) because the PL intensity is linearly proportional to $[\mathrm{S}_1]$. The key transition which could make TADF characteristics is the RISC. As the ISC and RISC quantum yield increases, the delayed part of the transient PL profiles becomes dominant. The high RISC quantum yield indicates the efficient harvesting of the triplet excited states to the singlet excited states (emissive states).[7,53,65,66] When $k_{\mathrm{r}}^{\mathrm{T}}$, $k_{\mathrm{nr}}^{\mathrm{T}} \ll k_{\mathrm{p}}$, $4k_{\mathrm{S}}k_{\mathrm{T}} - 4k_{\mathrm{isc}}k_{\mathrm{risc}} \ll \left(k_{\mathrm{S}} + k_{\mathrm{T}}\right)^2$, and $k_{\mathrm{r}}^{\mathrm{S}}$, $k_{\mathrm{nr}}^{\mathrm{S}}$, $k_{\mathrm{isc}} \gg k_{\mathrm{risc}}$, the prompt decay rate constant in Equation (1.8) could be simplified as the following equations.[7]

$$k_{\mathrm{p}} = k_{\mathrm{r}}^{\mathrm{S}} + k_{\mathrm{nr}}^{\mathrm{S}} + k_{\mathrm{isc}} \quad \cdots\cdots (1.12)$$

The PLQY of the exciplexes is not just the portion of the radiative decay rate constant of the singlet excited state when TADF takes place. The PLQY in exciplexes is the sum between the PLQY from prompt fluorescence and that from delayed fluorescence. The prompt PLQY (Φ_p) is the portion of the radiative decay rate constant of the singlet excited state which is $k_r^S/\left(k_r^S+k_{nr}^S+k_{isc}\right)$. The delayed PLQY ($\Phi_d$) could be written as the following equation.[7]

$$\Phi_d=\Phi_p\sum_{k=1}^{\infty}\left(\Phi_{isc}\Phi_{risc}\right)^k \quad \cdots\cdots (1.13)$$

where Φ_{isc} and Φ_{risc} are the ISC and RISC quantum yields, respectively. The ISC and RISC quantum yields could be expressed by $k_{isc}/\left(k_r^S+k_{nr}^S+k_{isc}\right)$ and $k_{risc}/\left(k_{nr}^T+k_{risc}\right)$ where k_{nr}^T is the nonradiative decay rate constant from the triplet state to the ground state, respectively, if exciplex phosphorescence is negligible. Then, the PLQY (Φ_{PL}) of the exciplexes could be expressed by the below equation.

$$\Phi_{PL}=\frac{k_r^S[S_1]}{G_S}=\frac{k_r^S}{k_r^S+k_{nr}^S+k_{isc}\left(1-\Phi_{risc}\right)} \quad \cdots\cdots (1.14)$$

The 100% PLQY could be achieved by two ways. The one way is when $k_r^S \gg k_{nr}^S, k_{isc}$. In that case, the delayed fluorescence becomes negligible in the PL process because the transition from the singlet excited states to the triplet excited states becomes negligible. The other way is when $k_r^S \gg k_{nr}^S$ and $\Phi_{risc}=1$. In this situation, triplet loss becomes zero even though the transition from the singlet excited states to the triplet excited states is considerable.

The ratio of prompt PLQY to total PLQY corresponds to the ratio of the concentration profile integrated from zero to infinity of S_1 without regeneration from

T_1 to that of S_1, which could be expressed by the following equation.

$$k_r^S = \Phi_{PL}\left(k_r^S + k_{nr}^S + k_{isc}\right)\frac{\int_0^\infty \left(C_p + C_d\right)\exp\left(-k_p t\right)dt}{\int_0^\infty C_p \exp\left(-k_p t\right) + C_d \exp\left(-k_d t\right)dt} \quad \cdots\cdots\cdots\cdots\cdots\cdots\cdots\cdots (1.15)$$

If Equation (1.12) is substituted into Equation (1.15), we could obtain k_r^S from the experimental data.

1.5. Diffusion of excited states

ETs cause the diffusion of excited species because it makes the excitation energy wander in space. When the ET takes place, excited species lose their energy and become ground state, resulting in the new excited species nearby the original ones from the ground state. There are two kinds of the ET. One is FRET and the other is DET. FRET is dominant mechanism when dipole-dipole coupling is large such as singlet exciton diffusion.[2,33] Excitons are the exited species in which a pair of an electron and a hole resides on one molecule, and exciplexes are the excited species of electron donor-acceptor molecular pairs.[1] The singlet excited states and ground state has the same spin multiplicity, resulting in the large transition dipole moment and large dipole-dipole coupling if orbital overlap between an electron and a hole is sufficient.[2] Note that the absorption coefficient is zero if the transition dipole moment between the excited state and the ground state is zero. On the other hand, DET is the only mechanism for triplet exciton diffusion of non-phosphorescent molecules because triplet excited states generally have the very low transition dipole moment inducing negligible dipole-dipole coupling.[33] Triplet excited states have the different spin multiplicity with the ground state, and it is the reason for the very low transition dipole moment because total spin is not conserved during the transition between the triplet excited states and ground state.

There are two requirements for DET to take place according to the Fermi golden rule. One is the electronic exchange integral between energy donor states and energy acceptor states. The electronic exchange integral drops exponentially with the separation between them, and DET was thought to occur when the energy donor

and acceptor are in physical contact.[67] However, the physical contact is not always the necessary condition for efficient long-range DET to occur, and the long-range DETs without the physical contact have been report, known as the superexchange ET.[68–70] The large coupling between π-conjugated molecules could expand the exchange integral between them to large separation when the energy donor and acceptor are π-conjugated molecules in the π-conjugated medium. It indicates that the physical contact between the energy donor and acceptor is not necessary for DET. The other is the spectral overlap between optical absorption of energy acceptors and emission of energy donors, which is the experimental view of the density of the isoenergetic energy-accepting states with energy donor states.

Thus, ET mechanisms (DET as well as FRET) have not been considered for the ET to exciplex states because of the lack of apparent CT absorption in standard steady-state absorption measurements in exciplex-forming systems.[2] It indicates that zero transition dipole moment for the transition from ground state to the exciplex state, resulting in zero dipole-dipole coupling for FRET and zero density of the isoenergetic energy-accepting states with energy donor states for DET. However, there are experimental results on the existence of sub-bandgap CT absorption in exciplex-forming systems with very low intensities employing elaborate measurements.[4,34,71] It should be noted that the DET rate constant does not depend on the magnitude of the transition dipole moment of the energy acceptor or dipole-dipole coupling, so that the considerable DET rate constant is possible even with so low extinction coefficient for the CT absorption unlike FRET.[72]

Chapter 2. Simple methods to measure intermolecular charge-transfer absorption of organic films

2.1. Introduction

Intermolecular charge transfer (CT) complexes of organic molecules have been of great interest in optoelectronic devices for efficient charge separation in organic photovoltaics (OPVs) and triplet harvesting in organic light-emitting diodes (OLEDs). Intermolecular CT complexes act as precursors for free polarons in OPVs.[3,73–76] Exciplexes, excited CT complexes, are exploited actively in OLEDs as triplet harvesters due to the small energy difference between singlet- and triplet-excited states.[7–9,77,78] Exciplexes have also been widely used as a host for efficient OLEDs.[79–81]

There are two species of intermolecular CT complexes of organic molecules. One is an electron donor–acceptor (EDA) complex, and the other is an excited charge-transfer complex (exciplex).[2,82–85] The difference between them lies in their optical absorptions. EDA complexes exhibit a new, broad and featureless absorption band that differs from those of individual organic molecules in a mixture.[2,84–87] In contrast, absorption in exciplex-forming molecules has not been detected in the sub-bandgap region by normal reflection–transmission measurements; thus, until recently, it was believed that no ground state interaction existed in mixed films, preventing direct optical excitation from the ground state to the CT state.[2,17,56,88] Exciplex emission also exhibits redshifted, broad and featureless bands, different from the emission bands of individual molecules.

Contrary to the popular belief that exciplexes are not optically generated directly, in recent reports direct exciplex CT absorption from the ground state of the polymers and fullerene derivatives blended films was detected in the sub-bandgap region by Fourier transform photocurrent spectroscopy (FTPS) and photothermal deflection spectroscopy (PDS) measurements.[4,20,34,35,59] However, to date, reflection–transmission measurements have not been applied to exciplex CT absorption detection due to the apparent insensitivity of the method; moreover, absorptions due to small-molecular exciplexes in films have yet to be reported.

In this study, we used normal reflection–transmission measurements to measure the very small extinction coefficient for direct CT absorption from the ground state in an exciplex-forming mixed film fabricated by vacuum deposition; our method does not require the use of FTPS or PDS. The absorbances of thick exciplex-forming mixed films were measured in the sub-bandgap region using the transfer-matrix method combined with ellipsometry measurements to obtain the extinction coefficient for the intermolecular CT state; values as low as 10^{-4} were obtained, which is comparable to those of a sensitive PDS method executed on thin films. Furthermore, we developed another method for extraction of the very small extinction coefficients from absorbance only exploiting the thin-film interference and Fresnel equations.

2.2. Experimental

2,4,6-tris[3-(diphenylphosphinyl)phenyl]-1,3,5-triazine (PO-T2T) and 4,4′,4″-tris (3-methyl-phenylphenylamino) triphenylamine (m-MTDATA) were purchased from Nichem Fine Technology, and 1,1-bis[(di-4-tolylamino)phenyl]cyclohexane (TAPC) was purchased from Shine Materials Technology. m-MTDATA:PO-T2T mixed films and neat films of m-MTDATA and PO-T2T were fabricated via thermal deposition at a rate of 1 Å s^{-1} for on precleaned fused silica substrates (thickness: 1 mm) at a base pressure of < 5 × 10^{-7} Torr. TAPC:PO-T2T mixed films and neat films of TAPC and PO-T2T were deposited at a rate of 2 Å s^{-1} for the same condition with the m-MTDATA:PO-T2T system. A variable angle spectroscopic ellipsometer (VASE) (M-2000; J. A. Woolam) was used to obtain the refractive index and extinction coefficient values. PL spectra and absorbances were measured using a spectrofluorometer (Photon Technology International, Inc.) with an incorporated monochromator (Acton Research Co.) and a Cary 5000 UV−Vis−NIR spectrophotometer, respectively. Film thickness was measured by a surface profilometer (Alpha Step IQ; KLA Tenco) and the variable angle spectroscopic ellipsometer.

2.3. Extinction coefficients from the combination of the ultra-violet-visible spectrophotometer and ellipsometry measurements

Small molecules of PO-T2T and m-MTDATA were used in this study.[89] PO-T2T has an electron-withdrawing triazine unit, and m-MTDATA has electron-donating triphenylamine units, as shown in Figure 2.1(a). Exciplex formation in the 1:1 (molar ratio) mixed film was confirmed by the appearance of a new, featureless and redshifted photoluminescence (PL) band with a peak at 650 nm, which differed from PL emission of neat films when m-MTDATA was excited at 350 nm Figure 2.1(b). The PL peak at 425 nm corresponding to m-MTDATA emission was also observed in the mixed film, indicating that m-MTDATA exciton formation was incomplete. Note that the 580-nm and 700-nm peaks of the PO-T2T neat and mixed films, respectively, originate from the second-harmonic frequency of the excitation sources. Figure 2.1(c) shows the absorbances of 50-nm-thick neat film and mixed films on fused silica. The baseline of the absorbance measurement was set to air. No new absorption peak in the sub-bandgap region was observed in the mixed film, and the absorbance of the mixed film well matched the weighted average of the neat films; these results corroborate exciplex formation between m-MTDATA and PO-T2T in the mixed film. Figure 2.1(d) displays the measured refractive indices and extinction coefficients of the 50-nm-thick neat and mixed films using ellipsometry. The calculated absorbances using the transfer-matrix method employing the refractive indices and extinction coefficients were in good agreement with the experimental absorbances of the thin films shown in Figure 2.1(c). No new band was detected in the

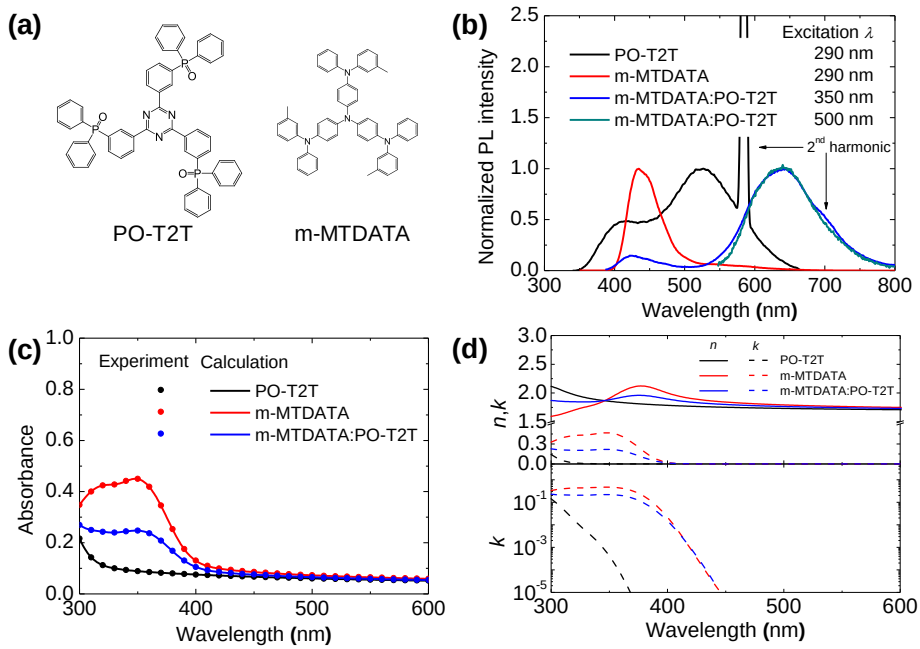

Figure 2.1. (a) Molecular structures of PO-T2T and m-MTDATA. (b) PL spectra of PO-T2T and m-MTDATA neat films (excitation wavelength: 290 nm) and the m-MTDATA:PO-T2T mixed film with a molar ratio of 1:1 (excitation wavelength: 350 and 500 nm), in which the second-harmonic peaks of the excitation are also observed. (c) Experimental and calculated absorbances of PO-T2T and m-MTDATA neat films and the m-MTDATA:PO-T2T mixed film with a molar ratio of 1:1 and thickness of 50 nm on fused silica substrates. (d) Refractive indices and extinction coefficients of PO-T2T and m-MTDATA neat films and the m-MTDATA:PO-T2T mixed film with a molar ratio of 1:1 from ellipsometry measurements of 50-nm-thick films on a linear scale (up) and logarithm scale (down) for the extinction coefficients.

mixed film.

We used the simple transfer-matrix method in the calculation of the absorbance of the film deposited on fused silica substrates. The absorbance is as follows:

$$\text{Absorbance} = -\log T \,, \quad \cdots\cdots (2.1)$$

where T is the transmissivity of the sample. T is given below for light at normal incidence with respect to the fused silica surface:

$$T = (1 - R_{\text{air,fs}}) T_{\text{film}} \sum_{n=0}^{\infty} \left(R_{\text{air,fs}} R_{\text{film}} \right)^n \quad \cdots\cdots (2.2)$$

where $R_{\text{air,fs}}$ is the reflectivity between air and fused silica calculated based on the Fresnel equation [Equation (2.3)]. T_{film} and R_{film} are the transmissivity and reflectivity, respectively, arising from the film between fused silica and air, as calculated using the transfer-matrix method (Equation (2.4)–(2.6) below):[90,91]

$$R_{\text{air,fs}} = \left| \frac{n_{\text{fs}} - 1}{n_{\text{fs}} + 1} \right|^2 , \quad \cdots\cdots (2.3)$$

$$T_{\text{film}} = \frac{1}{n_{\text{fs}}} \left| \frac{2 n_{\text{fs}}}{(A + B) n_{\text{fs}} + (C + D)} \right|^2 , \quad \cdots\cdots (2.4)$$

$$R_{\text{film}} = \left| \frac{(A + B) n_{\text{fs}} - (C + D)}{(A + B) n_{\text{fs}} + (C + D)} \right|^2 , \quad \cdots\cdots (2.5)$$

where n_{fs} is the refractive index of the fused silica, which can be obtained by measuring the transmissivity of the fused silica substrates in the transparent wavelength region, and A, B, C, and D are the elements of the transfer matrix M, represented by

$$M = \begin{bmatrix} A & B \\ C & D \end{bmatrix} = \begin{bmatrix} \cos(2\pi(n + ik)d / \lambda) & -i \sin(2\pi(n + ik)d / \lambda) / (n + ik) \\ -i \sin(2\pi(n + ik)d / \lambda)(n + ik) & \cos(2\pi(n + ik)d / \lambda) \end{bmatrix} \quad \cdots\cdots (2.6)$$

where n, k, and d are the refractive index, extinction coefficient, and thickness of

the film, respectively, and λ is the free-space wavelength of incident light.

Interestingly, PL emission from the mixed film at an excitation wavelength of 500 nm (xenon lamp) was observed, as shown in Figure 2.1(b); this absorption was not detected by the two measurements in the mixed film. The emission spectrum is in good agreement with the exciplex band in the PL spectrum of the mixed film at an excitation wavelength of 350 nm. Thus, sub-bandgap absorption was present; this absorption corresponds to intermolecular CT state absorption between m-MTDATA and PO-T2T emitting exciplex luminescence.

To measure the very small absorption corresponding to the intermolecular CT state, we fabricated mixed films of greater thicknesses: 465, 938, 1,404, and 1,846 nm. To investigate the sub-bandgap absorption of neat films, we also fabricated PO-T2T neat films with thicknesses of 450, 900, 1341, and 1,743 nm and m-MTDATA neat films with thicknesses of 508, 968, 1,395, and 1,800 nm. Figure 2.2(a), 2.2(b), and 2.2(c) (red line) show the experimental and calculated absorbances, along with the refractive index and extinction coefficient of the 50-nm film for the PO-T2T neat films, m-MTDATA neat films, and m-MTDATA:PO-T2T mixed films, respectively; experimental absorbances exceeding 4 are not reliable due to equipment limitations. One should note that the oscillation of the absorbance in the sub-bandgap region originates from the interference effect in the sample with the fused silica/film/air structure. The calculated absorbances well fit the experimental absorbances for the neat films, as presented in Figure 2.2(a) and 2.2(b), revealing that the sub-bandgap absorption is negligible in the neat films. In contrast to the neat films, the mixed films showed large differences between the calculated and experimental absorbances, especially in the sub-bandgap wavelength range (410–550 nm);

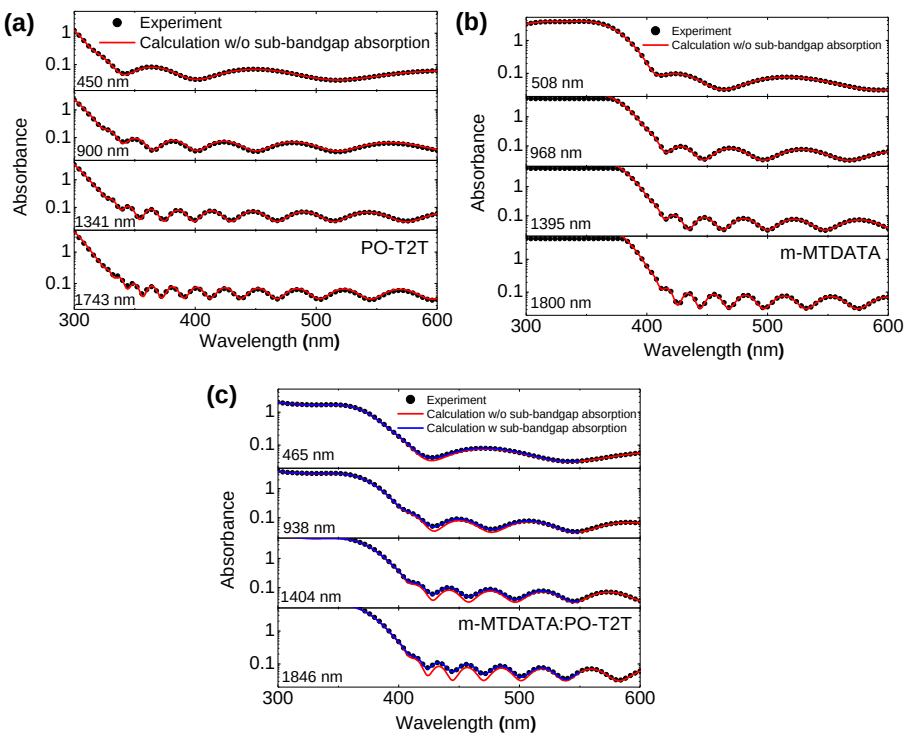

Figure 2.2. Experimental absorbances and calculated absorbances of (a) m-MTDATA and (b) PO-T2T neat films with various thicknesses on fused silica substrates employing the refractive indices and extinction coefficients from ellipsometry measurements for the 50-nm-thick films, and (c) experimental absorbances and calculated absorbances without and with sub-bandgap absorption for the m-MTDATA:PO-T2T mixed films (molar ratio 1:1) of various thicknesses. (The limit of absorbance of the equipment is 4.)

the difference increased with the film thickness, implying CT absorption in the mixed film.

The extinction coefficient of the mixed film was extracted from the fitting of the absorbance using the transfer-matrix method; the refractive index was measured by ellipsometry, as shown in Figure 2.1(d). With known values of $T(\lambda)$, $n(\lambda)$, and d, $k(\lambda)$ can be obtained using Equation (2.1)–(2.6), assuming that the influence of sub-bandgap absorption on the refractive index of the film is negligible. Figure 2.3(a) shows the calculated extinction coefficient of the mixed film. There was no significant difference between the calculated extinction coefficients and the extinction coefficients obtained from the ellipsometry measurements for the 50-nm film for the given wavelength range under the onset wavelength of the mixed film. In contrast, there was a significant difference between calculated and experimental extinction coefficients in the sub-bandgap wavelength region. The extinction coefficients extracted from different film thicknesses were consistent, up to 10^{-4}, for sub-bandgap wavelengths; this is comparable to the sensitivity of PDS technique executed on thin films. Gaussian fitting was carried out by the Levenberg–Marquardt algorithm. An iterative procedure was employed to minimize the reduced chi-square value in order for obtaining optimal fitting parameters. The Gaussian fitting in the sub-bandgap wavelength region reflected inhomogeneous broadening of the CT transition in films. Calculated absorbances using this extinction coefficient and the refractive index from ellipsometry measurements of the 50-nm film well fit the experimental absorbances with various thicknesses, as shown in Figure 2.2(c).

The PL spectrum of m-MTDATA:PO-T2T mixed film at an excitation wavelength of 500 nm, and extinction coefficients of the m-MTDATA and PO-T2T

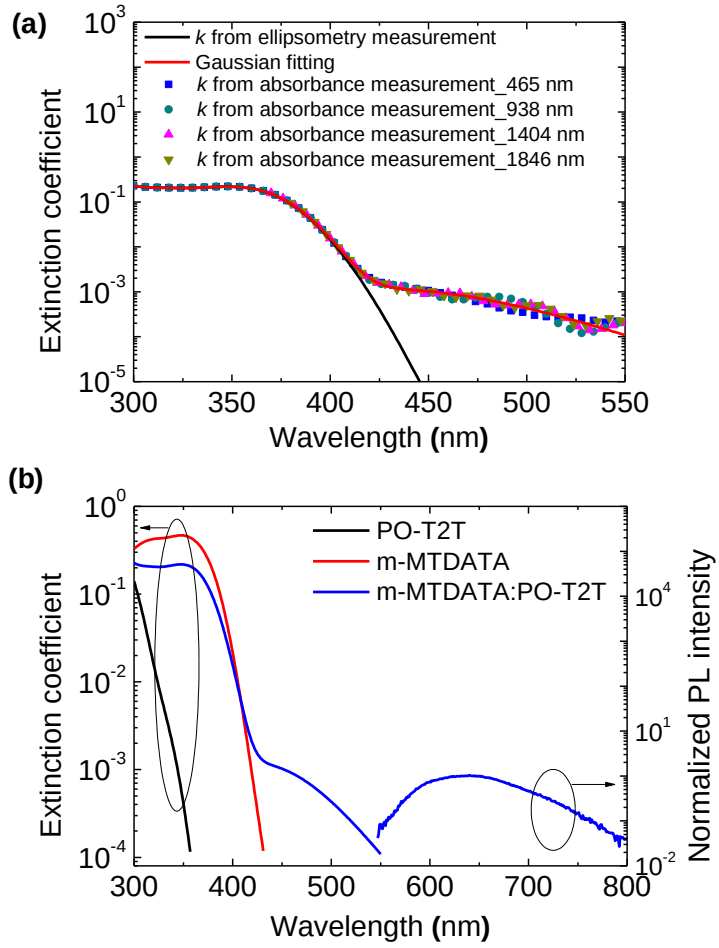

Figure. 2.3. (a) Extinction coefficients of the m-MTDATA:PO-T2T mixed film with a molar ratio of 1:1 from ellipsometry measurements of the 50-nm-thick film and the experimental absorbances for the mixed films of thicknesses of 465, 938, 1,404, and 1,846 nm, and the extinction coefficient of the mixed film with Gaussian fitting for the sub-bandgap energy region. (b) Extinction coefficients of the m-MTDATA and PO-T2T neat films and the m-MTDATA:PO-T2T mixed film with a molar ratio of 1:1, and PL spectra of the mixed film at an excitation wavelength of 500 nm.

neat films and the m-MTDATAT:PO-T2T mixed film, are shown in Figure 2.3(b). Not only the exciplex PL at an excitation wavelength of 500 nm, but also the similar onset of the sub-bandgap absorption and the PL band of m-MTDATA:PO-T2T exciplexes, imply that sub-bandgap absorption of the m-MTDATA:PO-T2T mixed film originates from the intermolecular CT state between m-MTDATA and PO-T2T, emitting exciplex luminescence. The presence of the sub-bandgap absorption corresponding to intermolecular CT state absorption between m-MTDATA and PO-T2T emitting exciplex luminescence implies that the term 'exciplex' would be inappropriate considering that the term originated from the absence of a new sub-bandgap absorption band. The intensity of the peak extinction coefficient for the singlet m-MTDATA:PO-T2T intermolecular CT state at 430 nm would be around 10^{-3}, which is about 400 times smaller than that at a wavelength of 348 nm for the m-MTDATA S_1 state. One should note that the method described in this paper can only be applied to homogeneous and uniform films because all the equations were derived for a one dimensional uniform film without considering the scattering in bulk and at the surface.

2.4. Extinction coefficients from the ultraviolet-visible spectrophotometer measurements

Another exciplex was investigated for its absorption band. PO-T2T form the exciplex with TAPC whose molecular structure is shown in Figure 2.4(a), and it exhibits orange emission. Figure 2.4(b) shows the steady-state PL spectra of the TAPC:PO-T2T blended film with a molar ratio of 1:1 along with those of the PO-T2T and TAPC neat films. The redshifted emission band of the blended film indicates that TAPC and PO-T2T form exciplexes in the blended film.

For the purpose of extracting extinction coefficients for intermolecular CT absorption, we measured the absorbance of an TAPC neat film and an TAPC:PO-T2T mixed film (thickness: 1.0, 1.5, and 2.0 μm) deposited on fused silica substrates; the film thicknesses were measured by a surface profilometer. The absorbances of TAPC and TAPC:PO-T2T films are shown in Figure 2.4(c) and 2.4(d), respectively. Absorbance was measured with respect to the normal incidence of light on the fused silica substrate, and the baseline for the absorbance measurement was set to that of air. Films with thicknesses of around 1 μm induced thin-film interference, resulting in oscillation of the absorbance. The absorbance of the film on the fused silica substrate is equal to $-\log(1-R-A)$, where R and A correspond to the reflectivity and absorptivity of the film on the fused silica substrate, respectively.[90–92]

Optical bandgaps of PO-T2T and TAPC in neat films are 4.0 eV[92,93] and 3.5 eV, respectively, from onsets of their absorption spectra. The absorbance of the

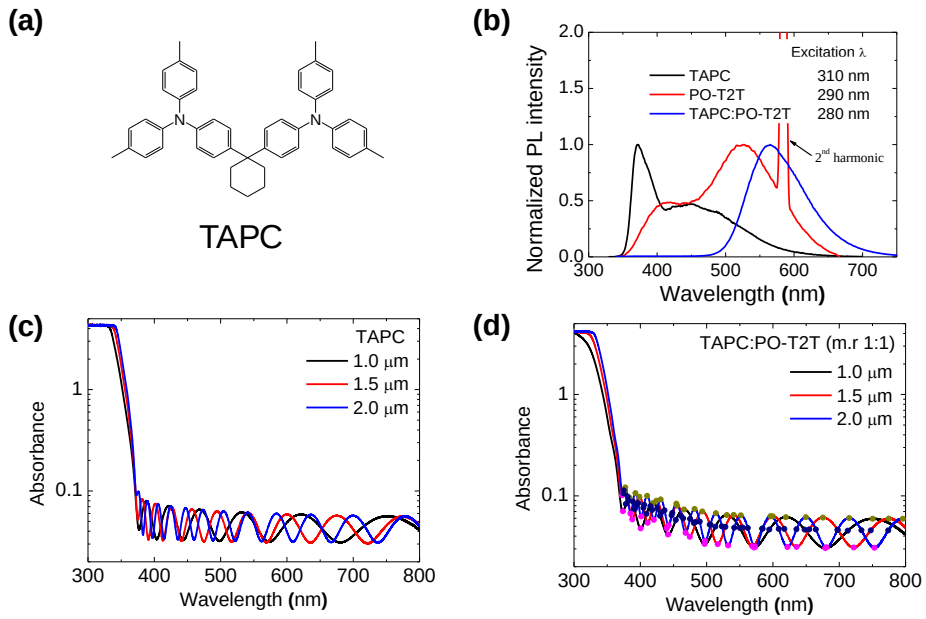

Figure 2.4. (a) Molecular structure of TAPC. (b) Steady-state PL spectra of the TAPC and PO-T2T neat films and the TAPC:PO-T2T blended film (m.r. 1:1). (c) Absorbances of the TAPC neat films with thicknesses of 1.0, 1.5, and 2.0 μm. (d) Absorbances of the TAPC:PO-T2T blended film (m.r. 1:1) with thicknesses of 1.0, 1.5, and 2.0 μm, where the absorbance points are denoted by dark yellow, navy, and magenta points, at which destructive, constructive, and middle interference, respectively, takes place for the transmitted waves. The maximum absorbance limit of the equipment is around 4.

TAPC:PO-T2T film was higher than that of the TAPC film in the sub-bandgap wavelength region. This indicates that a new absorption band is generated with a very small extinction coefficient when TAPC and PO-T2T are in close proximity.

When the difference in extinction coefficients at the interface of the films is negligible compared to the difference in the refractive indices at the interface, T_{film} and R_{film} can be expressed as follows, considering thin-film interference:

$$T_{\text{film}} = \frac{{a_{\text{T}}}^2}{n_{\text{fs}}\left(1-2b\cos\phi+b^2\right)}, \quad \cdots\cdots (2.7)$$

$$R_{\text{film}} = \left(r_1\cos\phi+\frac{a_{\text{R}}\left(1-b\cos\phi\right)}{1-2b\cos\phi+b^2}\right)^2+\left(-r_1\sin\phi+\frac{a_{\text{R}}b\sin\phi}{1-2b\cos\phi+b^2}\right)^2. \quad \cdots\cdots (2.8)$$

a_{T}, a_{R}, b, and ϕ are given by

$$a_{\text{T}} = t_1t_2\exp\left(-2\pi kd/\lambda\right), \quad \cdots\cdots (2.9)$$

$$a_{\text{R}} = \left(1-r_1^2\right)r_2\exp\left(-4\pi kd/\lambda\right), \quad \cdots\cdots (2.10)$$

$$b = -r_1r_2\exp\left(-4\pi kd/\lambda\right), \quad \cdots\cdots (2.11)$$

$$\phi = \frac{4\pi nd}{\lambda}, \quad \cdots\cdots (2.12)$$

where $r_1 = \left(n_{\text{fs}}-n\right)/\left(n_{\text{fs}}+n\right)$, $r_2 = \left(n-1\right)/\left(n+1\right)$, $t_1 = 2n_{\text{fs}}/\left(n_{\text{fs}}+n\right)$, and $t_2 = 2n/\left(n+1\right)$.

Thin-film interference can be used to obtain the exact thickness, refractive index, and small extinction coefficient of films in the sub-bandgap wavelength region. First, the refractive index of the film can be obtained based on the absorbance at the absorbance points where the destructive interference of transmitted waves takes place and the extinction coefficients are zero. Second, the exact film thickness can be calculated from the wavelength at the absorbance points where destructive

interference occurs. The refractive index can also be obtained from the exact film thickness. Finally, the film's extinction coefficient can be determined based on the exact thickness and refractive index of the film.

The exact thickness and refractive index of the film are required for calculating the extinction coefficient from the absorbance when the difference between the reflectivity and absorptivity of the film is small. When the film thickness is around 1 μm, the absorptivity becomes comparable to the reflectivity in the sub-bandgap wavelength region, as shown in Fig. 2.4(d).

T_{film} can be written as follows, at the absorbance points where the destructive interference of the transmitted waves occurs ($\phi = \pi, 3\pi, 5\pi, 7\pi, \cdots$) and the extinction coefficients are zero ($k = 0$) based on Equation (2.7):

$$T_{\text{film}} = \frac{4n^2 n_{\text{fs}}}{\left(n^2 + n_{\text{fs}}\right)^2} \quad \cdots\cdots (2.13)$$

Combining Equation (2.13) with Equation (2.2) and (2.3) results in the following equation considering that R_{film} is equal to $(1 - T_{\text{film}})$ when the extinction coefficients of the films are zero:

$$n = \left\{ \frac{-\left(n_{\text{fs}}{}^2 - 4n_{\text{fs}}T^{-1} + 1\right) + \left[\left(n_{\text{fs}}{}^2 - 4n_{\text{fs}}T^{-1} + 1\right)^2 - 4n_{\text{fs}}{}^2\right]^{0.5}}{2} \right\}^{0.5} . \quad \cdots\cdots (2.14)$$

The absorbance points corresponding to destructive interference of the transmitted waves are denoted by dark yellow points in Figure 2.4(d) for the TAPC:PO-T2T film, corresponding to the local maxima of the oscillating absorbance. The results of Equation (2.14) are shown in Figure 2.5(a) as filled points.

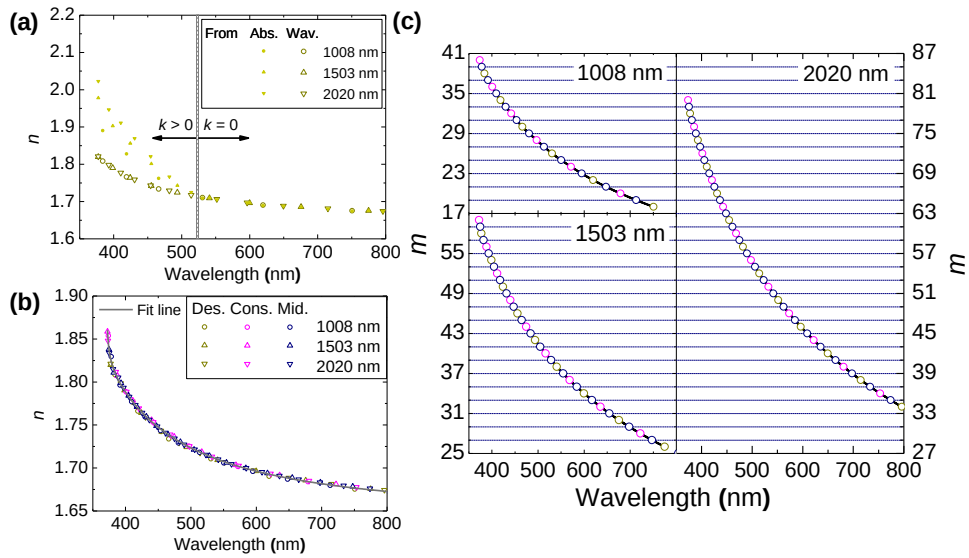

Figure 2.5. (a) Refractive indices of the TAPC:PO-T2T films with various thicknesses calculated from the absorbances (closed) at which destructive interference of the transmitted waves occurs, and refractive indices calculated from the wavelengths (open) of destructive interference based on the exact film thicknesses. (b) Refractive indices of the TAPC:PO-T2T films with various thicknesses calculated from wavelengths where destructive (dark yellow), constructive (magenta), and middle (navy) interference of the transmitted waves occurs, and their fit line. (c) *m* of the TAPC:PO-T2T mixed films with various thicknesses calculated from wavelengths where destructive (dark yellow), constructive (magenta), and middle (navy) interferences of the transmitted waves occurs, and an interpolation line for *m* of the destructive and constructive interference.

Employing this refractive index, the exact film thickness is given by

$$m = \frac{8nd}{\lambda}, \quad (2.15)$$

where m is the number of wavelengths required to pass through a film with a thickness of $8d$; m = 2, 6, 10, 14… for wavelengths with destructive interference. The restriction for m provides a key to solve one equation with two unknowns (m and d), where the approximate thickness of the film derived from surface profilometer measurements provides the restriction for d. The exact film thicknesses of TAPC:PO-T2T films with approximate thicknesses of ~1.0, ~1.5, and ~2.0 μm, as measured by a surface profilometer, were determined to be 1,008, 1,503, and 2,020 nm, respectively.

The refractive index at wavelengths of the destructive interference can be obtained using Equation (2.15), based on the exact film thickness in the sub-bandgap wavelength region. n is a continuous function of λ, indicating that m is also a continuous function of λ given a constant film thickness; the refractive index is plotted as dark yellow open points in Figure 2.5(a) and 2.5(b).

We determined the wavelengths at which constructive interference of the transmitted waves occurs as the local minima for the oscillating absorbance, denoted by magenta points in Figure 2.4(d). The refractive indices of the films were obtained using Equation (2.15), where m = 4, 8, 12, 16… for the wavelengths of constructive interference, shown as magenta points in Figure 2.5(b).

m was then determined as a function of λ using Equation (2.15), as shown in Figure 2.5(c). The interpolation of m allows the wavelengths of the "middle interference" (m = 1, 3, 5, 7…) of the transmitted waves takes place to be determined. Middle interference takes place when the phase difference between the transmitted

waves is an odd multiple of π/2. The wavelengths where middle interference of transmitted waves occur are denoted by navy points in Figure 2.5(c) and 2.4(d). The refractive indices at the wavelengths of middle interference, derived from Equation (2.15), are plotted as navy points in Figure 2.5(b).

Given the exact thicknesses and refractive indices of the films at the wavelengths of destructive, constructive, and middle interference, the extinction coefficient can be calculated from the absorbance. The substitution of Equation (2.3), (2.7)–(2.12) into Equation (2.2) provides an analytical solution for the extinction coefficient, with Equation (2.16), (2.17), and (2.18) used for destructive, constructive, and middle interference, respectively, considering that ϕ in Equation (2.12) is equal to $m\pi/2$, according to Equation (2.15).

$$k = -\frac{\lambda}{4\pi d}\ln\left\{\frac{-H + 8n_{fs}n^2 - \left[\left(H - 8n_{fs}n^2\right)^2 - T^2\left(n^2-1\right)^3\left(n^2 - {n_{fs}}^4\right)\right]^{0.5}}{T\left(n-1\right)^3\left(n - {n_{fs}}^2\right)}\right\} \quad \cdots\cdots\cdots (2.16)$$

$$k = -\frac{\lambda}{4\pi d}\ln\left\{\frac{H + 8n_{fs}n^2 - \left[\left(-H - 8n_{fs}n^2\right)^2 - T^2\left(n^2-1\right)^3\left(n^2 - {n_{fs}}^4\right)\right]^{0.5}}{T\left(n-1\right)^3\left(n - {n_{fs}}^2\right)}\right\} \quad \cdots\cdots\cdots (2.17)$$

$$k = -\frac{\lambda}{4\pi d}\ln\left\{\frac{8n_{fs}n^2 - \left[\left(-8n_{fs}n^2\right)^2 - T^2\left(n^2-1\right)^3\left(n^2 - {n_{fs}}^4\right)\right]^{0.5}}{T\left(n-1\right)^3\left(n - {n_{fs}}^2\right)}\right\} \quad \cdots\cdots\cdots (2.18)$$

where H is equal to $T\left(n^2 - {n_{fs}}^2\right)\left(n^2-1\right)$.

The calculated extinction coefficients are shown in Figure 2.6(a). The similar onsets of the exciplex PL band and sub-bandgap absorption band indicate that the sub-bandgap absorption band arises from optical absorption to the exciplex state. The fitting for the extracted refractive indices and extinction coefficients was carried

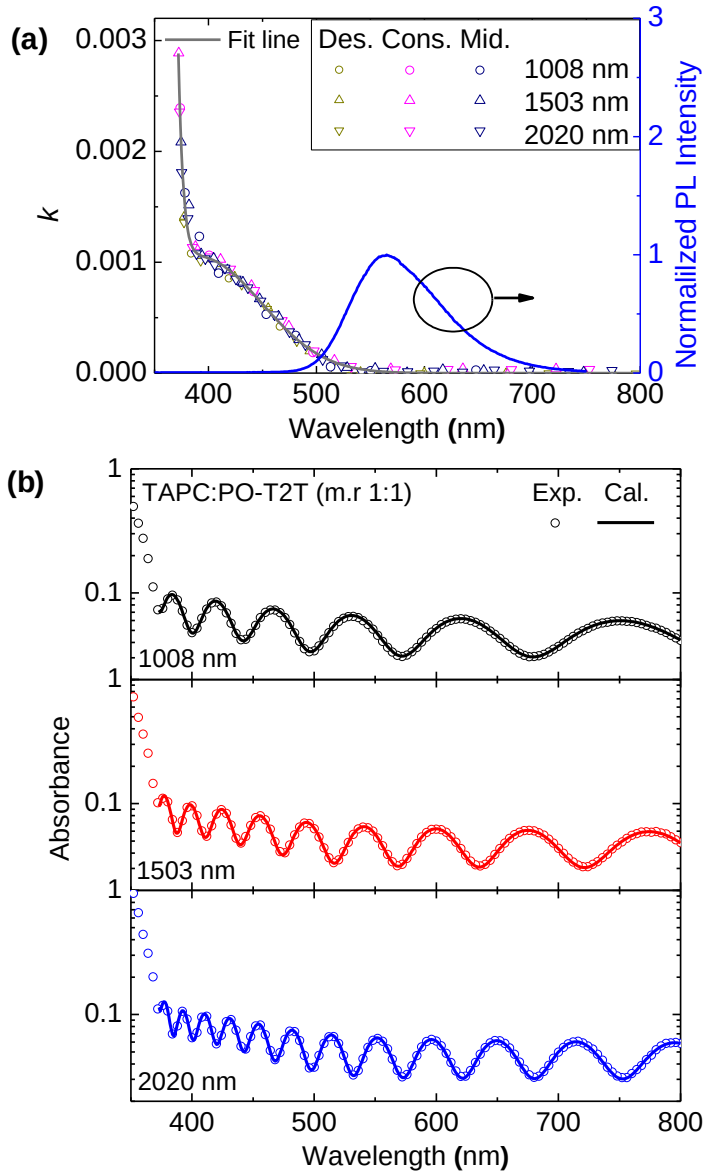

Figure 2.6. (a) Extinction coefficients of the TAPC:PO-T2T films with various thicknesses for destructive (dark yellow), constructive (magenta), and middle (navy) interference, and their fit line. (b) Experimental absorbances of the TAPC:PO-T2T films with various thicknesses on the fused silica substrates and calculated absorbances in the sub-bandgap wavelength region.

out using the Sellmeier equation and multiple Gaussian functions, respectively; the fit lines are shown in Figure 2.5(b) and 2.6(a) as solid lines. The refractive indices and extinction coefficients of the films derived from the fit lines and the exact film thicknesses were used to calculate absorbance using the transfer-matrix method (Equation (2.1)-(2.6)).[92] The calculated absorbances well matched the experimental data, as shown in Figure 2.6(b), demonstrating the utility of the method for extracting very small extinction coefficients from the absorbance.

2.5. Conclusion

In this work, we demonstrated that simple reflection–transmission measurements can be employed in the analysis of very small sub-bandgap CT absorption of an exciplex-forming mixed film, with an accuracy approaching 10^{-4} for the extinction coefficient if thick films with thicknesses of 1-2 micrometers are used. The sensitivity is comparable to that of PDS executed on thin films. Considering the difficulties associated with measuring the very small intermolecular CT absorption for exciplex-forming films, the methods introduced in this study is expected to lead to further advances in this area.

Chapter 3. Diffusion mechanism of exciplexes in organic semiconductors

3.1. Introduction

Excited-state charge transfer complexes (exciplexes) are formed by partial charge transfer in the excited state between electron donor molecules and nearby electron acceptor molecules after the photo-excitation of the molecules.[1,2] Exciplexes are widely observed in nature, such as photosynthetic systems, and also organic optoelectronic devices such as organic photovoltaics (OPVs) or organic light-emitting diodes (OLEDs), where heterojunctions between electron donor and acceptor molecules are employed. Exciplexes have long been considered as an obstacle because they have low emission efficiency in OLEDs and reduce the dissociation probability of charge transfer (CT) states in OPVs. Recently, however, exciplexes have been actively used as thermally assisted delayed fluorescence (TADF) emitters in OLEDs to take advantage of their higher luminescent exciton ratio, due to their small energy difference between the singlet and triplet excited states.[6–8,11] Exciplexes have also been used as host materials in highly efficient OLEDs, exploiting low driving voltage, good charge balance, and low efficiency roll-off.[94–96]

Exciplexes are known for a new emission band red-shifted from molecular emission bands, but the absence of the absorption band for the exciplex state when electron donors and acceptors are close together.[1,2] The formation, electronic structure, and excited state dynamics of exciplexes in films have been actively researched in recent years;[1,3,32,7,8,26–31] however, the diffusion of exciplexes has not been studied

until very recently, primarily because of the lack of apparent CT absorption in exciplex-forming systems measured by standard steady-state absorption experiments, which is a necessary condition for diffusion to take place via energy transfer (ET) mechanisms. The lack of apparent CT absorption in standard steady-state absorption experiments in exciplex-forming systems is the reason for the term 'exciplex'.[2]

There are a couple of papers describing the diffusion of exciplex or polaron pairs. C. Deibel et al. suggested that the diffusion of polaron pairs might account for the efficiency loss in OPVs by applying Monte Carlo simulations.[97] M. A. Baldo and coworkers have reported that CT exciplex states can be transported via an 'inchworm' mechanism.[36] The spatial distribution of the photoluminescence (PL) intensity of exciplexes over the decay time of CT exciplex states was measured, and the diffusion of exciplexes was confirmed. This phenomenon was explained through geminated charge recombination at different sites, from which CT exciplex states are initially formed. The movement distance of CT exciplex states was in the range 5–10 nm for ~20 μs. It was discussed that Förster-type resonance energy transfer (FRET) for diffusion of CT exciplex states would not be effective because of the negligibly low optical absorption of CT exciplex states, and that Dexter-type exchange energy transfer (DET) would also not be effective because CT exciplex states are weakly bound.

Here, we report that there is not one single mechanism for exciplex diffusion, and that DET is the dominant mechanism based on the analysis of the time-resolved PL measurements of high-energy exciplexes and low-energy exciplexes. Even though the CT absorption is orders of magnitude weaker than the normal resonance absorption,[4,20,25,34,35,71] recent reports and our own observation for the sub-bandgap CT absorption in organic electron donor-acceptor systems support that the

exciplex-exciplex ET takes place. The exciplex-exciplex ET means that ET from exciplex #1 to exciplex #2. In that case, exciplex #1 lose its excitation energy and exciplex #2 is generated from the ground state near exciplex #1. When D and A represent the electron donor and acceptor molecules, respectively, and δ is the degree of CT in the exciplex state, the exciplex-exciplex ET could be described by $\left[\left(D_1^{\delta_1+}A_1^{\delta_1-}\right)^* + \left(D_2A_2\right) \rightarrow (D_1A_1) + \left(D_2^{\delta_2+}A_2^{\delta_2-}\right)^*\right]$ where $\left(D_1^{\delta_1+}A_1^{\delta_1-}\right)^*$ and $\left(D_2^{\delta_2+}A_2^{\delta_2-}\right)^*$ represent the exciplex #1 to lose its excitation energy and exciplex #2 to gain its excitation energy, respectively.

3.2. Experimental

Four donor molecules of 4,4′-bis(3-methylcarbazol-9-yl)-2,2′-biphenyl (mCBP), di-[4-(*N*,*N*-ditolyl-amino)-phenyl]cyclohexane (TAPC), tris(4-carbazoyl-9-ylphenyl)amine (TCTA), and 4,4′,4″-tris (3-methyl-phenylphenylamino) triphenylamine (m-MTDATA) and one acceptor molecule of (1,3,5-triazine-2,4,6-triyl)tris(benzene-3,1-diyl))tris(diphenylphosphine oxide) (PO-T2T) were used for the exciplex-forming materials. They were purchased from Nichem Fine Technology and used as received without further purification. All organic films were deposited by thermal evaporation at a rate of 1 Å s^{-1} on precleaned quartz substrates under vacuum at a base pressure of $< 5 \times 10^{-7}$ Torr. Extinction coefficients were measured using variable angle spectroscopic ellipsometry (VASE, J. A. Woolam M-2000 spectroscopic ellipsometer). A spectrofluorometer (Photon Technology International, Inc.) with an incorporated monochromator (Acton Research Co.) was used for steady-state PL spectra measurements. A nitrogen gas laser with an excitation wavelength of 337 nm (3.68 eV) and a pulse width of 800 ps (KEN-2X, Usho) combined with a streak camera (C10627, Hamamatsu Photonics) was used for time-resolved PL experiments.

3.3. Energy transfer from high-energy exciplexes to low-energy exciplexes

We conducted two different experiments to investigate the ET from exciplexes to other kinds of exciplexes. The first experiment exploited a bilayer system with two different kinds of exciplexes. The second one was carried out for a co-doped system with two different kinds of exciplexes where two different kinds of electron donor molecules were co-doped (5 mol.% each) into an electron acceptor host.

Firstly, an exciplex-forming TAPC:PO-T2T mixed film (1:1 molar ratio, 2 nm thick) was stacked on another exciplex-forming mCBP:PO-T2T mixed film (1:1 molar ratio, 5 nm thick) (Film A in Figure 3.1(a)), and the emission characteristics of the bilayer film were compared with those of the non-stacked single-layer films. The structures for molecules in the films are shown in Figure 3.1(a). The energy levels of the mCBP, TAPC, and PO-T2T excitons, and the mCBP:PO-T2T and TAPC:PO-T2T exciplexes are shown in Figure 3.1(b). Formation of exciplexes in the mCBP:PO-T2T and TAPC:PO-T2T films was confirmed by the featureless red-shifted emission from the constituent materials as shown in Figure 3.2.[93,98] mCBP and TAPC were used as electron donors and PO-T2T was used as an electron acceptor for the exciplexes. The thickness of the films was adjusted for clear observation of the interface quenching effect (or ET) in the transient PL experiments. If the films are too thick, the interface quenching effect will be buried by strong bulk effect because the interface effect is limited at the interface no matter how thick the films are. If they are too thin, the signal must be too small to clearly detect. Figure 3.2 also

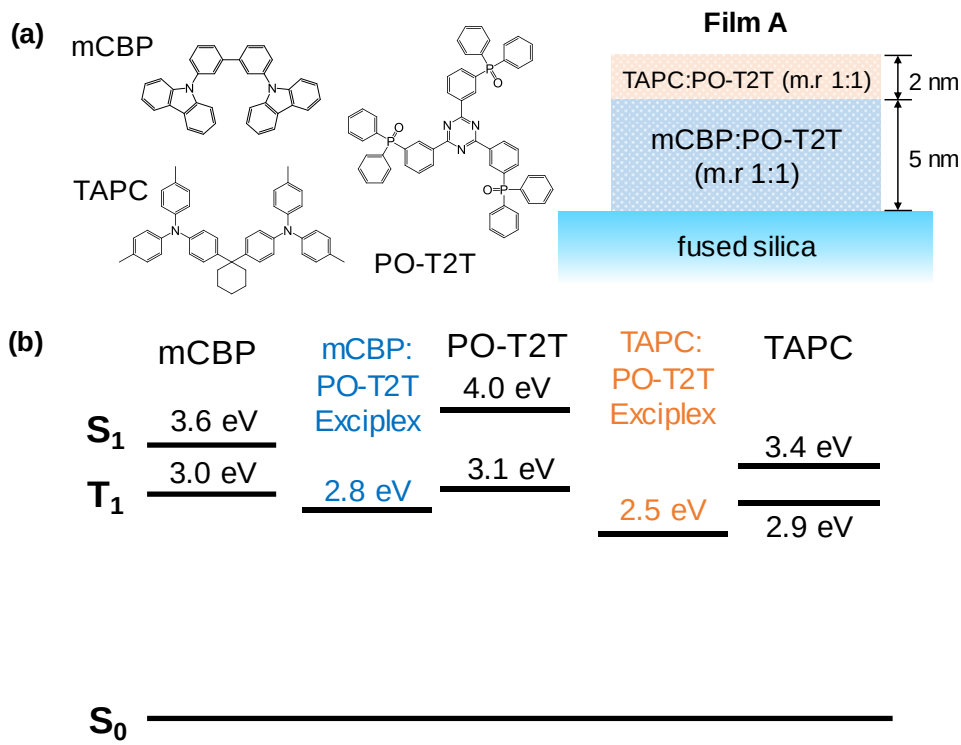

Figure 3.1. (a) Molecular structures of mCBP, TAPC, and PO-T2T and a bilayer structure of Film A. (b) Energy levels of mCBP, TAPC, and PO-T2T excitons and mCBP:PO-T2T and TAPC:PO-T2T exciplexes in the films, where S_1 and T_1 represent the lowest excited singlet and triplet excited states, respectively.

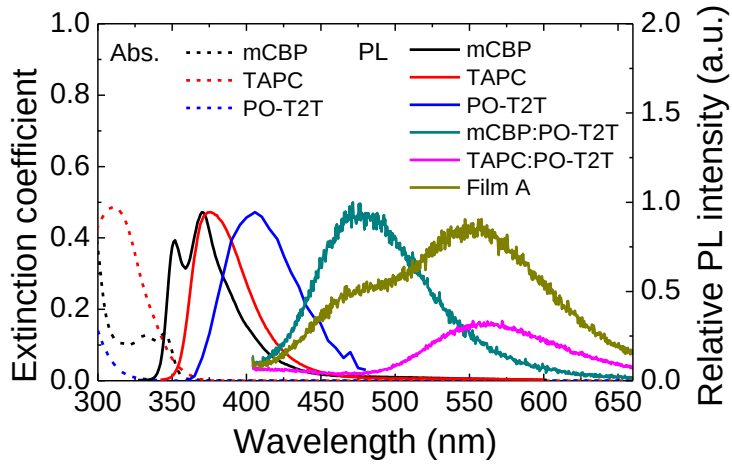

Figure 3.2. Extinction coefficients of mCBP, TAPC, and PO-T2T films, steady-state PL spectra of an mCBP film, a TAPC solution in methylene chloride at 10^{-4} M, and a PO-T2T solution,[93] and time-resolved PL spectra of an mCBP:PO-T2T film (5 nm thick), a TAPC:PO-T2T film (2 nm thick), and Film A integrated for 9 μs after excitation at 337 nm.

compares the time-resolved emission spectra integrated for 9 μs after excitation when the films were excited with a N_2 pulsed laser (337 nm wavelength with a pulse width of 0.8 ns). The emission from the bilayer film is composed of the exciplex emissions from the consisting layers. The longer wavelength emission from the TAPC:PO-T2T layer with the peak wavelength of 560 nm is significantly increased and the exciplex emission from the mCBP:PO-T2T layer with the peak wavelength of 475 nm was reduced significantly in Film A compared to the single layer emissions. The energy levels of the mCBP, TAPC, and PO-T2T singlet excitons were estimated from the onset of their absorption spectra. The energy levels of the mCBP, TAPC, and PO-T2T triplet excitons and mCBP:PO-T2T and TAPC:PO-T2T singlet exciplexes were estimated from the onset of their integrated emission spectra. The triplet energy levels of exciplexes are similar to the singlet levels due to small overlap between the highest occupied molecular orbital (HOMO) and the lowest unoccupied molecular orbital (LUMO) because they are mainly located in different materials, i.e., HOMO in the donor molecule and LUMO in the acceptor molecule, respectively.[7,53,99,100] The normalized transient PL intensities from the single layers are compared to those of the bilayer for the mCBP:PO-T2T exciplex emission (detection wavelength 455–475 nm) and the TAPC:PO-T2T exciplex emission (detection wavelength 620–660 nm) in Figure 3.3(a) and 3.3(b), respectively. The results show that the lifetime of the delayed emission of the mCBP:PO-T2T exciplex in the stacked layer is significantly reduced compared to that of the single layer. In contrast, the lifetime of delayed emission from the TAPC:PO-T2T exciplex in the stacked layer is significantly increased compared to that of the single layer. The transient results show that ET takes place from the mCBP:PO-T2T exciplex to the TAPC:PO-T2T exciplex.

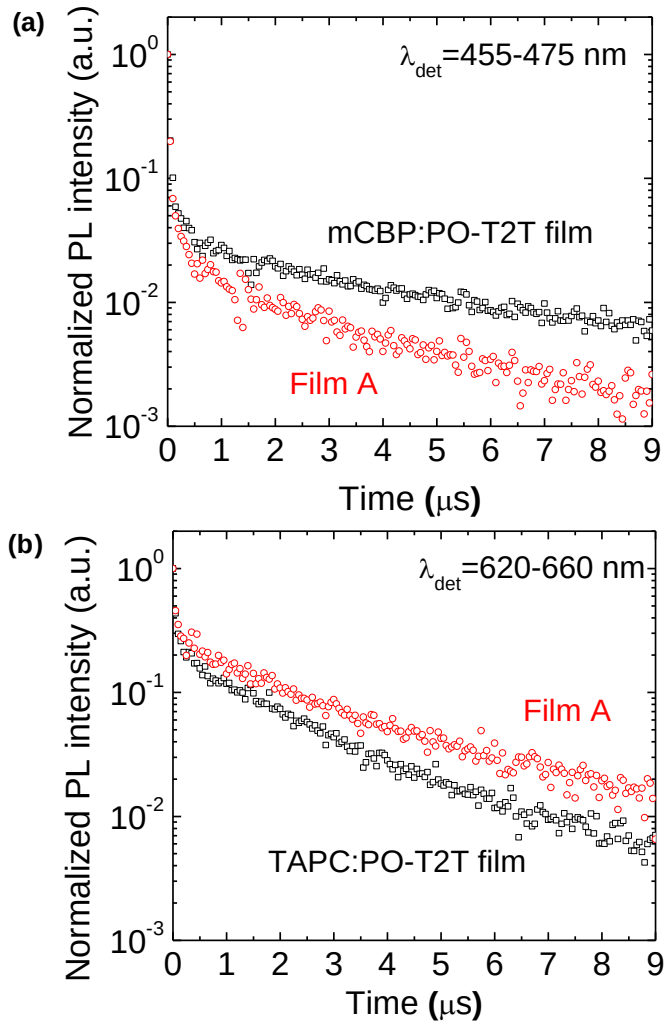

Figure 3.3. (a) Normalized transient PL intensities for the mCBP:PO-T2T film (m.r. 1:1) and Film A in the wavelength range of 455 to 475 nm. (b) Those for the TAPC:PO-T2T (m.r. 1:1) film and Film A in the wavelength range of 620 to 660 nm.

Similar behavior was observed in a different exciplex-forming system where two electron donor molecules [TCTA and m-MTDATA] were co-doped in an electron acceptor host [PO-T2T] at 5 mol.% each (Film B in Figure 3.4(a)). The molecular structures of TCTA and m-MTDATA are shown in Figure 3.4(a). The energy levels of the system are shown in Figure 3.4(b), and were estimated using the same methods as those in Figure 3.1(b). The featureless redshifted emission spectra of the mixed films of TCTA:PO-T2T and m-MTDATA:PO-T2T in Figure 3.5 confirm the formation of exciplexes between TCTA or m-MTDATA and PO-T2T. The extinction coefficients of TCTA, m-MTDATA, and PO-T2T neat films and m-MTDATA:PO-T2T (m.r. 1:1) mixed film [92] are shown in Figure 3.5 along with the time-resolved emission spectra of a TCTA:PO-T2T (m.r. 5:95) doped film, an m-MTDATA:PO-T2T (m.r. 5:95) doped film, and Film B integrated for 500 ns after excitation when the electron donors in the films were selectively excited by a N_2 pulsed laser at the wavelength of 337 nm. Again the emission from Film B is composed of the emissions from the TCTA:PO-T2T exciplexes and m-MTDATA:PO-T2T exciplexes, which are the high-energy exciplexes and low-energy exciplexes, respectively. The intensity of the TCTA:PO-T2T exciplex in Film B is significantly reduced to 23% compared to the singly doped TCTA:PO-T2T (m.r. 5:95) film and the m-MTDATA:PO-T2T exciplex emission increased to 1.8 times of the singly doped film. It indicates that the energy is transferred from the excited states involving TCTA molecules to those involving m-MTDATA molecules considering the energy levels of the singlet excitons of TCTA and m-MTDATA, and the singlet exciplexes of the TCTA:PO-T2T and m-MTDATA:PO-T2T. The transient PL profiles of the TCTA:PO-T2T exciplex emission from Film B to that from the singly doped TCTA:PO-T2T film measured in the wavelength range 510 to 530 nm, where the

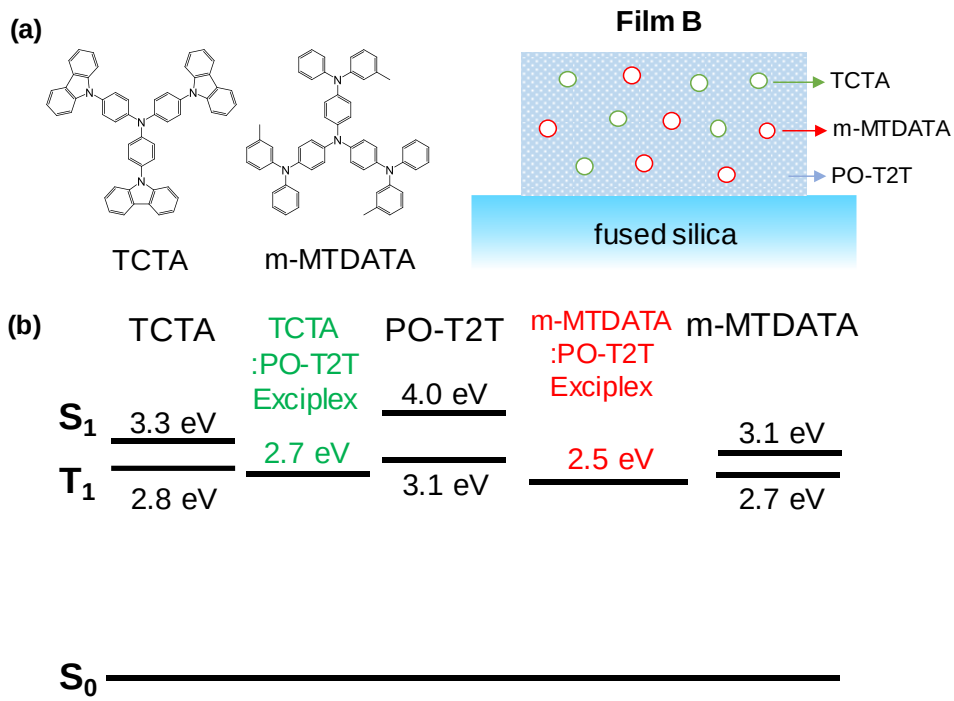

Figure 3.4. Molecular structures of TCTA and m-MTDATA and a PO-T2T film co-doped with TCTA and m-MTDATA (Film B). (b) Energy levels of S_1 and T_1 of TCTA, m-MTDATA and PO-T2T excitons, and TCTA:PO-T2T and m-MTDATA:PO-T2T exciplexes in the films.

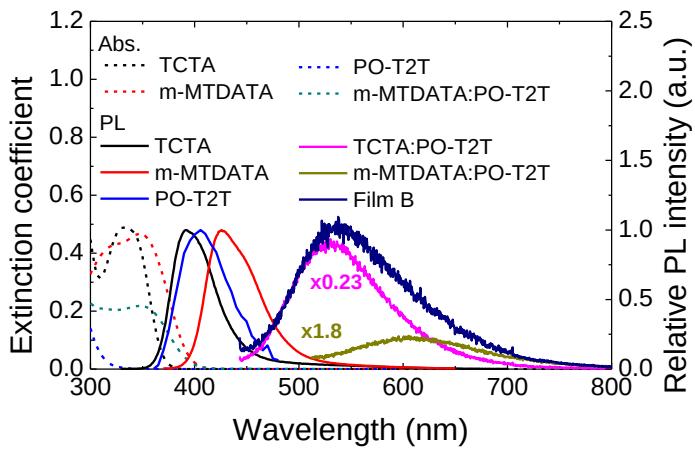

Figure 3.5. Extinction coefficients of TCTA, m-MTDATA, and PO-T2T films and m-MTDATA:PO-T2T (m.r. 1:1) film, steady-state PL spectra of a TCTA film, an m-MTDATA film, a PO-T2T solution,[93] and time-resolved PL spectra integrated for 500 ns after excitation of aTCTA:PO-T2T (m.r. 5:95) film (×0.23), an m-MTDATA:PO-T2T (m.r. 5:95) film (×1.8), and Film B.

TCTA:PO-T2T exciplex emission is dominant are compared in Figure 3.6(a). The decay rate constant for the emission of the TCTA:PO-T2T exciplexes in Film B was faster than that in the singly doped TCTA:PO-T2T film. On the other hand, the decay rate constant of the m-MTDATA:PO-T2T exciplexes in Film B was slower than that in the singly doped m-MTDATA:PO-T2T film in the detection-wavelength range of 700 to 800 nm, where m-MTDATA:PO-T2T exciplex emission is dominant, as shown in Figure 3.6(b).

The reduction of the lifetime and the intensity of the high-energy exciplex PL and their increase of the low-energy exciplex PL in the bilayer structure (Figure 3.1) and in the doped layer (Figure 3.4) clearly indicate that the ET from high-energy exciplexes to low-energy exciplexes takes place. This is the first observation of the possibility of ET from exciplexes to nearby exciplexes to our best knowledge, resulting in the diffusion of exciplexes.

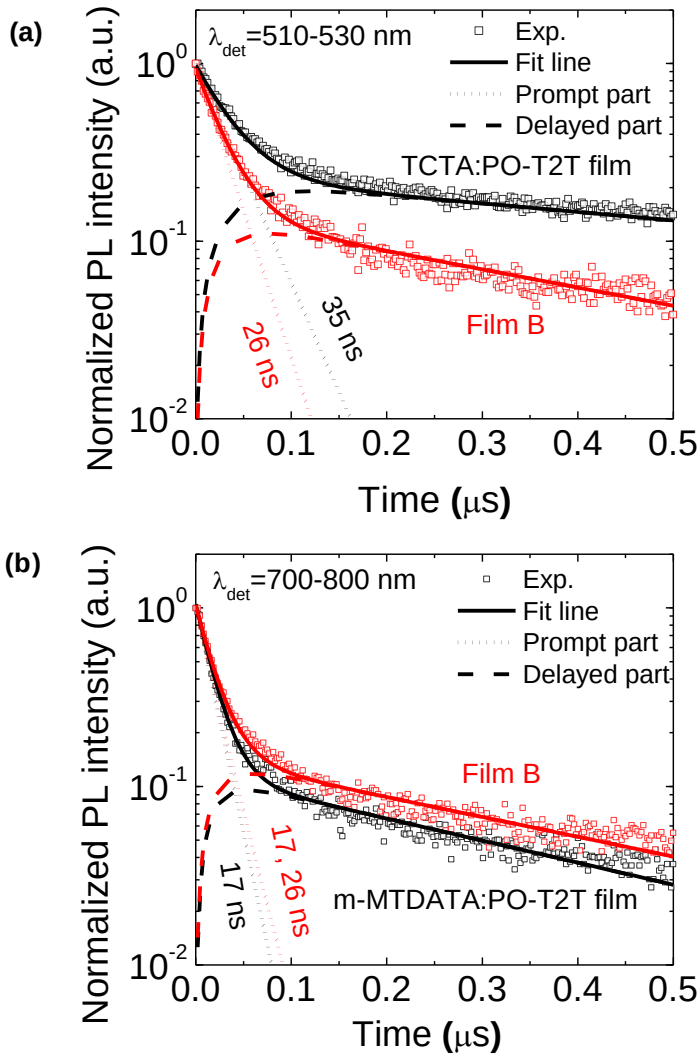

Figure 3.6. (a) Normalized transient PL intensities (empty squares), fit lines of the total (solid lines), prompt (dotted line) and delayed (dashed line) parts for the TCTA:PO-T2T film (m.r. 5:95) and Film B in the wavelength range of 510 to 530 nm. The decay time constants for the prompt parts are also given. (b) Those for the m-MTDATA:PO-T2T (m.r. 5:95) film and Film B in the wavelength range of 700 to 800 nm. The decay time constants for the prompt parts are also given.

3.4. Energy-transfer kinetics

To ensure that the ET from the high-energy exciplex to the low-energy exciplex in Film B can describe their transient decay profiles quantitatively, we carried out the fitting of the transient PL profiles for the TCTA:m-MTDATA:PO-T2T mixed film (m.r. 5:5:90) as shown in Figure 3.6(a) and 3.6(b). Firstly, the three transient PL profiles for the TCTA:PO-T2T exciplex in the TCTA:PO-T2T film and Film B and the m-MTDATA:PO-T2T exciplex in the m-MTDATA:PO-T2T film were fitted by a bi-exponential decay model considering the TADF of the exciplexes as follows;[7,101]

$$I_{\text{norm.PL}}(t) = I_{\text{p}}(t) + I_{\text{d}}(t) = e^{-k_{\text{p}}t} + C_{\text{d}}\left(e^{-k_{\text{d}}t} - e^{-k_{\text{p}}t}\right), \quad \cdots\cdots (3.1)$$

where t is the time after excitation, $I_{\text{norm.PL}}$ (t), I_{p} (t), and I_{d} (t) are the normalized transient PL intensity, prompt transient PL intensity, and delayed transient PL intensity from exciplexes, respectively, k_{p} and k_{d} are the prompt and delayed decay rate constants, respectively, and C_{d} is the pre-exponential constant for the delayed decay. The prompt transient PL intensity is the single-exponential term due to the decay of the singlet excited state into the ground state and triplet exited state by intersystem crossing, corresponding to the first term in the right-hand side of Equation (3.1). The delayed decay of the exciplex originates from the intersystem crossing from the singlet excited state to the triplet excited state, followed by the reverse intersystem crossing from the triplet excited state to the singlet excited state, of which intensity corresponds to the second term in the right-hand side of Equation (3.1). (1 - C_{d}) corresponds to the pre-exponential constant for the single prompt decay exponential term (C_{p}) for the normalized transient PL intensity. The three transient PL profiles are fitted very well using Equation (3.1) as represented by solid lines in Figure 3.6(a) and 3.6(b) except the transient PL profile of the m-MTDATA:PO-T2T exciplex in

Film B in Figure 3.6(b). The extracted fitting parameters are summarized in Table 3.1.

Secondly, the transient PL profile of the MTDATA:PO-T2T exciplex in Film B was fitted and the result is shown in Figure 3.6(b), exhibiting excellent fittings for them. The ET rate constant, k_{ET}, from the TCTA:PO-T2T exciplex to the m-MTDATA:PO-T2T exciplex in Film B was calculated as the difference between the prompt decay rate constants of TCTA:PO-T2T exciplexes in the TCTA:PO-T2T film and Film B,[7] which is 9.7×10^6 s^{-1}. Then, we fitted the prompt transient PL profiles for the m-MTDATA:PO-T2T exciplex in Film B using the experimentally obtained k_{ET} value. The differential rate equations for the prompt part of transient PL profiles in Film B are written as follows.

$$\frac{d\left[(\mathrm{T{:}P})^*\right]}{dt} = -k_p^{\mathrm{T:P}}\left[(\mathrm{T{:}P})^*\right] - k_{ET}\left[(\mathrm{T{:}P})^*\right] \quad \cdots\cdots (3.2)$$

$$\frac{d\left[(\mathrm{m{:}P})^*\right]}{dt} = -k_p^{\mathrm{m:P}}\left[(\mathrm{m{:}P})^*\right] + k_{ET}\left[(\mathrm{T{:}P})^*\right] \quad \cdots\cdots (3.3)$$

where [(T:P)*] and [(m:P)*] are the concentrations of the singlet TCTA:PO-T2T exciplexes and singlet m-MTDATA:PO-T2T exciplexes in Film B, respectively, $k_p^{\mathrm{T:P}}$ and k_{ET} are the prompt decay rate constant of the TCTA:PO-T2T exciplex in the TCTA:PO-T2T film (2.84×10^7 s^{-1}) and the ET rate constant from the singlet TCTA:PO-T2T exciplex to the m-MTDATA:PO-T2T exciplex (9.7×10^6 s^{-1}), respectively, and $k_p^{\mathrm{m:P}}$ is the prompt decay rate constant of the m-MTDATA:PO-T2T exciplex in the m-MTDATA:PO-T2T film which is 5.80×10^7 s^{-1}. The rate constants are summarized in Table 3.1. We just analyzed the transient PL profiles in the prompt region for the TCTA:m-MTDATA:PO-T2T system because the triplet-triplet ET

Table 3.1. Fitting parameters for the normalized transient PL profiles of the TCTA:PO-T2T exciplexes in the TCTA:PO-T2T film and Film B and those of the m-MTDATA:PO-T2T exciplexes in the m-MTDATA:PO-T2T film and Film B.

Detection wavelength	Film	C_p	k_p (s^{-1})	k_d (s^{-1})
510-530 nm	TCTA:PO-T2T	0.77	2.84×10^7	1.09×10^6
	Film B	0.85	3.81×10^7	2.36×10^6
700-800 nm	m-MTDATA:PO-T2T	0.89	5.80×10^7	2.85×10^6
	Film B	0.70	5.80×10^7	2.56×10^6
		0.16	3.81×10^7	

from TCTA:PO-T2T exciplex to m-MTDATA excitons as well as to m-MTDATA:PO-T2T exciplex can occur considering their energy levels as shown in Figure 3.4, which complicates the analysis. The initial concentration ratio of the TCTA:PO-T2T exciplexes to m-MTDATA:PO-T2T exciplexes ($C_0^{\mathrm{T:P}} / C_0^{\mathrm{m:P}}$) was set as 2/5 considering the extinction coefficients of TCTA and m-MTDATA at the excitation wavelength of 337 nm and the singlet-singlet ET from the TCTA exciton to m-MTDATA exciton by virtue of considerable spectral overlap between the TCTA emission spectrum and the m-MTDATA absorption spectrum as shown in Figure 3.5.

The normalized solutions of the differential rate equations are

$$I_{\mathrm{p}}^{\mathrm{T:P}} = e^{-\left(k_{\mathrm{p}}^{\mathrm{T:P}} + k_{\mathrm{ET}}\right)t} \quad \cdots\cdots (3.4)$$

$$I_{\mathrm{p}}^{\mathrm{m:P}} = \frac{k_{\mathrm{p}}^{\mathrm{m:P}} - k_{\mathrm{p}}^{\mathrm{T:P}} - \left(1 + C_0^{\mathrm{T:P}} / C_0^{\mathrm{m:P}}\right) k_{\mathrm{ET}}}{k_{\mathrm{p}}^{\mathrm{m:P}} - k_{\mathrm{p}}^{\mathrm{T:P}} - k_{\mathrm{ET}}} e^{-k_{\mathrm{p}}^{\mathrm{m:P}} t} + \frac{\left(C_0^{\mathrm{T:P}} / C_0^{\mathrm{m:P}}\right) k_{\mathrm{ET}}}{k_{\mathrm{p}}^{\mathrm{m:P}} - k_{\mathrm{p}}^{\mathrm{T:P}} - k_{\mathrm{ET}}} e^{-\left(k_{\mathrm{p}}^{\mathrm{m:P}} + k_{\mathrm{ET}}\right)t} . \quad \cdots\cdots (3.5)$$

The first term in the right-hand side of Equation (3.5) indicates that the more initial excited energy acceptors increase the influence of decay rate constant of the intrinsic energy acceptor on the transient PL profiles. The prompt part of the TCTA:PO-T2T exciplexes in Film B is a single-exponential line with a decay time constant of 26 ns and that of the m-MTDATA:PO-T2T exciplexes in Film B is a two-exponential line with the decay time constants of 17 ns and 26 ns which are $1/k_{\mathrm{p}}^{\mathrm{m:P}}$ and $1/\left(k_{\mathrm{p}}^{\mathrm{T:P}} + k_{\mathrm{ET}}\right)$, respectively. The fitting results using the parameters in Table 3.1 are shown in Figure 3.6(b) as the red dotted line. From the tail-fitting for the delayed part of the m-MTDATA:PO-T2T exciplex in Film B, the fit line of the entire transient PL profile for the m-MTDATA:PO-T2T exciplex in Film B well matches with the experimental values as shown in Figure 3.6(b). Because of the larger number of the

m-MTDATA:PO-T2T exciplex than the TCTA:PO-T2T exciplex in Film B at the excitation moment, the pre-exponential constant for the decay time constant of 17 ns and 26 ns is 0.81 and 0.19, respectively, leading to small change of the transient PL profiles for the m-MTDATA:PO-T2T exciplex than those for the TCTA:PO-T2T exciplex. The extracted parameters for the fit line (solid lines) in Figure 3.6 are included in Table 3.1. The very good fittings confirm that ET takes place indeed from the TCTA:PO-T2T exciplex to the m-MTDATA:PO-T2T exciplex.

3.5. Concentration-dependent energy transfer rate

To investigate the relationship between the ET rate constant and the distance between the energy donor and acceptor, we conducted concentration-dependent exciplex-quenching experiments with various molar ratios. Total 16 films (doped films) were fabricated: eight TCTA:PO-T2T films with molar ratios of *x*: 100 - *x* and eight TCTA:m-MTDATA:PO-T2T films with molar ratios of *x*: *x*: 100 – 2*x*, respectively, where *x* = 3.0, 3.5, 4.0, 4.5, 5.0, 5.5, 6.0, and 6.5. The thickness of the films was 50 nm. The doping concentrations of the films were kept low to maintain identical local environments for the dopants and ensure that the photo-physical characteristics of the TCTA:PO-T2T exciplex was not influenced by the addition of m-MTDATA molecules. The transient PL intensities of the films are shown in Figure 3.7. The transient PL profiles were fitted by a bi-exponential decay model using Equation (3.1) as described before to extract the k_{ET} values. The transient behaviors of the TCTA:PO-T2T exciplexes in the TCTA:m-MTDATA:PO-T2T films with different doping concentrations are well fitted by the bi-exponential decays and the fitting parameters are summarized in Table 3.2. The prompt decay rate constants of the TCTA:PO-T2T exciplexes in the TCTA:PO-T2T films do not change much with the different doping concentrations. In contrast, the prompt decay rate constants of the TCTA:PO-T2T exciplexes in the TCTA:m-MTDATA:PO-T2T films increased significantly with the doping concentration. The k_{ET} values are the difference between the prompt decay rate constants of TCTA:PO-T2T exciplexes in the TCTA:PO-T2T and TCTA:m-MTDATA:PO-T2T mixed films with the same TCTA concentrations as described in the previous section. The k_{ET} values are plotted in the

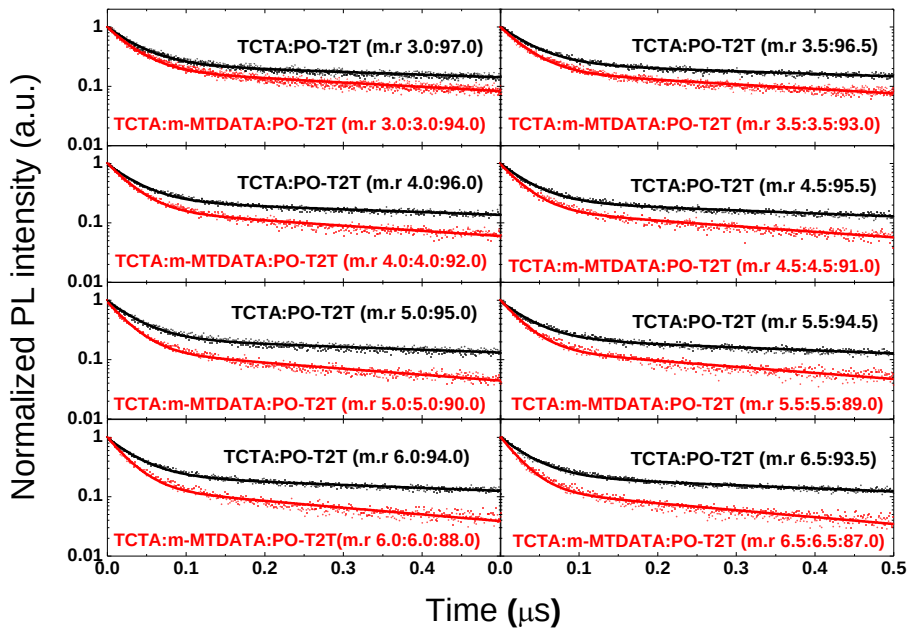

Figure 3.7. Normalized transient PL intensities in the wavelength range 510 to 530 nm, where the PL of the TCTA:PO-T2T exciplex is dominant in TCTA:PO-T2T films and TCTA:m-MTDATA:PO-T2T films with various molar ratios (points), and fit lines by a two-exponential decay model (line) using the parameters in Table 3.2.

Table 3.2. Pre-exponential constants and decay rate constants for the prompt and delayed decays of transient PL intensities in the wavelength range 510 to 530 nm, where PL of the TCTA:PO-T2T exciplex is dominant in TCTA:PO-T2T and TCTA:m-MTDATA:PO-T2T films with various molar ratios and the corresponding ET rate constants.

Molar ratio of m-MTDATA	TCTA:PO-T2T			TCTA:m-MTDATA:PO-T2T			k_{ET} [10^6 s^{-1}]
	C_p	k_p [10^6 s^{-1}]	k_d [10^6 s^{-1}]	C_p	k_p [10^6 s^{-1}]	k_d [10^6 s^{-1}]	
3.0	0.76	27.7 ±1.1	1.04 ±0.03	0.81	32.9 ±1.5	1.60 ±0.07	5.2 ±0.9
3.5	0.76	27.0 ±0.4	0.99 ±0.04	0.82	33.3 ±0.7	1.78 ±0.06	6.3 ±0.4
4.0	0.76	28.8 ±0.9	1.08 ±0.04	0.84	35.7 ±0.5	2.05 ±0.07	6.9 ±0.5
4.5	0.77	29.4 ±0.1	1.17 ±0.08	0.83	36.8 ±0.4	2.18 ±0.18	7.4 ±0.2
5.0	0.77	28.4 ±1.0	1.09 ±0.01	0.85	38.1 ±0.5	2.36 ±0.04	9.7 ±0.6
5.5	0.76	29.0 ±2.2	1.18 ±0.01	0.85	38.4 ±0.5	2.39 ±0.15	9.5 ±1.1
6.0	0.75	29.1 ±0.4	1.16 ±0.05	0.86	40.1 ±0.3	2.65 ±0.14	11.0 ±0.3
6.5	0.78	29.3 ±3.0	1.23 ±0.08	0.87	42.5 ±2.8	2.74 ±0.21	13.2 ±2.1

semi-logarithmic plot against $C_{\text{m-MTDATA}}^{-1/3}$ in Figure 3.8(a). The ET rate constant decreases with the separation between the high-energy exciplex and the low-energy exciplex.

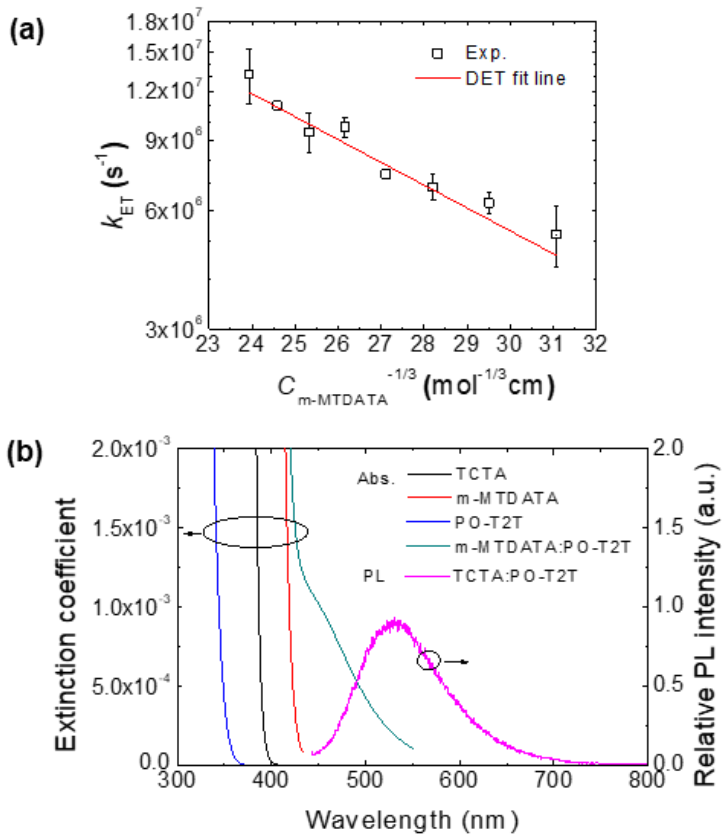

Figure 3.8. (a) A plot of experimental values (square) of the logarithm scale of k_{ET} vs. $C_{m\text{-}MTDATA}^{-1/3}$, and a DET fit line (solid line). (b) Extinction coefficients of TCTA, m-MTDATA, and PO-T2T films and m-MTDATA:PO-T2T (m.r. 1:1) film below 0.002 and the time-resolved PL spectra integrated for 500 ns after excitation of aTCTA:PO-T2T (m.r. 5:95) film.

3.6. Spectral overlap for the exciplex-exciplex energy transfer

Experimental results shown in the previous sections clearly indicate that the ET takes place between exciplexes. However, it seems to be counterintuitive since the exciplex is generally thought to be formed through CT only in the excited state between donor and acceptor molecules at photo-excitation and direct CT absorption from the ground state to the exciplex states does not take place. Therefore, the ET process must be carefully analyzed before we conclude that 'direct' ET between exciplex states indeed takes place. The direct ET is the ET from energy donors to energy acceptors without generation of any other species other than the energy acceptors during the process of ET. There are two mechanisms for the direct ET; FRET and DET. Both mechanisms require the CT absorption from the ground state to the exciplex state for the exciplex-exciplex ET. In order to investigate whether there exists the CT absorption in the exciplex, we selected the TCTA:m-MTDATA:PO-T2T system and measured the CT absorption of the energy-accepting exciplex (m-MTDATA:PO-T2T). Figure 3.8(b) shows the extinction coefficients of an m-MTDATA:PO-T2T (m.r. 1:1) mixed film along with the extinction coefficients of TCTA, m-MTDATA, and PO-T2T neat films.[92] The exciplex-forming mixed film only showed clear absorption in the sub-bandgap region at the longer wavelength than 420 nm even though it is very weak. Thick films were used for the purpose of detecting the intermolecular CT absorption by a simple absorption equipment of reflection/transmission measurement. Then, absorbance for the exciplex-forming mixed film in the sub-bandgap wavelength region was analyzed using the transfer-matrix method to obtain extinction coefficient for the intermolecular CT state as low as 10^{-4}. Details are described in ref. 91.

The indirect ET mechanisms were also considered for the ET from the high-energy exciplex to the low-energy exciplex. The indirect ET could have polaron pairs as intermediate products during the process of ET different from the direct ET. Polaron pairs could be generated by exciplex dissociation, and they could recombine into exciplexes apart from the dissociated exciplex in various ways. The Langevin recombination, trap-assisted recombination, and geminate recombination are considered in this section. Recently, the indirect ET via the geminate recombination was reported as the 'inchworm' mechanism.[36]

3.7. Dexter-type energy transfer

DET can be considered as a mechanism for the ET considering that the extinction coefficient of the CT absorption for the exciplexes is very small in the order of 10^{-3}. We considered DET between the nearest energy-donating exciplex (TCTA:PO-T2T exciplex) and energy-accepting exciplex (m-MTDATA:PO-T2T exciplex), and ET between more separated pairs was ignored because the DET rate constant decreases exponentially with the separation distance as follows;[102]

$$k_{\mathrm{DET}} = NKJ \exp(-\beta R), \quad \cdots\cdots (3.6)$$

where k_{DET} is the DET rate constant, N the number of nearest energy-accepting species with the separation of R, K the experimental factor related to the specific orbital interactions, J the spectral overlap integral normalized for the molar extinction coefficient of the energy-accepting species, and β the attenuation factor arising from the electronic exchange integral that is considered to drop exponentially in the tail of molecular orbitals.[67,68] The nearest distances between the TCTA:PO-T2T exciplexes and the m-MTDATA:PO-T2T exciplexes in the mixed films were calculated using Equation (3.7) in the Wigner-Seitz approximation,[103] where TCTA and m-MTDATA molecules doped in bulk PO-T2T at low concentrations are assumed to be uniformly dispersed:

$$\frac{4}{3}\pi\left(\frac{R}{2}\right)^3 = \left(\frac{N_{\mathrm{d}}}{V}\right)^{-1} = \left(2N_{\mathrm{A}}C_{\text{m-MTDATA}}\right)^{-1} \quad \cdots\cdots (3.7)$$

where R (in units of cm) is the distance between the nearest TCTA:PO-T2T exciplexes and m-MTDATA:PO-T2T exciplex which corresponds to the distance between TCTA and m-MTDATA molecules in this system, N_{d} is the number of dopants in volume of V, N_{A} is Avogadro's number, and $C_{\text{m-MTDATA}}$ is the molar

concentration of m-MTDATA in the TCTA:m-MTDATA:PO-T2T mixed film (in units of mol cm^{-3}) calculated from the molar ratio of mixed films under the assumption that all films had a density of 1 g cm^{-3}. The grazing incident small angle X-ray scattering (GISAXS) was measured for the mixed film with the highest doping concentration [TCTA:m-MTDATA:PO-T2T (m.r. 6.5:6.5:87) film] to investigate whether the dopant molecules form aggregates or not. Figure 3.9(a) shows the GISAXS image for the film, and the horizontal line cut of the image is shown in Figure 3.9(b). The GISAXS image were measured for 5 s, and X-rays with an energy of 11.57 KeV are incident with an angle of 0.15° relative to the surface of the film. A 'Guinier knee' is not observed in the horizontal line cut. This indicates that doping molecules do not form aggregate in the film.[104,105]

Substituting this equation into the DET rate constant equation results in

$$\log k_{\mathrm{DET}} = \log(NKJ) - \frac{\beta}{2.303}\left(\frac{3}{\pi N_{\mathrm{A}}}\right)^{1/3} C_{\text{m-MTDATA}}{}^{-1/3} \quad \cdots\cdots (3.8)$$

The linear fit line of k_{ET} against $C_{\text{m-MTDATA}}{}^{-1/3}$ in the semilogarithmic plot in Figure 3.8(a) indicates that the ET rate constant decreases exponentially with the distance between the TCTA:PO-T2T exciplex and the m-MTDATA:PO-T2T exciplex in the mixed films, demonstrating that ET takes place by DET. The attenuation factor arising from the electronic exchange integral was 1.1 nm^{-1}, and the pre-exponential constant NKJ = 2.9×10^{8} s^{-1} from the fitting by Equation (3.8). S. R. Forrest et al. reported that the diffusion of the triplet excited states of phosphors takes place via Dexter-type exchange mechanism.[69] DET between the phosphors have the attenuation factors of 1.2 ~ 1.5 nm^{-1} and the pre-exponential constants of 6.4×10^{6} s^{-1}~3.0×10^{8} s^{-1} which are the similar values with our results.[69] It indicates that the ET

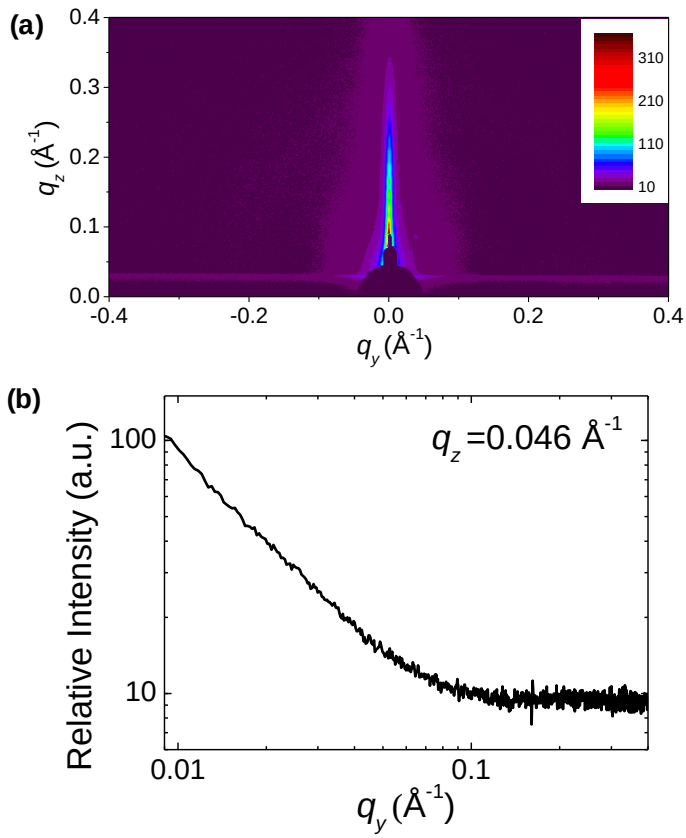

Figure 3.9. (a) GISAXS images measured for TCTA:m-MTDATA:PO-T2T (m.r. 6.5:6.5:87) films. (b) Horizontal GISAXS line cut of the TCTA:m-MTDATA:PO-T2T (m.r. 6.5:6.5:87) film at q_z = 0.046 Å $^{-1}$.

between the exciplexes also takes place by Dexter-type exchange mechanism in organic films. The DET process from exciplexes to exciplexes can be explained using a molecular-orbital diagram schematically represented by Figure 3.10(a) to explain the exchange mechanism.

There are two requirements for DET to take place by the Fermi golden rule. One is the spectral overlap between absorption of energy acceptors and emission of energy donors which is satisfied in the exciplex systems as discussed in the beginning of Section 4. The other one is the electronic exchange integral between energy donor states and energy acceptor states. The electronic exchange integral drops exponentially with the separation between them. Because of the reason, DET has been thought to occur only when the energy donor and acceptor are in physical contact.[67] However, the physical contact is not always a necessary condition for efficient long-range DET to occur, and the long-range DETs without the physical contact have been reported, known as the superexchange ET which is the exchange ET with the influence of intervening states.[68–70] The large coupling between π-conjugated molecules could expand the exchange integral between them to large separation when the energy donor and acceptor are π-conjugated molecules in the π-conjugated medium. It indicates that the physical contact between the energy donor and acceptor is not a necessary condition for DET.

The long-range DET with small attenuation factors around 1 nm^{-1} can be explained by the state energy diagram shown in Figure 3.10(b),[70,106–108] where v_1, v, and v_2 are the electronic exchange integrals between the states of the energy-donating exciplex and medium molecule, between the states of the medium molecules, and

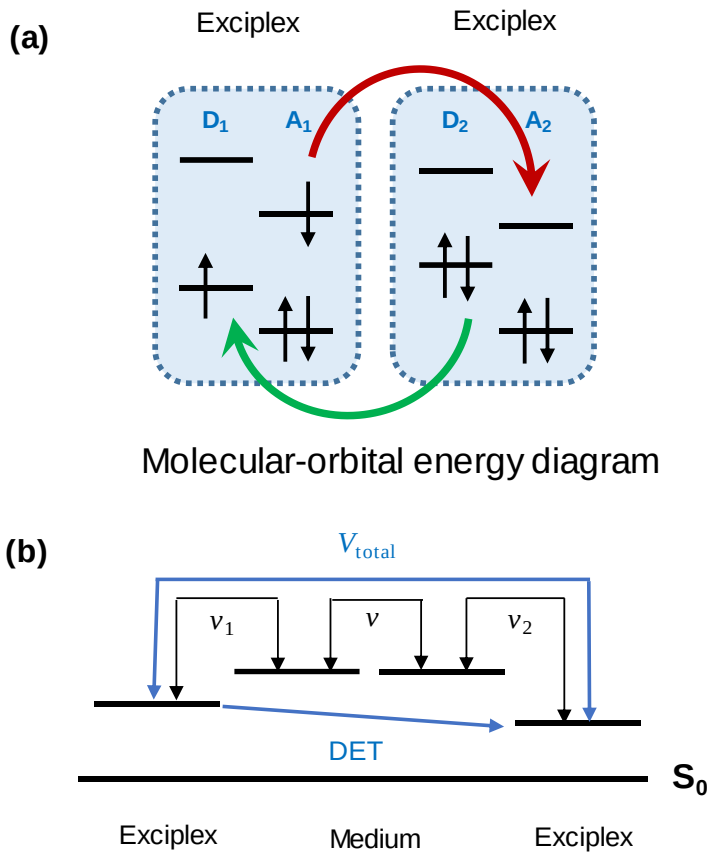

Figure 3.10. (a) Schematic molecular-orbital energy diagrams of DET from an exciplex to another exciplex. (b) Schematic state energy diagrams of DET from an exciplex to another exciplex in π-conjugated molecular films.

between the states of the medium molecule and the energy-accepting exciplex, respectively. As a result of the first-order perturbation theory, V_{total} is the superexchange electronic exchange integral which is the indirect electronic exchange integral via intermediate states (medium states).[68,69,107,108] The small β in organic π-conjugated films can be explained by large coupling between π-conjugated molecules, according to McConnell's relation.[68,69,106–108] According to this theory, β can be expressed by:[106–108]

$$\beta = \frac{2}{R_0} \ln \left| \frac{\Delta}{v} \right| \quad \cdots\cdots (3.9)$$

where R_0 is the length of the repeating units between energy donors and acceptors, Δ is the energy difference between the energy donor states and localized states of the repeating units, and v is the exchange integral between the repeating units. This equation indicates that the large v could lead to the decrease of β, i.e., the large coupling between excitonic states of small π-conjugated molecules could increase the possibility of DET between an energy donor and an energy acceptor with large separation. When the electronic exchange integrals between π-conjugated molecules are negligible, the electronic exchange integral for the superexchange ET becomes negligible, resulting in large β requiring direct physical contact.[2,108] Therefore, the small β in exciplex-forming blended films must be caused by large coupling between π-conjugated molecules according to McConnell's relation.

Other mechanisms are also considered for the ET process. However, ET rate constants of other mechanisms were negligible compared to those of the exchange mechanism in the system investigated in this study as follows.

3.8. Förster-type energy transfer

The FRET rate constant (k_{FRET}) can be expressed by the following equation.[109]

$$k_{FRET} = \frac{9000 \ln 10}{128 \pi^5 N_A} \frac{N_R \kappa^2 k_r}{n^4} \frac{\int I_D(\lambda) \varepsilon_A(\lambda) \lambda^4 d\lambda}{\int I_D(\lambda) d\lambda} \frac{1}{R^6} \quad \cdots\cdots (3.10)$$

where k_{FRET} is the FRET rate constant, N_R is the number of energy acceptors with separation of R from an energy donor, κ^2 is the dipole orientation factor, k_r is the radiative rate constant of the energy-donating states, n is the refractive index of the medium, λ is the wavelength (in units of cm), I_D is the emission spectrum of the energy-donating states, ε_A is the molar extinction coefficient of energy-accepting states (in units of L cm^{-1} mol^{-1}), and R is the distance between the energy donors and acceptors (in units of cm). Based on the assumption that TCTA and m-MTDATA molecules doped into bulk of PO-T2T molecules at low concentrations are uniformly dispersed in the Wigner-Seitz approximation,[103] the number of the nearest energy-accepting species is 6 in TCTA:m-MTDATA:PO-T2T doped films. Again, we only consider the FRET between the nearest energy-donating exciplex and energy-accepting exciplex because the FRET between the second nearest energy donor-acceptor pairs would be more than 10 times smaller than that. The dipole orientation factor was assumed to be 2/3 for randomly oriented energy donors and energy acceptors. The refractive index of the medium of TCTA:m-MTDATA:PO-T2T doped films was determined to be 1.73 which is same as the refractive index of PO-T2T neat films at the wavelength of 500 nm. The nearest distance between the TCTA:PO-T2T exciplexes and the m-MTDATA:PO-T2T exciplexes could be calculated by Equation (3.7). The emission spectrum of the TCTA:PO-T2T singlet exciplex is depicted in

Figure 3.8(b). The molar extinction coefficient of the m-MTDATA:PO-T2T singlet exciplex (in units of L cm^{-1} mol^{-1}) could be obtained by Equation (3.11).

$$\varepsilon_A = \frac{4\pi\kappa}{\lambda} C_{\text{m-MTDATA}}{}^{-1} = \frac{4\pi\kappa M_w}{1000\lambda\rho_{film}} \quad \cdots\cdots (3.11)$$

where κ is the extinction coefficient of m-MTDATA:PO-T2T singlet exciplexes as shown in Figure 3.8(b),[92] ρ_{film} is the density of the film (in units of g cm^{-3}), and M_W is the sum of molecular weights of m-MTDATA and PO-T2T (in units of g mol^{-1}) for the m-MTDATA:PO-T2T (m.r. 1:1) film. All films were assumed to have a density of 1 g cm^{-3}. The k_r of the TCTA:PO-T2T singlet exciplex could be obtained from the following equation derived from the two-exponential decay model for TADF emission.[7]

$$k_r = k_p \Phi_{PL} \frac{\int_0^\infty I_p(t)\,dt}{\int_0^\infty I_{\text{norm.PL}}(t)\,dt} \quad \cdots\cdots (3.12)$$

where k_r and k_p are the fluorescence rate constant and prompt decay rate constant of exciplexes, respectively, and Φ_{PL} is the PL quantum yield (PLQY) of exciplexes. The PLQY of the TCTA:PO-T2T exciplexes was measured to be 35%. The k_r of the TCTA:PO-T2T singlet exciplex was calculated to be 1.5×10^6 s^{-1} given Equation (3.1) and the transient PL characteristics from the TCTA:PO-T2T films summarized in Table 3.2. The calculated values of Equation (3.10) are plotted as dashed lines in Figure 3.11. The FRET rate constants are almost one order of magnitude smaller than the experimental ET rate constants which are fitted by the Dexter-type exchange mechanism. Not only that, the concentration dependence of the FRET rate constants does not follow the experimental data [$\propto R^{-6}$ for FRET vs. $e^{-\beta R}$ for DET]. The much smaller FRET rate constant of the exciplex can be understood from the very small extinction coefficient for CT absorption. These results reveal that FRET is not the

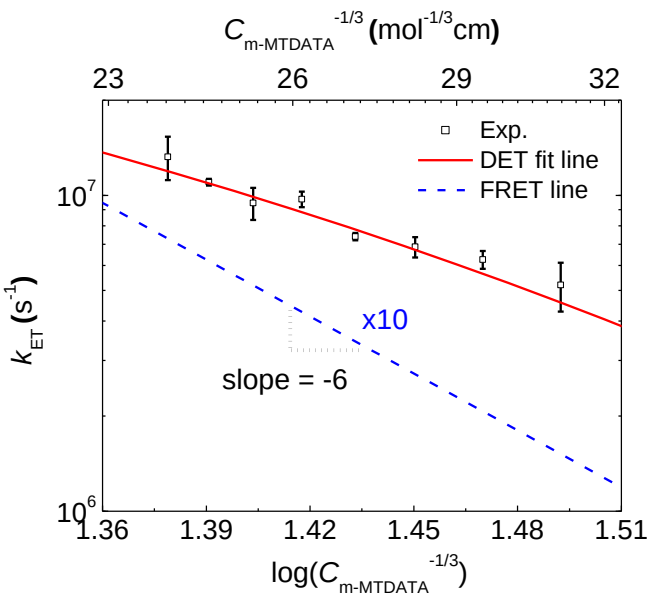

Figure 3.11. A plot of experimental values (empty square) of the logarithm scale of k_{ET} vs log($C_{m\text{-}MTDATA}^{-1/3}$), a DET fit line (solid line), and calculated FRET rate constants (×10) by Equation (3.10) (dashed line).

dominant mechanism for the exciplex diffusion.

3.9. Exciplex dissociation followed by Langevin recombination

We considered three indirect ET cases: exciplex dissociation followed by Langevin recombination, trap-assisted recombination, or geminate recombination. We first considered Langevin recombination which is the recombination of free electrons and holes. Langevin recombination is a bimolecular process different from trap-assisted recombination or geminate recombination.

The mCBP:PO-T2T exciplexes and TCTA:PO-T2T exciplexes which are the high-energy exciplexes in each system could be dissociated into the free polarons, and they can recombine into the low-energy exciplexes in the organic films. The transient behavior of the exciplex emission must depend on the density of the charged species at the moment of photo-excitation since Langevin recombination is a bimolecular process. The initial numbers of free electrons and holes are both proportional to the intensity of the excitation light. The square dependence of exciplex generation rate will result in the excitation intensity dependence of decay rate constants if Langevin recombination is dominant process for the generation of the singlet exciplex states. The transient PL profiles for the mCBP:PO-T2T film (m.r. 1:1) and TCTA:PO-T2T film (m.r. 5:95) where the high-energy exciplexes for each system only exist exhibit negligible change with different excitation light intensities, as shown in Figure 3.12(a) and 3.12(b), respectively. The excitation light intensities were controlled by neutral-density (ND) filters with different optical densities ranging from 25 to 800 μW. These results indicate that bimolecular recombination or Langevin recombination hardly participate in the decay of the exciplexes to ground states.

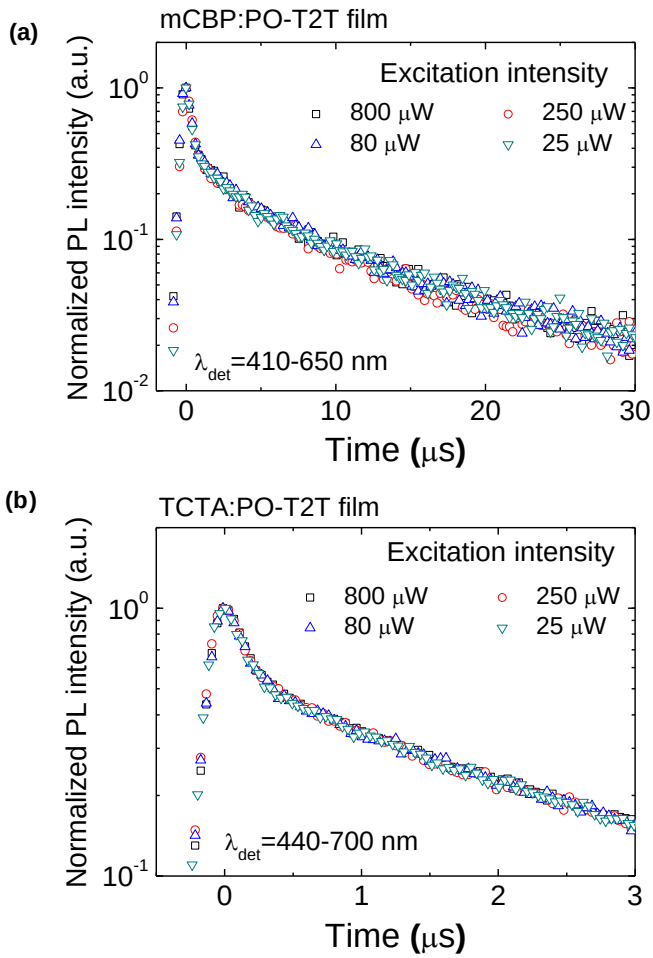

Figure 3.12. (a) Normalized transient PL profiles of an mCBP:PO-T2T film (m.r. 1:1) excited by a 337 nm pulsed laser light (N_2 laser) at different intensities in the wavelength range of 410 to 650 nm. (b) Those of a TCTA:PO-T2T film (m.r. 5:95) at different intensities in the wavelength range of 440 to 700 nm.

3.10. Exciplex dissociation followed by trap-assisted recombination

Indirect ET via trap-assisted recombination of polarons formed by the dissociation of exciplexes could occur. The TCTA:PO-T2T exciplexes dissociate into polarons, and then trap-assisted recombination occurs to form the m-MTDATA:PO-T2T exciplexes, as depicted in Equation (3.13).

$$\left(\text{TCTA:PO-T2T}\right)^* \underset{k_{CR}}{\overset{k_{CS}}{\rightleftarrows}} \text{TCTA}^+ \cdots \text{PO-T2T}^- \xrightarrow{k_{TR}} \left(\text{m-MTDATA:PO-T2T}\right)^* \quad (3.13)$$

k_{CS}, k_{CR}, and k_{TR} is the rate constants for exciplex dissociation, geminate recombination, and trap-assisted recombination, respectively. When a steady-state approximation for the concentrations of intermediates is applied described by Equation (3.14),

$$k_{CS}\left[\left(\text{TCTA:PO-T2T}\right)^*\right] - k_{CR}\left[\text{TCTA}^+ \cdots \text{PO-T2T}^-\right] - k_{TR}\left[\text{TCTA}^+ \cdots \text{PO-T2T}^-\right] = 0 \quad \cdots\cdots (3.14)$$

the quenching rate constant of TCTA:PO-T2T exciplexes in the above reaction could be expressed by

$$\begin{aligned} k_{ET}\left[\left(\text{TCTA:PO-T2T}\right)^*\right] &= k_{CS}\left[\left(\text{TCTA:PO-T2T}\right)^*\right] - k_{CR}\left[\text{TCTA}^+ \cdots \text{PO-T2T}^-\right] \\ &= k_{CS}\left(1 - \frac{1}{k_{TR}/k_{CR} + 1}\right)\left[\left(\text{TCTA:PO-T2T}\right)^*\right] \end{aligned} \quad \cdots (3.15)$$

k_{TR} in Equation (3.15) could be expressed by the following equation.[110]

$$k_{TR} = \frac{q\mu_n n_{trap}}{\varepsilon\varepsilon_0} = \frac{q\mu_n N_A C_{\text{m-MTDATA}}}{\varepsilon\varepsilon_0} \quad \cdots\cdots (3.16)$$

where q is the elementary charge, μ_n is the electron mobility in the film (in units of $cm^2\ V^{-1}\ s^{-1}$), n_{trap} is the density of the traps for holes corresponding to the density of m-MTDATA in the TCTA:m-MTDATA:PO-T2T mixed film, $C_{\text{m-MTDATA}}$ is the molar

concentration of m-MTDATA in the films (in units of mol cm^{-3}), ε is the dielectric constant of the film, and ε_0 is the vacuum permittivity. We considered that m-MTDATA molecules behave as hole traps when the trap-assisted recombination engages in the ET from the TCTA:PO-T2T exciplexes to the m-MTDATA:PO-T2T exciplexes in the TCTA:m-MTDATA:PO-T2T films, not only because m-MTDATA has higher HOMO levels than TCTA and PO-T2T, but also logically the positive polaron originated from TCTA must be trapped in m-MTDATA for the ET to take place from the TCTA:PO-T2T exciplexes to the m-MTDATA:PO-T2T exciplexes by the trap-assisted recombination. Thus, we used the molecular density of m-MTDATA in the films as the trap density. For the TCTA:m-MTDATA:PO-T2T film with $\varepsilon = 4$ and $\mu_n = 1.2\times10^{-5}$ $cm^2/V\cdot s$,[98] Equation (3.15) becomes,

$$k_{ET} = k_{CS}\left(1-\frac{1}{3.3\times10^{12}/k_{CR}\times C_{\text{m-MTDATA}}+1}\right) \quad \cdots\cdots(3.17)$$

The value of k_{CS} and k_{CR} are not known for the TCTA:m-MTDATA:PO-T2T film. Instead of determining the values by experiment, we used approximate values taken from a similar exciplex system in literature, where an 1:1 mixed film of m-MTDATA:tri[3-(3-pyridyl)mesityl]borane (3TPYMB) was used as an exciplex-forming mixed film to report $k_{CS}/k_{CR} = 1.36\times10^{-3}$ and the binding energy of the m-MTDATA:3TPYMB exciplex of 0.17 eV.[99] If we assume the exciplex binding energies in small-molecular π-conjugated organic films are similar, then $k_{CS}/k_{CR} = 1.36\times10^{-3}$ must be similar in the both systems. Using the relationship, the k_{ET} values are calculated for different k_{CR} values of 5×10^7 s^{-1}, 1×10^8 s^{-1}, 5.3×10^8 s^{-1},[110] 1×10^9 s^{-1}, and 5×10^9 s^{-1}, and are compared with the experimental data and DET fitting in Figure 3.13. The ET rate constants via trap-assisted recombination of polaron pairs generated from the dissociation of exciplexes are almost two orders of magnitude

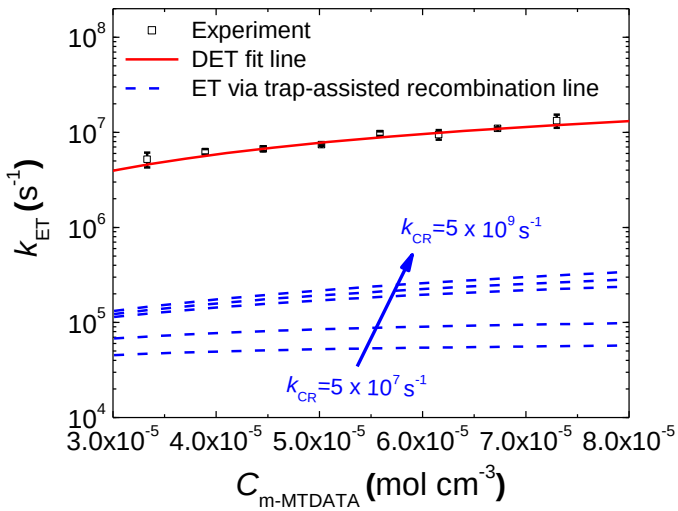

Figure 3.13. A plot of experimental values (empty square) of logarithm scale of k_{ET} vs. $C_{m\text{-}MTDATA}$, a DET fit line (solid line), and possible lines of rate constants for ET via trap-assisted recombination (Equation (3.17) when k_{CR} values are 5×10^7 s^{-1}, 1×10^8 s^{-1}, 5.3×10^8 s^{-1},[110] 1×10^9 s^{-1}, and 5×10^9 s^{-1}) (dashed line).

smaller than the experimental ET rate constants which are fitted by the Dexter-type exchange mechanism. Therefore, exciplex diffusion via trap-assisted recombination must be negligible compared to the DET.

3.11. Exciplex dissociation followed by geminate recombination ('Inchworm' mechanism)

Finally, we consider the inchworm mechanism of exciplex diffusion reported in ref. 34 based on the magneto-PL observed from exciplex and Monte Carlo simulation, where an electron and a hole dissociated from an exciplex hop to neighboring molecules incoherently, and recombine geminately. There are two arguments that we thought the inchworm mechanism would not be dominant in the exciplex-forming system. The first one is that the supporting data for explaining inchworm mechanism are not powerful. The magnetic field data were used to support the inchworm mechanism. However, it should be noted that the interpretation about magnetic field effect in exciplexes is controversial at this moment.[111,112] Baldo and coworkers et al. claimed that the magnetic field data for an exciplex could be explained by the presence of polaron pairs in exciplex-forming films inducing hyperfine interaction (HFI).[36,99] Splitting of T_+ and T_- could induce decrease of intersystem crossing rate by HFI when a magnetic field is applied. However, the magnetic field response is too broad to explain the effect by the HFI. When applied magnetic fields are about one order of magnitude greater than the hyperfine coupling, intersystem crossing between $T_\pm$ and S is shut off.[113] Considering that typical values of hyperfine coupling constants are 1-10 mT,[113] the magnetic field effect should saturate in the range of 10-100 mT. It is clearly shown in the magneto-electroluminescence of poly[2-methoxy-5-(2-ethylhexyloxy)-1,4-phenylenevinylene] (MEH-PPV) based OLEDs.[112] The magneto-electroluminescence of MEH-PPV OLED devices at constant current saturates at ~100 mT, where the magnetic field effect is governed by HFI.[113] On the other hand, the magnetic field effect for exciplex reported by Baldo

et al. saturates at ~300 mT and the full width at half maximum (FWHM) of the magnetic field effect is ~66 mT, which are not easy to be explained by the HFI between polaron pairs. Instead, Z. Valy Vardeny et al. analyzed the magnetic field effects on the PL of an exciplex by the Δg mechanism.[112] They also pointed out that the FWHM of the magnetic field effect on the PL of the exciplex of 32 mT is too large for the magnetic field effect to originate from HFI. They concluded that magneto-reverse intersystem crossing between singlet and triplet exciplex states caused by Δg mechanism would have a large contribution in the magnetic field effect for the exciplex by analyzing the activation energy of the magnetic field effect of the exciplex. M. E. Flatté, et al. also reported that the Δg mechanism is dominant over HFI in the same system.[114] In addition, the magnetic field effect was reported in TADF molecules (intra-molecular CT molecules) where the dissociation of the exciton is hardly expected, resulting in negligible density of polaron pairs inducing HFI.[115] The authors attributed the effect to the spin-orbit coupling rather than HFI.

Second, exciplex dissociation rate constant is too small to explain the large ET rate constant. The inchworm mechanism has three steps; dissociation of exciplexes into electrons and holes, incoherent hopping of the electrons and holes in bound state, and geminate recombination of the electrons and holes. The processes are sequential so that the slowest step must be the rate determining step. M. A. Baldo and coworkers have reported the rate constant for the exciplex dissociation into the polaron pair as 7.2×10^{5} s^{-1} and the geminate recombination of the polaron pairs as 5.3×10^{8} s^{-1}.[99] Also, the geminate recombination rate constant in various organic electron donor-acceptor films were reported as 1×10^{7}~5×10^{9} s^{-1}.[4] Given the exciplex binding energy of ~0.17 eV,[99] the exciplex dissociation rate constant is in the range

from 1×10^4 s^{-1} up to 7×10^6 s^{-1}. It implies that the ET rate constant via the inchworm model must saturate to 7×10^6 s^{-1} no matter how large the rate constant for charge hopping after exciplex dissociation is. This value is too small to explain our reported ET values with the maximum value of 1.3×10^7 s^{-1}.

To sum up, we think that it may be a feasible mechanism, but it is too early to conclude that the magnetic field effect on the PL of exciplexes is the crucial evidence for the presence of a pair of an electron and a hole for the inchworm mechanism inducing HFI. Therefore, the inchworm mechanism would not be a dominant mechanism in the exciplex-forming systems in this study. Further study is required to clarify whether the inchworm mechanism can be applicable to exciplex-forming systems.

3.12. Exciplex-exciplex energy transfer in organic semiconductors

The DET process would be dominant in polymer organic OPVs as well. We obtained the similar absorption coefficient for the intermolecular CT state in the m-MTDATA:PO-T2T mixed film [92] with those in the polymer:[6,6]-phenyl C_{61} butyric acid methyl ester (PCBM) mixed films exploited in OPVs as shown in Figure 3.14.[34] Thus, the order of FRET rate constant in the mixed film we investigated would be similar with that in the polymer:PCBM mixed films exploited in OPVs. FRET rate constant is linearly proportional to both the radiative rate constant of an energy donor and the spectral overlap with molar extinction coefficient of an energy acceptor as shown in Equation (3.10). The order of magnitude of radiative rate constants of singlet exciplexes would be similar between small molecular systems and polymer systems because the radiative rate constant is related to the extinction coefficient according to the following equation based on the one-dimensional oscillator theory.[2]

$$k_{\mathrm{r}} = 3\times10^{-9}\overline{\nu_0}^{2}\int \varepsilon d\bar{\nu} \quad \cdots\cdots (3.18)$$

where k_{r} is the radiative rate constant, ε is the molar extinction coefficient, and $\overline{\nu_0}$ is the peak-wavenumber for the molar extinction coefficient. Then, the order of magnitude of spectral overlap would be also similar because the attenuation coefficient for the CT state in the m-MTDATA:PO-T2T mixed film is similar with those in the polymer:PCBM mixed films as shown in Figure 3.14. Therefore, the DET must be considered for the exciplex-exciplex ET in OPVs along with dissociation of CT states followed by geminated or non-geminated recombinations.

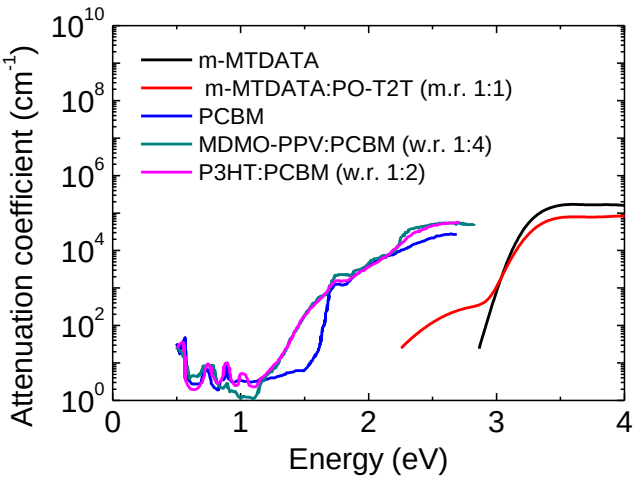

Figure 3.14. Attenuation coefficients of the m-MTDATA neat film, the m-MTDATA:PO-T2T mixed film with the molar ratio of 1:1, the PCBM neat film,[34] poly[2-methoxy-5-(3′,7′-dimethyloctyloxy)-1,4-phenylenevinylene] (MDMO-PPV):PCBM mixed film with the weight ratio of 1:4,[34] and poly(3-hexylthiophene-2,5-diyl) (P3HT):PCBM mixed film with the weight ratio of 1:2.[34]

3.13. Conclusion

It is demonstrated that ETs from exciplexes to other kinds of exciplexes upon ET using time-resolved PL spectroscopy. The ET from the high-energy exciplexes to the low-energy exciplexes is supported by the observation for the sub-bandgap CT absorption in exciplex-forming films to satisfy the necessary condition of the spectral overlap between absorption and emission spectra for the ET process to take place. The ET can be explained by the superexchange mechanism based on the concentration-dependent ET rate constants. We concluded that DET could be the dominant mechanism for exciplex diffusion in our investigated exciplex-forming systems after investigating other possibilities. The diffusion mechanism must be widely applied for most of optoelectronic materials in OLEDs and OPVs. As the importance of exciplexes or CT states in organic photonic devices such as OLEDs and OPVs has increased in recent years, the ET process discussed in this study must be taken into account and play an important role in understanding device characteristics and will contribute to the design of molecules and devices with improved performance. The result of the ET is the generation of other kinds of exciplexes with different photo-physical characteristics from the quenched exciplexes. This could be utilized for the optoelectronic devices.

Chapter 4. Exciplex generation by energy transfer from excitons

4.1. Introduction

Excitons and excited-state charge-transfer complexes (exciplexes) are two key players in organic optoelectronic devices. Organic lighting-emitting diodes (OLEDs) and organic photovoltaics (OPVs) usually employ type-II heterojunctions where exciplexes could be generated.[3,5] Excitons and exciplexes can be generated from each other and this interaction greatly influences the device performance. Two kinds of the interactions are widely known in the transformation between the excited states and have a great impact on the optoelectronic devices, which are exciplex generation from excitons by charge transfer (CT) and exciton generation from exciplexes by energy transfer (ET).

Excitons can be transformed into exciplexes by CT whose rate constant is faster than that of the exciton decay to the ground state if conditions are satisfied. The fast CT transition leads to the negligible intensity of molecular photoluminescence (PL) bands in exciplex-forming blended films compared to the neat films.[7,8,56] The exciplex formation by CT could be a trigger for generating free polaron pairs from excitons optically generated in OPVs.[3,17,73–76] On the other hand, excitons can be generated from exciplexes by ET, and this interaction is exploited for high efficiency of OLEDs.[6,7,9,10,12–14,78] Conventional fluorescent organic dyes have little ability of transition from triplet excited states to singlet excited states. Instead of the

them, exciplexes exhibiting the small energy gap between the lowest singlet and triplet excited states play a key role in the triplet harvesting in order to increase the luminescent excited states via reverse intersystem crossing in OLEDs. Furthermore, exciton generation from exciplexes by CT was also reported in blended films of poly(9,9-dioctylfluorene-co-benzothiadiazole) (F8BT) with poly(9,9-dioctylfluorene-co-bis-*N*,*N*-(4-butylphenyl)-bis-*N*,*N*-phenyl-1,4-phenylenediamine) (PFB).[3] A. C. Morteani reported that the F8BT excitons are regenerated from the PFB:F8BT exciplexes by endothermically back transfer.

However, exciplex generation from excitons by ET have not been reported, although the other three kinds of transitions for exciplex or exciton generation from each other (exciton generation from exciplex via ET and CT, and exciplex generation from exciton via CT) have been reported. It has not been considered due to the lack of the optical absorption for the exciplex state from the ground state.[2,17,56,88] In order for ET to occur, the spectral overlap between emission spectra of energy donors and absorption spectra of energy acceptors should be present according to the Fermi golden rule. The lack of the absorption band for the exciplex state has excluded discussion on the possibility of the formation of the exciplexes by ET.

Here, we show exciplexes can be formed from the exciton by ET in organic films. The qualitative and quantitative analysis of the transient PL profiles of the exciton and the exciplex in an organic film indicates that ET engages in generation of the exciplex from the exciton. Recent observation of CT absorption in polymer films and small organic molecular films support the possibility of the ET process.[4,20,34,35,59,92]

4.2. Experimental

A tris(8-hydroxyquinoline)aluminum (Alq_3), a di-[4-(*N*,*N*-ditolyl-amino)-phenyl]cyclohexane (TAPC), and an (1,3,5-triazine-2,4,6-triyl)tris(benzene-3,1-diyl))tris(diphenylphosphine oxide) (PO-T2T) were employed in this paper and purchased from Nichem Fine Technology and used without further purification. All organic films with the thickness of 50 nm were thermal deposited on pre-cleaned fused silica substrates at a base pressure of $< 5 \times 10^{-7}$ Torr with a rate of 1 Å s^{-1}. A variable angle spectroscopic ellipsometry (VASE, J. A. Woolam M-2000 spectroscopic ellipsometer) and a spectrofluorometer (Photon Technology International, Inc.) with an incorporated monochromator (Acton Research Co.) were employed for measuring extinction coefficients and steady-state photoluminescence (PL) spectra, respectively. The steady-state PL spectrum of TAPC molecules dissolved in methylene chloride at 10^{-4} M was measured at the excitation wavelength of 330 nm. Time-resolved PL spectra and transient PL profiles were measured by a streak camera (C10627; Hamamatsu Photonics) excited by a nitrogen gas laser with a pulse wavelength of 337 nm and a pulse width of 800 ps (KEN-2X; Usho).

4.3. Result and discussion

The exciton-exciplex ET was investigated using three kinds of films deposited by thermal evaporation; an Alq_3:PO-T2T singly doped film with a molar ratio of 6:94, a TAPC:PO-T2T (T:P) (m.r. 6:94) singly doped film, and an Alq_3:TAPC:PO-T2T (m.r. 6:6:88) co-doped film (Film A). The molecular structures of Alq_3, TAPC, and PO-T2T are shown in Figure 4.1(a). The steady-state PL spectra of a TAPC solution and a PO-T2T solution[93] are shown in Figure 4.1(b). The time-resolved PL spectra of the doped films were integrated for 800 ns after excitation by a N_2 pulsed laser (pulse width of 0.8 ns) at a wavelength of 337 nm and are compared in the same figure. The PL spectrum of the singly doped Alq_3:PO-T2T film exhibits only Alq_3 emission with a peak at 514 nm and a full-width at half maximum of 97 nm.[116] It indicates that Alq_3 and PO-T2T do not form exciplexes. In contrast, the TAPC-doped PO-T2T film exhibits a featureless spectrum largely redshifted from the solution PL spectra of TAPC and PO-T2T molecules, indicating that TAPC and PO-T2T form exciplexes.[93] The emission intensity of Alq_3 is higher than the T:P exciplex in the singly doped films. Film A co-doped with Alq_3 and TAPC in PO-T2T exhibits a broader emission than the Alq_3 and the T:P exciplex and it can be de-convoluted into the Alq_3 and the T:P exciplex emissions represented by the dark yellow filled areas. Interestingly, the emission intensity of the T:P exciplex is higher than that of Alq_3 in Film A while that of Alq_3 is higher than that of the T:P exciplex in the singly doped films. It implies that ET takes place from the Alq_3 excitons to the T:P exciplexes in Film A.

Comparison of the transient PL intensities of the Alq_3 and the T:P exciplex

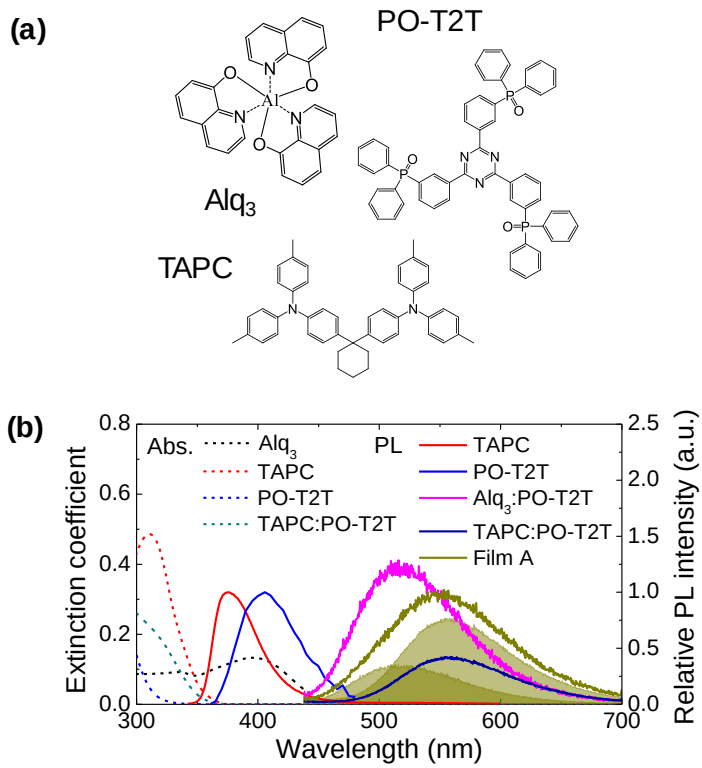

Figure 4.1. (a) Molecular structures of Alq_3, TAPC, and PO-T2T. (b) Extinction coefficients of Alq_3, TAPC, PO-T2T, TAPC:PO-T2T (m.r. 1:1) films, steady-state PL spectra of a TAPC solution and a PO-T2T solution,[93] and time-resolved PL spectra integrated for 800 ns after excitation moment of an Alq_3:PO-T2T (m.r. 6:94) film, a TAPC:PO-T2T (m.r. 6:94) film, and Film A which is de-convoluted into the two emissions (dark yellow filled areas).

in the singly doped films and Film A shown in Figure 4.2 gives clearer evidences of ET from the Alq_3 excitons to the T:P exciplexes. The lifetime of the Alq_3 excitons in Film A is shorter than in the singly doped film, indicating that there is another decay path of the Alq_3 excitons in Film A compared to the singly doped Alq_3:PO-T2T film. In contrast, the lifetime of the T:P exciplex in Film A is longer than that in the singly doped T:P film. The lifetime decrease of the Alq_3 exciton and the lifetime increase of the T:P exciplex as shown in Figure 4.2(a) and 4.2(b), respectively, indicate that ET from the Alq_3 exciton to the T:P exciplex occurs. One must note that the Alq_3 emission is eliminated from the emission of Film A in order for analyzing the transient PL profiles of the T:P exciplex in Figure 4.2(b). More details are provided in Supporting Information.

The quantitative analysis of the transient PL profiles was performed to confirm that the exciton-exciplex ET can be indeed described by ET. We used a single ET rate constant from the Alq_3 excitons to the T:P exciplexes to describe the transient PL profiles in Film A along with other decay rate constants extracted from the singly doped films without ET (black solid lines in Figure 4.2 for the Alq_3:PO-T2T and TAPC:PO-T2T films). Details of the analysis are described in Supporting Information. The calculated normalized transient PL profiles for the Alq_3 exciton and the T:P exciplex in Film A are plotted as red lines in Figure 4.2(a) and 4.2(b) , respectively, and are well matched with the experimental data, where the ET rate constant of 2.9×10^7 s^{-1} was used. This excellent match clearly confirms that ET from the Alq_3 exciton to the T:P exciplex takes place in Film A.

The absence of the spectral overlap between the PL spectrum of Alq_3 (pink solid line) and the absorption spectrum of the T:P film (green dashed line) in Figure

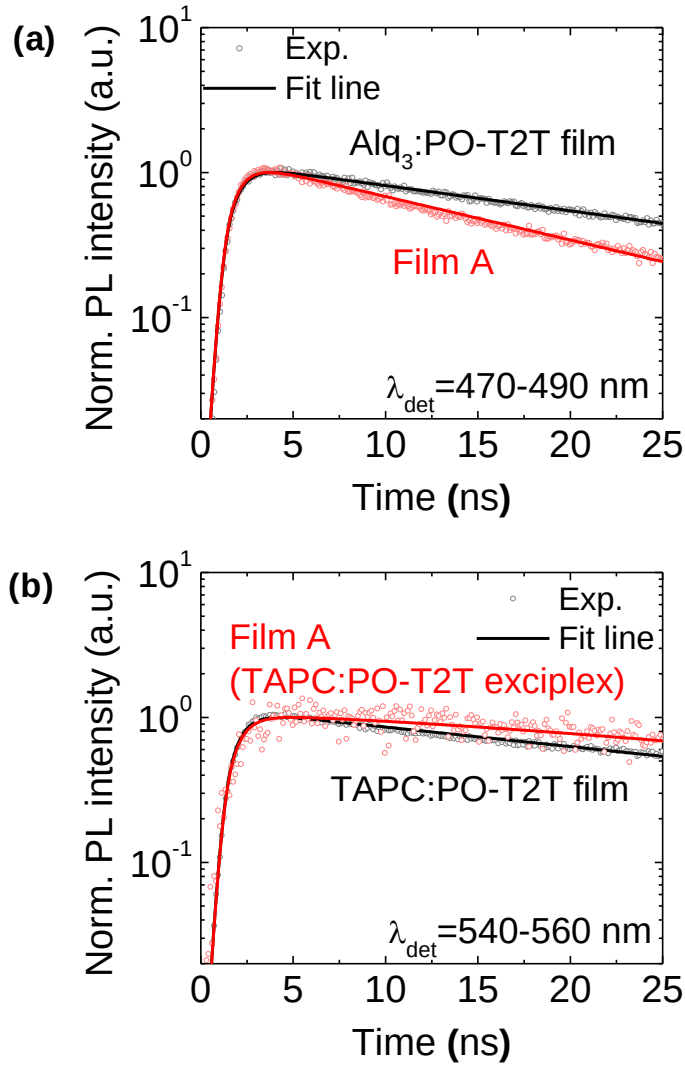

Figure 4.2. (a) Normalized transient PL intensities and fit lines for the Alq_3:PO-T2T (m.r. 6:94) film and Film A in the wavelength range of 470 to 490 nm. (b) Normalized transient PL intensities and fit lines for the T:P exciplex in T:P (m.r. 6:94) film and Film A in the wavelength range of 540 to 560 nm.

4.1(b) seems to be contradictory for ET to take place from the Alq_3 exciton to the T:P exciplex. However, a newly developed method allowed us to measure the very small extinction coefficient down to 10^{-4},[92] and it turns out that the CT absorption in the TAPC:PO-T2T film is present as shown in Figure 4.3. As a result, there is a good enough spectral overlap between the PL spectrum of Alq_3 and the CT absorption spectrum of the T:P pairs so that ET from the Alq_3 excitons to the T:P exciplexes is now possible. Details of the ET mechanisms is under study and will be reported separately.

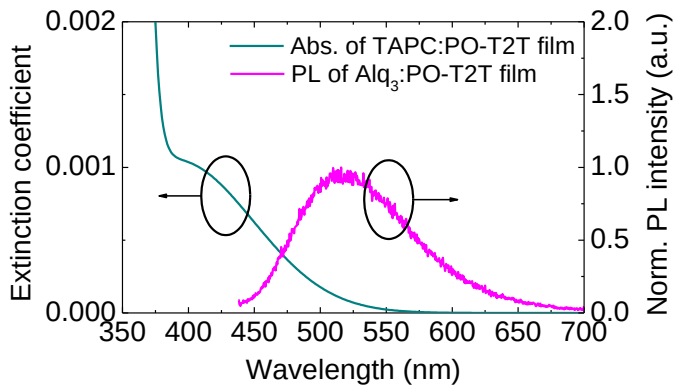

Figure 4.3. An extinction coefficient of the T:P (m.r. 1:1) film below 0.002 and the time-resolved PL spectra of an Alq_3:PO-T2T (m.r. 6:94) film integrated for 800 ns after excitation moment.

4.4. Conclusion

In conclusion, we observed the exciplex generation from the exciton by ET in the organic film. The exciton quenching as well as the lifetime increase of the exciplex when they are close together implies that the exciton-exciplex ET takes place. The spectral overlap and quantitative analysis for the transient PL profiles support the exciton-exciplex ET. The exciplex generation from excitons by ET is the newly recognized phenomenon, and it could help the deep understanding for the organic optoelectronic devices where exciplexes and excitons are simultaneously present.

4.5. Appendix

A. Transient PL profiles of the TAPC:PO-T2T exciplex in Film A

The transient PL profiles of the TAPC:PO-T2T (T:P) exciplexes in the singly doped T:P film (black circles) and Film A (red circles) in the wavelength rage of 540 to 560 nm are shown in Figure 4.2(b). One must note that the transient PL intensity of Film A in the detection wavelength range of 540 to 560 nm is the sum of those from the T:P exciplexes and the Alq_3 excitons apparent from Figure 4.1(b). Because the transient PL profiles of the Alq_3 excitons does not vary with the detection wavelength and the PL intensity in the detection range of 540 nm to 560 nm is the same with that in the detection range of 470 nm to 490 nm $\left(\int_{540nm}^{560nm} I_{Alq_3}^{Alq_3}(t)d\lambda = \int_{470nm}^{490nm} I_{Alq_3}^{Alq_3}(t)d\lambda\right)$ as shown in Figure 4.4(a), we could think that the transient PL intensity of Film A in the detection wavelength range of 540 to 560 nm is the sum of those from the T:P exciplex in the detection wavelength range of 540 to 560 nm and the Alq_3 exciton in the detection wavelength range of 470 to 490 nm $\left[\int_{540nm}^{560nm} I_{\text{Film A}}(t)d\lambda = \int_{540nm}^{560nm}\left(I_{\text{Film A}}^{\text{exciplex}}(t) + I_{\text{Film A}}^{Alq_3}(t)\right)d\lambda = \int_{540nm}^{560nm} I_{\text{Film A}}^{\text{exciplex}}(t)d\lambda + \int_{470nm}^{490nm} I_{\text{Film A}}^{Alq_3}(t)d\lambda\right]$. Then, the difference between the transient PL intensities in the detection wavelength of 540 to 560 nm and that of 470 to 490 nm in Film A corresponds to the transient PL intensity from the T:P exciplex in Film A as depicted in Figure 4.4(b) and Figure 2(b) as red circles.

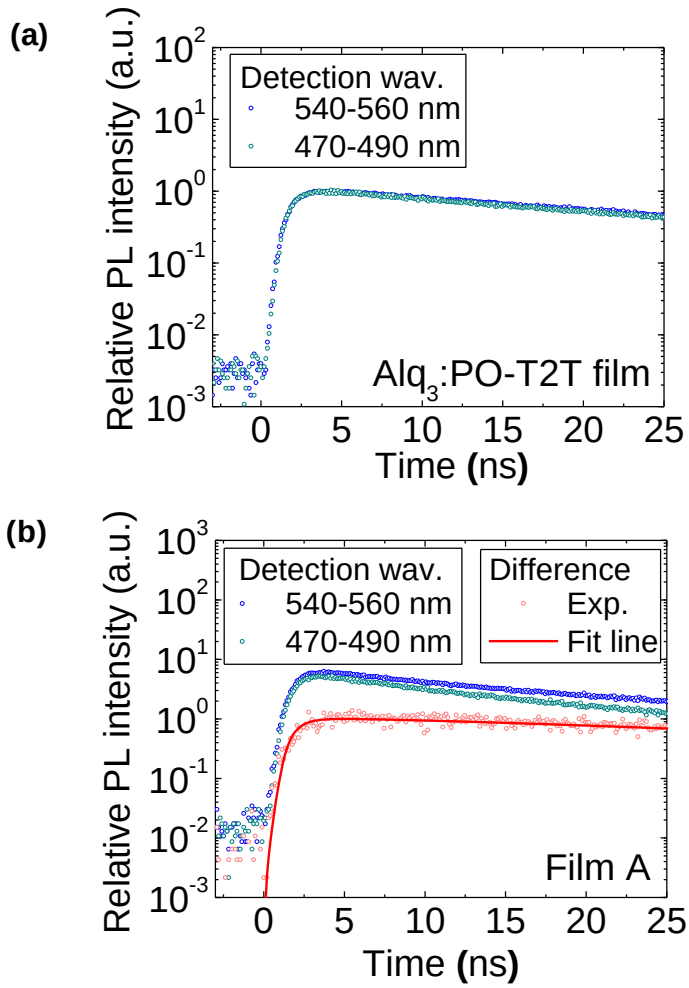

Figure 4.4. (a) Relative transient PL intensities of Alq_3:PO-T2T (m.r.6:94) doped film in the detection wavelength of 540 to 560 nm and that of 470 to 490 nm. (b) Relative transient PL intensity of Film A in the detection wavelength of 540 to 560 nm and that of 470 to 490 nm and the difference between them along with a fit line for the difference.

B. Quantitative analysis of the transient PL profiles

More quantitative analysis of the transient PL profiles was performed to understand the exciton-exciplex energy transfer (ET). We could calculate the transient PL profiles of the Alq_3 exciton and the T:P exciplex in the films employing Equation (4.1).[117,118]

$$I_{\text{norm}}(t) = \frac{1}{I_{\max}} \int_0^t R(t')D(t-t')dt' \quad \cdots\cdots (4.1)$$

where t is the time after the onset of the pulse, $I_{\text{norm}}(t)$ is the measured normalized transient PL profile, $I_{\max}$ is the maximum transient PL intensity in a detection time range, $R(t)$ is the measured pulse profile, and $D(t)$ is the δ-pulse response function of excited species when a pule is applied at $t = 0$. Equation (4.1) indicates that the measured transient PL profiles are distorted by the slow electronic response of the detector, and it is the convolution of the instrument response function and δ-pulse response of excited species. $R(t)$ could be obtained from the response function as shown in Figure 4.5.

$D(t)$ in Equation (4.1) can be obtained using the concentration profiles of the Alq_3, TAPC singlet excitons and the T:P singlet exciplex described by following equations.

$$\frac{d\left[(\text{Alq}_3)^*\right]}{dt} = k_{\text{ET}}^{\text{exciton}}\left[(\text{TAPC})^*\right] - \left(k_{\text{d}}^{\text{exciton}} + k_{\text{ET}}^{\text{exciplex}}\right)\left[(\text{Alq}_3)^*\right] \quad \cdots\cdots (4.2)$$

$$\frac{d\left[(\text{TAPC})^*\right]}{dt} = -\left(k_{\text{ET}}^{\text{exciton}} + k_{\text{CT}}\right)\left[(\text{TAPC})^*\right] \quad \cdots\cdots (4.3)$$

$$\frac{d\left[(\text{T:P})^*\right]}{dt} = k_{\text{CT}}\left[(\text{TAPC})^*\right] - k_{\text{d}}^{\text{exciplex}}\left[(\text{T:P})^*\right] + k_{\text{ET}}^{\text{exciplex}}\left[(\text{Alq}_3)^*\right] \quad \cdots\cdots (4.4)$$

where $[(Alq_3)^*]$, $[(TAPC)^*]$, and $[(T:P)^*]$ are the singlet concentrations of Alq_3,

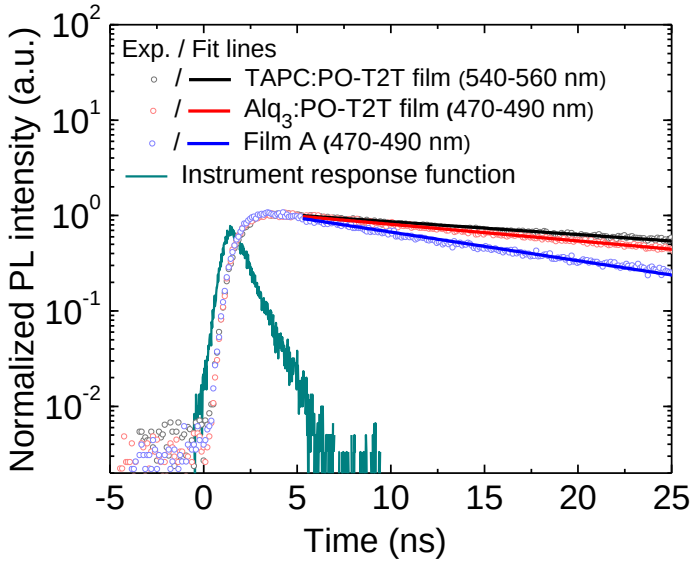

Figure 4.5. The normalized transient PL intensity and the tail-fit line for the T:P (m.r. 6:94) film in the wavelength range of 540 to 560 nm and those for the Alq_3:PO-T2T (m.r. 6:94) film and Film A in the wavelength range of 470 to 490 nm, and the instrument response function.

TAPC, and the T:P exciplex, respectively, $k_{ET}^{exciton}$ and k_{CT} are the exciton-exciton ET rate constant from TAPC to Alq_3 and the T:P exciplex generation rate constant from the TAPC exciton by charge transfer (CT), respectively, $k_d^{exciton}$ and $k_d^{exciplex}$ are the decay rate constants of the Alq_3 exciton and the T:P exciplex without quenchers, respectively, and $k_{ET}^{exciplex}$ is the ET rate constant from the Alq_3 excitons to the T:P exciplexes. We just analyzed the singlet excited states in the prompt time region where the influence of the reverse intersystem crossing from triplet excited states to singlet excited states on the concentration profiles of the singlet excited states is negligible. The intrinsic decay rate constant of the TAPC exciton was neglected in the Equation (4.3) because the TAPC emission was negligible compared to the T:P exciplex emission in the blends. The initial ratio for [(Alq_3)*], [(TAPC)*], and [(T:P)*] was set to be 1:*a*:0 considering that direct excitation from the ground state to the exciplex state is negligible.[92]

When solving the differential equations, the concentration profiles for the Alq_3 exciton and the T:P exciplex could be written as the following equations.

$$\left[\left(Alq_3\right)^*\right] = C_1 e^{-\left(k_{ET}^{exciton}+k_{CT}\right)t} + C_2 e^{-\left(k_d^{exciton}+k_{ET}^{exciplex}\right)t} \quad \cdots\cdots (4.5)$$

$$\left[\left(T{:}P\right)^*\right] = C_3 e^{-\left(k_{ET}^{exciton}+k_{CT}\right)t} + C_4 e^{-\left(k_d^{exciton}+k_{ET}^{exciplex}\right)t} + C_5 e^{-k_d^{exciplex}t} \quad \cdots\cdots (4.6)$$

The pre-exponential factors in Equation (4.5) and (4.6) could be written as the following equations.

$$C_1 = \frac{a k_{ET}^{exciton}}{k_{ET}^{exciplex} + k_d^{exciton} - k_{CT} - k_{ET}^{exciton}} \quad \cdots\cdots (4.7)$$

$$C_2 = \frac{k_{ET}^{exciplex} + k_d^{exciton} - k_{CT} - \left(1+a\right)k_{ET}^{exciton}}{k_{ET}^{exciplex} + k_d^{exciton} - k_{CT} - k_{ET}^{exciton}} \quad \cdots\cdots (4.8)$$

$$C_3 = \frac{a\left(k_{CT}{}^2 - k_d^{exciton} k_{CT} + k_{CT} k_{ET}^{exciton} - k_{CT} k_{ET}^{exciplex} - k_{ET}^{exciton} k_{ET}^{exciplex}\right)}{\left(k_{CT} + k_{ET}^{exciton} - k_d^{exciplex}\right)\left(k_{ET}^{exciplex} + k_d^{exciton} - k_{CT} - k_{ET}^{exciton}\right)} \quad \cdots\cdots (4.9)$$

$$C_4 = \frac{k_{ET}^{exciplex}\left((1+a)k_{ET}^{exciton} + k_{CT} - k_{ET}^{exciplex} - k_d^{exciton}\right)}{\left(k_{ET}^{exciplex} + k_d^{exciton} - k_d^{exciplex}\right)\left(k_{ET}^{exciplex} + k_d^{exciton} - k_{CT} - k_{ET}^{exciton}\right)} \quad \cdots\cdots (4.10)$$

$$C_5 = \frac{(1+a)k_{CT}k_{ET}^{exciplex} + (1+a)k_{ET}^{exciton}k_{ET}^{exciplex} + ak_d^{exciton}k_{CT} - ak_d^{exciplex}k_{CT} - k_d^{exciplex}k_{ET}^{exciplex}}{\left(k_{ET}^{exciplex} + k_d^{exciton} - k_d^{exciplex}\right)\left(k_{CT} + k_{ET}^{exciton} - k_d^{exciplex}\right)} \quad \cdots\cdots$$

$$\cdots\cdots (4.11)$$

The concentration profiles (Equation (4.5) and (4.6)) are linearly proportional to $D(t)$ in Equation (4.1). There are six parameters in Equation (4.5)-(4.11). All parameters other than $k_{ET}^{exciton}$ and k_{CT} could be obtained from the experimental data. $k_d^{exciton}$ and $k_d^{exciplex}$ are 4.0×10^7 s^{-1} and 3.1×10^7 s^{-1} from the tail fitting, respectively. $k_{ET}^{exciplex}$ is 2.9×10^7 s^{-1} corresponding to the difference between the decay rate constants of Alq_3 in the Alq_3:PO-T2T film and Film A. The decay rate constants are obtained from the tail fitting of the transient PL profiles as shown in Figure 4.5 considering that $D(t)$ is linearly proportional to $I_{norm}(t)$ in the time region where $R(t)/I_{max}$ is negligible compared to $I_{norm}(t)$ in Equation (4.1). a is 2 because the extinction coefficient of TAPC is two times larger than that of Alq_3 at excitation wavelength of 337 nm as shown in Figure 4.1(b). In order to fit the transient PL intensities of the Alq_3 exciton and the T:P exciplex as shown in Figure 4.2(a) and 4.2(b), respectively, we made an assumption for $k_{ET}^{exciton}$, and set k_{CT} as fitting parameter.

When the radiative rate constant of the TAPC singlet exciton is assumed to be 10^8 s^{-1}, $k_{ET}^{exciton}$ was calculated as 4×10^9 s^{-1} by using the Förster ET rate equation considering the nearest energy donor-acceptor pairs and random orientations of the participating species.[72,109] When the fitting parameter, k_{CT} was set to be 2×10^{10} s^{-1},

the normalized transient PL profiles calculated from Equation (4.1) for the Alq_3 exciton and the T:P exciplex are plotted as red lines in Figure 4.2(a) and 4.2(b) as well as 4.4(b), respectively, and were well matched with the experimental ones in Film A. The black lines in Figure 4.2(a) and 4.2(b) are the normalized transient profiles calculated from Equation (4.1) when $k_{ET}^{exciton}$ and $k_{ET}^{exciplex}$ were set to zero, which are well matches with the experimental ones from two-component films. Calculated transient PL profiles of the energy donor and energy acceptor species are well matches with the experimental ones, indicating that ET from the Alq_3 exciton to the T:P exciplex takes place in Film A.

Chapter 5. Summary and Conclusion

An excited-state charge-transfer complexes (exciplex) plays important roles in organic optoelectronic devices. It acts as a precursor before charge dissociation in organic photovoltaics (OPVs) and a triplet harvester in organic light-emitting diodes (OLEDs). Since thermally activated delayed fluorescence (TADF) was reported, its application in OLEDs has been actively researching employing its TADF characteristics. Exciplex diffusion in organic films, however, has not been studied much. The apparent lack of optical absorption band for an exciplex state makes generation of exciplexes by energy transfer (ET) considered improbable. However, it was reported that exciplex diffusion takes place indeed and its mechanism was proposed to be 'inchworm'-type rather than ET, recently. In this thesis, we reported that the diffusion mechanism of exciplex in organic films would take place dominantly by Dexter-type ET.

In Chapter 2, we reported the absorption band for an intermolecular charge-transfer (CT) state exhibiting exciplex luminescence. The extraction of the extinction coefficients for the exciplex state from absorbance was carried out. Two different methods were introduced. One is to employ the ellipsometry measurement as well as the ultraviolet-visible-near infrared (UV-Vis-NIR) spectrophotomer measurement, and the other is employ the UV-Vis-NIR spectrophotomer measurement only.

The presence of the absorption band for the exciplex state implies that exciplex generation by ET could take place. We concluded that exciplex diffusion could occur by ET based on concentration-dependent quenching experiments in Chapter 3. The exciplex-exciplex ET and the exponential decrease of the ET rate constants with

separation were observed. These indicate that the mechanism of this ET is exchange type.

Finally, we also report the exciton-exciplex ET in Chapter 4. Exciton generation from exciplexes by CT or ET and exciplex generation from excitons by CT are reported. However, exciplex generation from excitons by ET has not been reported because of a common belief that the CT absorption band for exciplexes is absent. From the analysis of the transient photoluminescence profiles of the exciton and exciplex, we could conclude that exciton-exciplex ET occurs in the organic semiconductor based on the presence of the CT absorption band for the exciplex.

Bibliography

1. Kavarnos, G. J. & Turro, N. J. Photosensitization by reversible electron transfer: theories, experimental evidence, and examples. *Chem. Rev.* **86**, 401–449 (1986).

2. Turro, N. J. *Modern Molecular Photochemistry*. (University Science Books, 1991).

3. Morteani, A. C., Sreearunothai, P., Herz, L. M., Friend, R. H. & Silva, C. Exciton regeneration at polymeric semiconductor heterojunctions. *Phys. Rev. Lett.* **92**, 247402–1 (2004).

4. Clarke, T. M. & Durrant, J. R. Charge photogeneration in organic solar cells. *Chem. Rev.* **110**, 6736–6767 (2010).

5. Kim, H.-B. & Kim, J.-J. Recent progress on exciplex-emitting OLEDs. *J. Inf. Disp.* **20**, 105–121 (2019).

6. Wang, J.-F. *et al*. Exciplex Electroluminescence from Organic Bilayer Devices Composed of Triphenyldiamine and Quinoxaline Derivatives. *Adv. Mater.* **10**, 230–233 (1998).

7. Goushi, K., Yoshida, K., Sato, K. & Adachi, C. Organic light-emitting diodes employing efficient reverse intersystem crossing for triplet-to-singlet state conversion. *Nat. Photonics* **6**, 253–258 (2012).

8. Park, Y.-S., Kim, K.-H. & Kim, J.-J. Efficient triplet harvesting by fluorescent molecules through exciplexes for high efficiency organic light-emitting diodes. *Appl. Phys. Lett.* **102**, 153306 (2013).

9. Hung, W. Y. *et al.* Highly efficient bilayer interface exciplex for yellow organic light-emitting diode. *ACS Appl. Mater. Interfaces* **5**, 6826–6831 (2013).

10. Jankus, V. *et al.* Highly efficient TADF OLEDs: How the emitter-host

interaction controls both the excited state species and electrical properties of the devices to achieve near 100% triplet harvesting and high efficiency. *Adv. Funct. Mater.* **24**, 6178–6186 (2014).

11. Liu, X. K. *et al.* Nearly 100% triplet harvesting in conventional fluorescent dopant-based organic light-emitting devices through energy transfer from exciplex. *Adv. Mater.* **27**, 2025–2030 (2015).

12. Chen, D. *et al.* Efficient exciplex organic light-emitting diodes with a bipolar acceptor. *Org. Electron. physics, Mater. Appl.* **25**, 79–84 (2015).

13. Oh, C. S., Kang, Y. J., Jeon, S. K. & Lee, J. Y. High Efficiency Exciplex Emitters Using Donor-Acceptor Type Acceptor Material. *Journal of Physical Chemistry C* vol. 119 22618–22624 (2015).

14. Zhang, L. *et al.* Efficient Organic Light-Emitting Diode through Triplet Exciton Reharvesting by Employing Blended Electron Donor and Acceptor as the Emissive Layer. *ACS Appl. Mater. Interfaces* **7**, 24983–24986 (2015).

15. Kim, H.-B., Kim, D. & Kim, J.-J. Exciplex: Its Nature and Application to OLEDs. in *Highly Efficient OLEDs: Materials Based on Thermally Activated Delayed Fluorescence* (ed. Yersin, H.) 331–376 (John Wiley & Sons, 2018).

16. Yersin, H. *Highly Efficient OLEDs: Materials Based on Thermally Activated Delayed Fluorescence*. (John Wiley & Sons, 2018).

17. Offermans, T., Van Hal, P. A., Meskers, S. C. J., Koetse, M. M. & Janssen, R. A. J. Exciplex dynamics in a blend of π-conjugated polymers with electron donating and accepting properties: MDMO-PPV and PCNEPV. *Phys. Rev. B - Condens. Matter Mater. Phys.* **72**, 045213 (2005).

18. Yin, C., Kietzke, T., Neher, D. & Hörhold, H. H. Photovoltaic properties and exciplex emission of polyphenylenevinylene- based blend solar cells. *Appl. Phys. Lett.* **90**, 1–4 (2007).

19. Westenhoff, S. Charge recombination in organic photovoltaic devices with

high open-circuit voltages. *J. Am. Chem. Soc.* **130**, 13653–13658 (2008).

20. Vandewal, K. *et al.* The relation between open-circuit voltage and the onset of photocurrent generation by charge-transfer absorption in polymer: Fullerene bulk heterojunction solar cells. *Adv. Funct. Mater.* **18**, 2064–2070 (2008).

21. Vandewal, K., Tvingstedt, K., Gadisa, A., Inganäs, O. & Manca, J. V. On the origin of the open-circuit voltage of polymer-fullerene solar cells. *Nat. Mater.* **8**, 904–909 (2009).

22. Veldman, D., Meskers, S. C. J. & Janssen, R. A. J. The energy of charge-transfer states in electron donor-acceptor blends: insight into the energy losses in organic solar cells. *Adv. Funct. Mater.* **19**, 1939–1948 (2009).

23. Schlenker, C. W. *et al.* Polymer triplet energy levels need not limit photocurrent collection in organic solar cells. *J. Am. Chem. Soc.* **134**, 19661–19668 (2012).

24. Rao, A. *et al.* The role of spin in the kinetic control of recombination in organic photovoltaics. *Nature* **500**, 435–9 (2013).

25. Vandewal, K. *et al.* Efficient charge generation by relaxed charge-transfer states at organic interfaces. *Nat. Mater.* **13**, 63–68 (2014).

26. Inai, Y., Sisido, M. & Imanishi, Y. Distance and Orientation Dependence of Electron Transfer and Excipiex Formation of Naphthyl and p-Dimethyianiiino Groups Fixed on a Helical Polypeptide Chain. *J. Phys. Chem.* **94**, 6237–6243 (1990).

27. Gould, I. R., Farid, S. & Young, R. H. Relationship Between Exciplex Fluorescence and Electron Transfer in Radical Ion Pairs. *J. Photochem. Photobiol. a-Chemistry* **65**, 133–147 (1992).

28. Bixon, M., Jortner, J. & Verhoeven, J. W. Lifetimes for Radiative Charge Recombination in Donor-Acceptor Molecules. *J. Am. Chem. Soc.* **116**, 7349–

7355 (1994).

29. Gould, I. R., Young, R. H., Mueller, L. J., Albrecht, a. C. & Farid, S. Electronic Structures of Exciplexes and Excited Charge-Transfer Complexes. *J. Am. Chem. Soc.* **116**, 8188–8199 (1994).

30. Verhoeven, J. W. *et al.* Electronic coupling in inter- and intramolecular donor-acceptor systems as revealed by their solvent-dependent charge-transfer fluorescence. *Rec. Trav. Chim. Pays Bas* **114**, 443–448 (1995).

31. Huang, Y. *et al.* Electronic structures of interfacial states formed at polymeric semiconductor heterojunctions. *Nat. Mater.* **7**, 483–489 (2008).

32. Graves, D., Jankus, V., Dias, F. B. & Monkman, A. Photophysical investigation of the thermally activated delayed emission from films of m-MTDATA:PBD exciplex. *Adv. Funct. Mater.* **24**, 2343–2351 (2014).

33. Mikhnenko, O. V., Blom, P. W. M. & Nguyen, T.-Q. Exciton diffusion in organic semiconductors. *Energy Environ. Sci.* **8**, 1867–1888 (2015).

34. Goris, L. *et al.* Observation of the subgap optical absorption in polymer-fullerene blend solar cells. *Appl. Phys. Lett.* **88**, 052113 (2006).

35. Goris, L. *et al.* Absorption phenomena in organic thin films for solar cell applications investigated by photothermal deflection spectroscopy. *J. Mater. Sci.* **40**, 1413–1418 (2005).

36. Deotare, P. B. *et al.* Nanoscale transport of charge-transfer states in organic donor-acceptor blends. *Nat. Mater.* **14**, 1130–1134 (2015).

37. Forrest, S. R. *et al.* ORGANIC ELECTRONICS AND OPTOELECTRONICS , STEPHEN R . FORREST AND MARK E . THOMPSON , GUEST EDITORS Introduction : Organic Electronics and Optoelectronics Spiro Compounds for Organic Optoelectronics Organic Semiconducting Oligomers for Use in Thin Film Tr. *Chem. Rev.* **107**, 953–1010 (2007).

38. Zhigang, R. L. *Organic Light-Emitting Materials and Devices*. (CRC Press, 2015).

39. Ge, Z. *et al.* Synthesis and properties of 3,8-bis[4-(9H-carbazol-9-yl)phenyl]-1,10-phenanthroline for phosphorescent OLEDs. *Chem. Lett.* **37**, 262–263 (2008).

40. Chen, Y.-M. *et al.* Carbazole–benzimidazole hybrid bipolar host materials for highly efficient. *J. Mater. Chem.* **21**, 14971–14978 (2011).

41. Zhang, X. *et al.* Theoretical investigation of dihydroacridine and diphenylsulphone derivatives as thermally activated delayed fluorescence emitters for organic light-emitting diodes. *RSC Adv.* **5**, 51586–51591 (2015).

42. Gaspar, D. J. & Polikarpov, E. *OLED Fundamentals: Materials, Devices, and Processing of Organic Light-Emitting Diodes*. (CRC Press, 2015).

43. Hughes, G. & Bryce, M. R. Electron-transporting materials for organic electroluminescent and electrophosphorescent devices. *J. Mater. Chem.* **15**, 94–107 (2005).

44. Jeon, S. O. & Lee, J. Y. Phosphine oxide derivatives for organic light emitting diodes. *J. Mater. Chem.* **22**, 4233–4243 (2012).

45. Sasabe, H., Seino, Y., Kimura, M. & Kido, J. A m -terphenyl-modifed sulfone derivative as a host material for high-efficiency blue and green phosphorescent OLEDs. *Chem. Mater.* **24**, 1404–1406 (2012).

46. Xu, X., Yu, G., Chen, S., Di, C. & Liu, Y. Synthesis and characterization of a quinoxaline compound containing polyphenylphenyl and strong electron-accepting groups, and its multiple applications in electroluminescent devices. *J. Mater. Chem.* **18**, 299–305 (2008).

47. Murata, H., Malliaras, G. G., Uchida, M., Shen, Y. & Kafafi, Z. H. Non-dispersive and air-stable electron transport in an amorphous organic semiconductor. *Chem. Phys. Lett.* **339**, 161–166 (2001).

48. Banal, J. L. *et al.* Electron Deficient Conjugated Polymers Based on Benzotriazole. *Polym. Chem.* **4**, 1077–1083 (2013).

49. Tekarli, S. M., Cundari, T. R. & Omary, M. A. Rational design of macrometallocyclic trinuclear complexes with superior ??-acidity and ??-basicity. *J. Am. Chem. Soc.* **130**, 1669–1675 (2008).

50. Young, R. H., Feinberg, A. M., Dinnocenzo, J. P. & Farid, S. Transition from charge-transfer to largely locally excited exciplexes, from structureless to vibrationally structured emissions. *Photochem. Photobiol.* **91**, 624–636 (2015).

51. Groenen, E. J. J. & van Velzen, P. N. T. An electro-optical study of the electronic structure of exciplexes of 9,10-dicyanoanthracene and of N,N-dimethylaniline. *Mol. Phys.* **35**, 19–31 (1978).

52. Cherpak, V. *et al.* Mixing of phosphorescent and exciplex emission in efficient organic electroluminescent devices. *ACS Appl. Mater. Interfaces* **7**, 1219–1225 (2015).

53. Hung, W. Y. *et al.* Balance the Carrier Mobility to Achieve High Performance Exciplex OLED Using a Triazine-Based Acceptor. *ACS Appl. Mater. Interfaces* **8**, 4811–4818 (2016).

54. Yuying, H., Junfeng, L., Xiaohong, F., Wenhao, F. & Bingshe, X. Theoretical studies on geometrical and electronic structure of electroplex at the NPB/PBD interface in organic light-emitting diodes. *Curr. Appl. Phys.* **10**, 744–748 (2010).

55. Kuzmin, M. G., Soboleva, I. V. & Dolotova, E. V. The behavior of exciplex decay processes and interplay of radiationless transition and preliminary reorganization mechanisms of electron transfer in loose and tight pairs of reactants. *J. Phys. Chem. A* **111**, 206–215 (2007).

56. Kulkarni, A. P. & Jenekhe, S. A. Blue-green, orange, and white organic light-emitting diodes based on exciplex electroluminescence of an oligoquinoline

acceptor and different hole-transport materials. *J. Phys. Chem. C* **112**, 5174–5184 (2008).

57. Itaya, A., Kitagawa, T., Moriyama, T., Matsushita, T. & Miyasaka, H. Picosecond-Microsecond Dynamics of Photoinduced Electron-Transfer Processes in Amorphous Solid Films of Dimeric Carbazolyl Compounds Doped with 1,2,4,5-Tetracyanobenzene. *J. Phys. Chem. B* **101**, 524–530 (1997).

58. Vandewal, K. *et al.* Fourier-Transform Photocurrent Spectroscopy for a fast and highly sensitive spectral characterization of organic and hybrid solar cells. *Thin Solid Films* **516**, 7135–7138 (2008).

59. Hallermann, M. *et al.* Charge transfer excitons in polymer/fullerene blends: The role of morphology and polymer chain conformation. *Adv. Funct. Mater.* **19**, 3662–3668 (2009).

60. Vanecek, M. & Poruba, A. Fourier-transform photocurrent spectroscopy of microcrystalline silicon for solar cells. *Appl. Phys. Lett.* **80**, 719–721 (2002).

61. Uoyama, H., Goushi, K., Shizu, K., Nomura, H. & Adachi, C. Highly efficient organic light-emitting diodes from delayed fluorescence. *Nature* **492**, 234–8 (2012).

62. Lim, B. T., Okajima, S., Chandra, A. K. & Lim, E. C. Radiationless transitions in electron donor-acceptor complexes: selection rules for S1 → T intersystem crossing and efficiency of S1 → S0 internal conversion. *Chem. Phys. Lett.* **79**, 22–27 (1981).

63. Gould, I. R., Boiani, J. A., Gaillard, E. B., Goodman, J. L. & Farid, S. Intersystem crossing in charge-transfer excited states. *J. Phys. Chem. A* **107**, 3515–3524 (2003).

64. Etherington, M. K., Gibson, J., Higginbotham, H. F., Penfold, T. J. & Monkman, A. P. Revealing the spin-vibronic coupling mechanism of thermally activated delayed fluorescence. *Nature Communications* vol. 7

13680 (2016).

65. Baldo, M., Adachi, C. & Forrest, S. R. Transient analysis of organic electrophosphorescence.II. Transient analysis of triplet-triplet annihilation. *Phys. Rev. B* **62**, 10967–10977 (2000).

66. Baleizão, C. & Berberan-Santos, M. N. Thermally activated delayed fluorescence as a cycling process between excited singlet and triplet states: Application to the fullerenes. *J. Chem. Phys.* **126**, 204510 (2007).

67. Speiser, S. Photophysics and Mechanisms of Intramolecular Electronic Energy Transfer in Bichromophoric Molecular Systems : Solution and Supersonic Jet Studies Photophysics and Mechanisms of Intramolecular Electronic Energy Transfer in Bichromophoric Molecular Systems. *Chem. Rev.* **96**, 1953–1976 (1996).

68. Harriman, A., Khatyr, A., Ziessel, R. & Benniston, A. C. An unusually shallow distance-dependence for triplet-energy transfer. *Angew. Chemie - Int. Ed.* **39**, 4287–4290 (2000).

69. Zhang, Y. & Forrest, S. R. Triplet diffusion leads to triplet–triplet annihilation in organic phosphorescent emitters. *Chem. Phys. Lett.* **590**, 106–110 (2013).

70. Albinsson, B. & Martensson, J. Excitation energy transfer in donor–bridge–acceptor systems. *Phys. Chem. Chem. Phys.* **12**, 7338–7351 (2010).

71. Klosterman, J. K., Iwamura, M., Tahara, T. & Fujita, M. Energy transfer in a mechanically trapped exciplex. *J. Am. Chem. Soc.* **131**, 9478–9479 (2009).

72. Förster, T. Zwischenmolekulare energiewanderung und fluoreszenz. *Ann. Phys.* **437**, 55–75 (1948).

73. Sariciftci, N. S., Smilowitz, L., Heeger, A. J. & Wudl, F. Photoinduced Electron Transfer from a Conducting Polymer to Buckminsterfullerene. *Science (80-.).* **258**, 1474–1476 (1992).

74. Mihailetchi, V. D., Koster, L. J. A., Hummelen, J. C. & Blom, P. W. M. Photocurrent generation in polymer-fullerene bulk heterojunctions. *Phys. Rev. Lett.* **93**, 216601 (2004).

75. Peumans, P. & Forrest, S. R. Separation of geminate charge-pairs at donor-acceptor interfaces in disordered solids. *Chemical Physics Letters* vol. 398 27–31 (2004).

76. Muntwiler, M., Yang, Q., Tisdale, W. A. & Zhu, X. Y. Coulomb barrier for charge separation at an organic semiconductor interface. *Phys. Rev. Lett.* **101**, 196403 (2008).

77. Jankus, V., Chiang, C. J., Dias, F. & Monkman, A. P. Deep blue exciplex organic light-emitting diodes with enhanced efficiency; P-type or E-type triplet conversion to singlet excitons? *Adv. Mater.* **25**, 1455–1459 (2013).

78. Liu, X. K. *et al.* Prediction and design of efficient exciplex emitters for high-efficiency, thermally activated delayed-fluorescence organic light-emitting diodes. *Adv. Mater.* **27**, 2378–2383 (2015).

79. Park, Y. S. *et al.* Exciplex-forming Co-host for organic light-emitting diodes with ultimate efficiency. *Adv. Funct. Mater.* **23**, 4914–4920 (2013).

80. Sun, J. W. *et al.* A fluorescent organic light-emitting diode with 30% external quantum efficiency. *Adv. Mater.* **26**, 5684–5688 (2014).

81. Shin, H. *et al.* Blue phosphorescent organic light-emitting diodes using an exciplex forming co-host with the external quantum efficiency of theoretical limit. *Adv. Mater.* **26**, 4730–4734 (2014).

82. Masuhara, H. & Mataga, N. Ionic Photodissociation of Electron Donor-Acceptor Systems in Solution. *Acc. Chem. Res.* **14**, 312–318 (1981).

83. Marcus, R. A. Relation between Charge Transfer Absorption and Fluorescence Spectra and the Inverted Region. *J. Phys. Chem.* **93**, 3078–3086 (1989).

84. Gould, I. R., Young, R. H., Moody, R. E. & Farid, S. Contact and Solvent-Separated Geminate Radical Ion Pairs in Electron- Transfer Photochemistry. *J. Phys. Chem.* **95**, 2068–2080 (1991).

85. Gould, I. R. *et al.* Radiative and nonradiative electron transfer in contact radical-ion pairs. *Chem. Phys.* **176**, 439–456 (1993).

86. Itaya, A., Egawa, A., Umehara, Y., Sakai, H. & Masuhara, H. Fluorescence dynamics of charge-transfer-complex films of poly(N-vinylcarbazole) and 1,2,4,5-tetracyanobenzene and molecular aspects of the disordered structure. *Polymer (Guildf).* **35**, 3149–3155 (1994).

87. Panda, P. *et al.* Charge transfer absorption for π-conjugated polymers and oligomers mixed with electron acceptors. *J. Phys. Chem. B* **111**, 5076–5081 (2007).

88. Kim, K.-H., Moon, C.-K., Sun, J. W., Sim, B. & Kim, J.-J. Triplet Harvesting by a Conventional Fluorescent Emitter Using Reverse Intersystem Crossing of Host Triplet Exciplex. *Adv. Opt. Mater.* **3**, 895–899 (2015).

89. Zhang, T. *et al.* Blue exciplex emission and its role as a host of phosphorescent emitter. *Org. Electron. physics, Mater. Appl.* **24**, 1–6 (2015).

90. Grant R. Fowles. *Introduction to modern optics*. (Courier Corporation, 1975).

91. K. J. Pascoe. *Relectivity and Transmissivity Through Layered Lossy Media: A User-Friendly Approach*. (Wright Patterson Air Force Base, Ohio, USA, 2001).

92. Kim, H.-B. & Kim, J.-J. A simple method to measure intermolecular charge-transfer absorption of organic films. *Org. Electron. physics, Mater. Appl.* **62**, 511–515 (2018).

93. Lee, J.-H. *et al.* An exciplex forming host for highly efficient blue organic light emitting diodes with low driving voltage. *Adv. Funct. Mater.* **25**, 361–366 (2015).

94. Park, Y. S., Jeong, W. I. & Kim, J. J. Energy transfer from exciplexes to dopants and its effect on efficiency of organic light-emitting diodes. *J. Appl. Phys.* **110**, 124519 (2011).

95. Kim, S. Y. *et al.* Organic light-emitting diodes with 30% external quantum efficiency based on a horizontally oriented emitter. *Adv. Funct. Mater.* **23**, 3896–3900 (2013).

96. Zhao, B. *et al.* Highly efficient red OLEDs using DCJTB as the dopant and delayed fluorescent exciplex as the host. *Sci. Rep.* **5**, 10697 (2015).

97. Strobel, T., Deibel, C. & Dyakonov, V. Role of polaron pair diffusion and surface losses in organic semiconductor devices. *Phys. Rev. Lett.* **105**, 266602 (2010).

98. Hung, W. Y. *et al.* The first tandem, all-exciplex-based WOLED. *Sci. Rep.* **4**, 1–11 (2014).

99. Hontz, E. *et al.* The Role of Electron-Hole Separation in Thermally Activated Delayed Fluorescence in Donor-Acceptor Blends. *J. Phys. Chem. C* **119**, 25591–25597 (2015).

100. Kim, K. H., Yoo, S. J. & Kim, J. J. Boosting Triplet Harvest by Reducing Nonradiative Transition of Exciplex toward Fluorescent Organic Light-Emitting Diodes with 100% Internal Quantum Efficiency. *Chem. Mater.* **28**, 1936–1941 (2016).

101. Baldo, M. a & Forrest, S. R. Transient analysis of organic electrophosphorescence: I. Transient analysis of triplet energy transfer. *Phys Rev B* **62**, 10958-- (2000).

102. D. L. Dexter. A Theory of Sensitized Luminescence in Solids. *J. Chem. Phys.* **21**, 836 (1953).

103. Ashcroft, N. W. & Mermin, N. D. *Solid State Physics*. (Holt, Rinehart and Winston, 1976).

104. Szarko, J. M. *et al.* When function follows form: Effects of donor copolymer side chains on film morphology and BHJ solar cell performance. *Adv. Mater.* **22**, 5468–5472 (2010).

105. Szarko, J. M., Guo, J., Rolczynski, B. S. & Chen, L. X. Current trends in the optimization of low band gap polymers in bulk heterojunction photovoltaic devices. *J. Mater. Chem.* **21**, 7849–7857 (2011).

106. McConnell, H. M. Intramolecular charge transfer in aromatic free radicals. *J. Chem. Phys.* **35**, 508 (1961).

107. Eng, M. P. & Albinsson, B. Non-exponential distance dependence of bridge-mediated electronic coupling. *Angew. Chemie - Int. Ed.* **45**, 5626–5629 (2006).

108. Albinsson, B., Eng, M. P., Pettersson, K. & Winters, M. U. Electron and energy transfer in donor–acceptor systems with conjugated molecular bridges. *Phys. Chem. Chem. Phys.* **9**, 5847–5864 (2007).

109. Pillai, S. & Van der Vliet, P. C. *FRET and FLIM Techniques*. (Elsevier, UK, 2009).

110. Kuik, M., Koster, L. J. A., Wetzelaer, G. A. H. & Blom, P. W. M. Trap-assisted recombination in disordered organic semiconductors. *Phys. Rev. Lett.* **107**, 256805 (2011).

111. Geng, R., Daugherty, T. T., Do, K., Luong, H. M. & Nguyen, T. D. A review on organic spintronic materials and devices: I. Magnetic field effect on organic light emitting diodes. *J. Sci. Adv. Mater. Devices* **1**, 128–140 (2016).

112. Basel, T. *et al.* Magnetic Field Enhancement of Organic Light-Emitting Diodes Based on Electron Donor–Acceptor Exciplex. *Adv. Electron. Mater.* **2**, 1500248 (2016).

113. Gould, I. R., Turro, N. J. & Zimmt, M. B. Magnetic field and magnetic isotope effects on the products of organic reactions. *Adv. Phys. Org. Chem.*

20, 1 (1984).

114. Wang, Y., Sahin-Tiras, K., Harmon, N. J., Wohlgenannt, M. & Flatté, M. E. Immense magnetic response of exciplex light emission due to correlated spin-charge dynamics. *Phys. Rev. X* **6**, 011011 (2016).

115. Hu, B. Understanding spin-dependent processes in TADF light-emitting materials based on magneto-optical studies (Conference Presentation). *Proc. SPIE* **10362**, 103620E (2017).

116. Wang, Z., Tsuboi, T., Liu, X. & Huang, W. Study of photoluminescence excitation spectra of tris(8-hydroxyquinoline) aluminum(III) (Alq3) in solutions and films. *Isr. J. Chem.* **54**, 927–930 (2014).

117. O'Connor, D. V., Ware, W. R. & Andre, J. C. Deconvolution of Fluorescence Decay Curves. A Critical Comparison of Techniques. *J. Phys. Chem.* **83**, 1333 (1979).

118. Jan F. Rabek. *Progress in photochemistry and photophysics volume VI*. (1992).

초 록

여기 상태 전하 이동 복합체인 엑시플렉스는 삼중항 여기자를 수확한다는 결과가 보고되면서 중요한 연구 주제가 되어왔다. 본래 인광 염료가 사용되지 않은 유기 발광 소자에서는 일중항 여기자만이 발광에 참여할 수 있고, 전하 재결합 시 일중항 여기자가 25%의 확률, 삼중항 여기자가 75%의 확률로 생성되기 때문에 형광 유기 발광 소자의 효율이 높지 못했다. 하지만, 유기 발광 소자에 엑시플렉스를 적용하여 삼중항 여기 상을 일중항 여기 상으로 전환시키는데 성공시킨 보고가 최근에 발표되었고, 이는 포논으로 낭비되는 75%의 삼중항 여기자를 광자로 전환시켜 이론적 최대 효율에 다다르는 높은 효율의 형광 유기 발광 소자 구현의 근거를 마련했다고 볼 수 있다.

유기 태양 전지에서도 엑시플렉스는 중요한 연구 주제 중 하나이다. 유기 태양 전지의 목적은 빛에 의해 생성된 여기자를 전자와 정공으로 분리시켜 전극으로 수집하는 것이다. 여기자를 분리시키기 위하여 헤테로 접합이 이용되는데, 여기자로부터 약하게 결합된 전자-정공 쌍이라고 할 수 있는 엑시플렉스가 헤테로 접합에서 생성될 수 있다. 이러한 연유로 엑시플렉스가 포함된 여기자의 분리 과정에 대한 이해가 유기 태양 전지의 효율을 높이는데 앞서 선행되어야 한다고 말할 수 있다.

이러한 유기 광전자 소자 내 엑시플렉스의 활용성과 중요성에도

불구하고 소자 내에서 엑시플렉스의 확산은 연구 대상이 되지 않았다. 여기 상의 확산은 여기 에너지 전이에 의해서 일어나는데 여기 에너지 전이는 에너지 주개의 발광 스펙트럼과 에너지 받개의 흡수 스펙트럼의 겹침을 필요로 한다. 하지만 엑시플렉스 상의 흡광 계수는 존재하지 않는다고 알려져 왔기 때문에 엑시플렉스의 확산은 고려되지 않았다.

이 학위 논문에서는 먼저 엑시플렉스 상의 흡광 계수를 보고한다. 수 마이크로미터 두께의 엑시플렉스 형성 박막에 대한 분광광도법을 실행하여 엑시플렉스 상에 대한 광학적 흡수를 관찰할 수 있었다. 흡광 계수의 추출은 박막의 흡광도를 이용하여 진행하였으며, 추가적으로 엘립소메트리 측정을 이용하는 방법과 그렇지 않은 방법 두 가지를 새로 도입하였다.

두번째로 엑시플렉스 확산에 대한 논의가 진행된다. 엑시플렉스 상의 흡광 계수의 보고로 엑시플렉스의 흡수 스펙트럼과 발광 스펙트럼 간의 스펙트럼 겹침이 존재하게 되고, 이로 인해 엑시플렉스-엑시플렉스 에너지 전이가 일어날 수 있다. 엑시플렉스-엑시플렉스 에너지 전이가 일어나는지 알아보기 위하여 높은 에너지의 엑시플렉스와 낮은 에너지의 엑시플렉스가 함께 도핑된 유기 박막을 제작하여 각각의 시간 전계 발광에 대한 분석을 진행하였다. 뿐만 아니라 농도 별 분석을 통해 엑시플렉스 간 거리 증가에 따른 에너지 전이 속도 상수의 지수 함수적 감소를 관찰하였고, 이는 덱스터 에너지 전이가 주로 엑시플렉스-엑시플렉스 에너지 전이에 기여한다는 것을 의미한다.

마지막으로, 에너지 전이에 의해 엑시플렉스로부터 여기자가 생성되는 현상을 보고한다. 여기자의 발광 스펙트럼과 엑시플렉스의 흡수 스펙트럼의 겹침이 존재하고, 이는 여기자-엑시플렉스 에너지 전이가 일어날 수 있다는 것을 의미한다. 이에 대한 실험적 규명을 위하여 여기자와 엑시플렉스가 함께 도핑된 유기 박막을 제작하여 여기자와 엑시플렉스의 발광 스펙트럼에 대한 시간 전계 정량 분석을 진행하였다. 여기자와 엑시플렉스가 가까이 있을 때 여기자 수명의 감소와 엑시플렉스 수명의 증가는 유기 박막에서 엑시톤-엑시플렉스 에너지 전이가 일어난 것을 실험적으로 보여준다.

주요어: 엑시플렉스, 확산, 에너지 전이, 전하 이동 흡수, 덱스터 에너지 전이

학번: 2014-21494